Department of Spatial Sciences

Using CORONA and Landsat Data for Evaluating and Mapping Long-term LULC Changes in Iraqi Kurdistan

Ashty Saleem

This thesis is presented for the Degree of
Doctor of Philosophy
of
Curtin University

May 2017

Declaration

To the best of my knowledge and belief this thesis contains no material previously published by any other person except where due acknowledgment has been made.

This thesis contains no material which has been accepted for the award of any other degree or diploma in any university.

Signature: 

Date: 16/05/2017

Dedication

This project dedicated to the spirit of my father and my senior brother (Azad) who pass away during my PhD journey. In addition, this historical work is dedicated to every individual Kurds living somewhere in this world. To the Kurdish nation, which always wanted to be independent as a country, free from discrimination, racism, and to live peacefully in their motherland “Kurdistan”. To the nation that deserves to live in the luxury that science can provide. Also, a humble dedication to every single person who believe in the equal opportunities for all humans living on this earth.

Abstract

Modern land expansion is regarded as having begun in the 1960s and since then the pattern of land cover has changed considerably in many parts of the world. The majority of change detection studies have used Landsat MSS, TM, ETM+, and LC8 imagery and other satellite imagery to quantify and map land use changes for many parts in our globe from the early 1970s until now. The timeline of the change detection analysis can be extended beyond the first Landsat satellite imagery by cross-referencing with CORONA imagery to start from the 1960s rather than 1970s. CORONA images have high spatial resolution (1.8 m); and therefore, have been used extensively for archaeological sites detection by visual interpretation around different parts of the world. They have also been used for creating land cover maps using on-screen manual digitising. In addition, these images have been used in some case studies for stereo analysis and digital elevation model creation by taking the advantage of the dual panoramic capability of those images. Since CORONA space photographs are panchromatic images (single band images), there are therefore limitations to using them in the automatic classification process due to the lack of spectral signature information from the surface elements. This has limited the use of those images in the field of remote sensing of land cover studies.

This research implements a new approach to classifying CORONA images by combining texture information with the original single band image using a change detection analysis for the Kurdistan region as a case study. The study area has an area covers approximately 45,000 km² and the study period is extended to the period 1969 to 2014 by using both Landsat data and CORONA data. The results of the maximum likelihood classification process for CORONA images showed that those images could be classified successfully and accurately. The accuracy assessment process for the CORONA image using point reference dataset showed an overall accuracy of 85 % and kappa coefficient of 0.80. In addition, using a region dataset as reference showed an overall accuracy of 84 % and kappa coefficient of 0.76. This study has demonstrated that CORONA images can be used to create a land use map automatically instead of by on-screen manual digitising. This study has also shown that the timeline of the change detection analysis can be extended by using CORONA's unique historical images to include the period before Landsat missions started in 1972. For the Kurdistan region case study, this data was necessary as many

of the changes occurred after 1974 when the Kurdish revolution collapsed. It was therefore important to acquire accurate information for the 1969 land cover map to show the status of the landscape before the changes during the period 1974 to 1991.

Land use and land cover changes in the landscape of the Kurdistan region have been enormous. These changes divided into three stages: The destruction and demolition of the landscape during 1974 to 1991. The second stage is the stage of freedom and minor changes in the landscape of Kurdistan region that began in 1992 and lasted until 2002. Finally, the last stage started from late 2003 until the present date; during this period, the Kurds were able to increase the built areas in Kurdistan region rapidly by investing most of the Kurdistan region budget which was received from central government in Baghdad. The economy growth and population increase were the main factors of the urban growth in the Kurdistan region areas. In addition, a positive non-linear relationship (R^2=0.89) was found between population increase and urban growth using the regression analysis approach for the study area period 1969 to 2014.

Acknowledgements

I would like to express my gratitude to my leading supervisor, Dr. Robert Corner from Curtin University, Department of Spatial Sciences for his supervision and valuable advice to reach the main objectives of the study. An enormous respect and thanks to Dr. Robert Corner again for his support after hearing that my brother passed away while I was in an advanced stage for completing my thesis writing. I am grateful to Professor Jason Ur from Harvard University for directing me to the CORONA Atlas for the Middle East website to obtain georeferenced CORONA images for my project. Also enormous thanks to “CORONA Atlas for the Middle East” Centre for Advanced Spatial Technologies (CAST), University of Arkansas and U.S. Geological Survey staff for allowing me to download valuable CORONA data from their websites. I am very thankful to Mrs. Lori Patterson from the Spatial Sciences administration staff for reading the thesis and offering succinct suggestion and advice to improve the readability of the thesis. I would like to thank my wife (Mrs. Dyary Ameen) for her patience and support while I was working on my research. My great gratitude to everyone wanting me to be successful in my approach. Finally, yet importantly, I would like to express my thankfulness to my God for the spiritual guidance, strength, and protection throughout my PhD research journey.

Table of contents

List of figures

List of tables

Acronyms

Acronym	Meaning
ALOS	Advanced Land Observation Satellite
ARGON	Classified military satellite systems code
ASTER	Advanced Spaceborne Thermal Emission and Reflection Radiometer
BOA	Below of Atmosphere
CAST	Centre for Advanced Spatial Technologies
CORONA	Classified military satellite mission code
DEM	Digital Elevation Model
DME	Dasymetric Mapping Extension
DNs	Digital Numbers
DOS	Dark Object Subtraction
ERDAS	Earth Resources Data Analysis System
ENVI	Environment for Visualising Images
ETM+	Enhanced Thematic Mapper+
FTT	Fast Fourier Transform
GCPs	Ground Control Points
GIFOV	Ground Instantaneous Field of View
GIS	Geographic Information System
GLCMs	Gray levels Co-occurrence matrix
IKONOS	Satellite images from Greek word "image"
IRS	Indian Remote Sensing
ISIS	Islamic State of Iraq and Syria
KAR	Kurdistan Autonomous Region
KH	Keyhole
KNA	Kurdistan National Assembly
KRG	Kurdistan Regional Government
LANYARD	Classified military satellite systems code

LDCM	Landsat Data Continuity Mission
LPS	Lecia Photogrammetric Suite
LUCC	Land use cover changes
LULC	Land use and land cover
KRG-MNR	Kurdistan Regional Government - Ministry of Natural Resources
MDC	Minimum Distance Classifier
MLC	Maximum likelihood Classifier
MNF	Minimum Noise Fraction
MSS	Multispectral Scanner
NASA	National Aeronautics and Space Administration
NITF	National Imagery Transmission Format
OLI	Operational Land Imager
RMSE	Root Mean Square Error
ROIs	Region of Interests
RPC	Rational Polynomial Coefficients
SVMC	Support Vector Machine Classifier
TIRS	Thermal Infrared Sensor
TM	Thematic Mapper
TOA	Top of Atmosphere
UGAT	Urban Growth Analysis Tool
UID	Unique Identification Number
UK	United Kingdom
US	United States
USGS	United States Geological Survey

Introduction

1.1 Background of the study

Modern land development is regarded as having begun in the 1960s, and since then the pattern of the landscape has changed significantly in many parts of the globe. A large numbers of studies have shown that there are only a few small areas on the Earth that are still unaffected by human activities (Kavzoglu 2008; Naik et al. 2008; Deng et al. 2009a). Due to human activities, the Earth's surface is being significantly transformed in different ways such as deforestation, forest degradation, urbanisation, population pressure, migration, and industrialisation (Ridd and Liu 1998). In addition, natural disasters (such as earthquakes, volcanoes, tsunamis, floods and bush fires) play their parts in making changes to the landscape pattern almost everywhere on the planet. Changes in the landscape are dynamic in nature and understanding those changes can provide a comprehensive knowledge of the interaction and relationship between anthropogenic activities and the environment (Meyer 1992). Changes in the Earth's landscape is usually described by the hybrid term, land use and land cover change.

Analysis of land use and land cover is an important factor in detecting and understanding global land status. Land use change has been a widespread focus and "hot spot" of global change research (Deng et al. 2009b). Land use/cover changes and their areal distributions are the essential and fundamental information for a widespread study in the physical and social sciences, parallel with the rapid global landscape transformation.

According to (Kavzoglu 2008), remote sensing is a key application in global-change science and land use/cover dynamics analysis; it is the most applicable data source for determining impacts on the environment and to monitor their effects. Remote sensing represents a major source of land cover data by providing spatially consistent coverage of large areas with both high spatial detail and temporal frequency (Jusoff and Senthavy 2003). From the 1960s until today, remote sensing has provided many studies with valuable information through a series of satellite imagery that started with the CORONA missions in the early 60s and has continued until today with many other generations of satellite such as the Landsat series. It provides the most reliable technique for a monitoring of different landscape structures and the net radiation and

heat fluxes associated with changed areas at the regional scale. The changes in surface biophysical parameters over the years can be examined in association with land use changes to demonstrate how these parameters respond to rapid change of surface elements (Zoran and Weber 2007).

From the beginning of the 1970s until now, the majority of land use /cover studies and change detection analysis studies use Landsat MSS, TM and ETM+ and other satellite imagery (Seto et al. 2002; Xiao et al. 2006; Porter-Bolland et al. 2007; Abdulaziz et al. 2009; Alphan et al. 2009; Deng et al. 2009b; Kesgin and Nurlu 2009; Sun et al. 2009b; Torres-Vera et al. 2009; Townshend et al. 2012; Yadav et al. 2012; Wong and Sarker 2014). The timeline of change detection analysis can be extended by cross-referencing with CORONA imagery to extend change detection analysis by starting from 1960s rather than 1970s. Because CORONA images are panchromatic image (single layer image), there are therefore limitations to their use in spectral classification processes. Despite this limitation, CORONA imagery has been used for many case studies for creating land cover and land use thematic maps. Those studies have included the identification of archaeological sites by on screen digitising (Tappan 2000; Ur 2003; Lorenz 2004; Andersen 2006; Ruelland 2011; Coskun Hepcan 2013), and visual interpretation (Challis 2002; Philip et al. 2002; Rigina 2003; Fowler 2004; Gheyle 2004; Wilkinson 2006; Beck 2007; Hritz 2013). Some case studies have been carried out using Stereo analysis and DEM generation (Goossens et al. 2006; Casana 2008; Lamsal 2011).

The landscape pattern of Kurdistan, the homeland of the Kurds, has experienced dramatic changes over the last six decades. The changes in the landscape of the area could be a result of human activities such as urbanisation and population increase. In addition, the behaviour of the Iraqi government to the Kurds and their land in the northern region of the country since 1960 may also be another factor for those changes in the landscape. The war between Iraq and Iran in 1980s could have contributed to those changes in Kurdistan region. Also the civil war between two main Kurdish parties in 1996 could be another factors of making the changes in the Kurdistan landscape. The arrival of Islamic State of Iraq and Syria (ISIS) could have impact of the changes in the study area. This research captures and quantifies changes in the landscape of the Kurdistan may be within by using a series of satellite images.

The high speed of urbanisation, industrialisation, population increase, and political turmoil in the Middle East region make environmental management a very important aspect for the Kurdistan region government. Land use patterns change over time in response to economic, social, and environmental forces (Ridd and Liu 1998) and understanding the nature of change in the use of land resources is essential for the proper planning, management, and regulation of those resources.

Because of the lack of land cover information for the study area for the early 1960s and a lack of socio-economic data due to political turmoil, CORONA imagery can play a significant role in detecting and mapping the status of land cover for the Kurdistan region for the period 1960-1972. Using high-resolution CORONA space imagery and multispectral Landsat satellite data is a powerful approach to form collective summary of maps of human activities for the period 1960 to 2014. In addition, it can provide a baseline for spatially distributed studies of urban area expansion. However, since Kurdistan is predominantly mountainous, difficulties connected with shadows may downgrade observations and interpretations of remotely sensed data.

1.2 Objectives and thesis outline

The main objective of this research is to investigate and develop new input data for supervised image classification methods from panchromatic (single layer) CORONA images using a combination of original Gray-levels (brightness) and textural information. The newly developed classification approach will then take advantage of the continuing between the CORONA and Landsat satellite series to detect and map the land use/ land cover (LULC) categories for the entire Kurdistan Region for the period 1969-2014. Change detection analysis will be performed for land use or cover changes over this period. This research will also investigate and highlight the connection between the Land use/Land cover changed areas and population pressures for the Kurdistan region using GIS techniques. The research objectives can be summarised as:

- Investigate and develop new semi-automatic classification technique for CORONA panchromatic images.
- Map LULC for entire Kurdistan Region (45,000 km²) for the period 1969 to 2014.

- Implement remote sensing and GIS technologies to explore and analyse the LULC changes in Kurdistan and its connection with population pressures.

In order to achieve the objectives of this research the following additional questions will be investigated and tested:

1. Can land use and land cover categories be detected and mapped using combined texture and brightness information from the CORONA panchromatic images?
2. Can these panchromatic images be classified to LULC maps with the same level of accuracy as multispectral Landsat images?
3. Is there any connection between LULC changes and population pressures in Kurdistan Region for the period 1969-2014?

1.3 Chapter summary

This chapter has outlined the background of the study and stated the objectives of the study. It also outlined further additional questions, directly related to the main objectives, to be answered during the progress of this research. The chapter discussed the timeline of modern development started; and the importance of remote sensing data for detecting and mapping local and global changes, which have occurred because of both human activities and the forces of Mother Nature. The chapter defined the factors which may be behind the changes in the landscape for many parts of the globe including Iraqi Kurdistan. It has pointed out the limitations of the previous study in using only Landsat data for their research and how the timeline can be extended by using the CORONA imagery. The chapter also highlighted the limitations of CORONA single band image. Finally, this chapter also included the importance of using CORONA data for this study, as there is a lack of information because of political turmoil for the region.

2 CORONA and Landsat satellite imagery

2.1 CORONA mission imagery

2.1.1 Background

The United States space programme included not only the open scientific program, but also classified satellites which were operated by the Air Force and the Central Intelligence Agencies. These induced the top-secret CORONA program (MacDonald 1995). CORONA operated from August 1960 to May 1972 and acquired photographic images covering nearly two billion square kilometres over a 12-year period (Leachtenauer 1997). The last flight of the secret CORONA missions took place on 24 May 1972 (Kostka 2002), but the images were not released and offered for public use until February 1995 (MacDonald 1995). This declassification of major U.S. satellite reconnaissance programs offered a significant source of imagery to the civil community such as environmental researchers, archaeologists, historians, and other users, with over 800,000 images having been taken from space for many parts of the Earth (Leachtenauer 1997).

Many researchers have reported that those images could significantly contribute the analysis of environmental processes and to understanding the main factors that affect the environment. In particular, the CORONA imagery could help to establish new ground reference data, especially for inaccessible regions around the world. Since that time, CORONA imagery has been used in change detection analyses as ground reference historical data in combination with late high resolution satellite data from IRS 1C and Landsat data (Rigina 2003). CORONA photographs make it possible to study and map land resources from the very beginning of the Space Age (Tappan 2000).

A rich database archive of CORONA images was completed after a large number of the CORONA images were released in three editions in 1996, 2002, and 2013. Those images are available for civilian access through the Internet and can be easy accessed through a user-friendly catalogue published on the website of the United States Geological Survey (http://edcsns17.cr.usgs.gov/ Earth Explorer) with low price (Kennedy 1998). Since September 2004, the imagery is no longer available as film

negatives, but only as digital images, which are very useful format for GIS and RS research.

2.1.2 Characteristics of CORONA images

The main advantages of CORONA images are their spatial coverage, spatial resolution (ranging between 6-40 Feet) as shown in Table 2.1, cost effectiveness and their easy availability. By cross-referencing with Landsat images, those images can extend the temporal coverage of the remotely sensed dataset for environmental monitoring studies back to early the 1960s. The proposed study is an example of such a case study. The only available images that cover the early sixties are CORONA images with a spatial resolution of 1.8 m, low cost and easy accessibility (Kennedy 1998).

Table 2.1: CORONA system types, characteristics, and operational time period.

Mission	System	Camera Type	Operation Periods	Resolution/ Feet	Resolution/ Metre	Ground Coverage (km)
CORONA	KH-1	single Panoramic	Aug 1960	40	12.20	15 x 210 to 42 x 580
CORONA	KH-2	single Panoramic	Dec 1960 to July 1961	30	9.15	15 x 210 to 42 x 580
CORONA	KH-3	single Panoramic	Aug 1961 to Dec 1961	25	7.63	15 x 210 to 42 x 580
CORONA	KH-4	two Panoramic	Feb1962 to Dec 1963	25	7.63	15 x 210 to 42 x 580
CORONA	KH-4A	two Panoramic	Aug 1963 to Sep 1969	9	2.75	17 x 232
CORONA	KH-4B	two Panoramic	Sep 1963 to May 1972	6	1.83	14 x 188
ARGON	KH-5	Frame	May 1962 to Aug 1964	460	140.30	483 x 483
LANYARD	KH-6	single Panoramic	July 1963 to Aug1963	6	1.83	12 x 64

CORONA imagery also has Stereo capabilities as shown in Table 2.1. Systems KH-4, KH-4A, and KH-4B were equipped with forward and backward looking cameras. They produce their images in stereo form with the best resolution being 6 feet (1.8 m) for the KH-4B system. Stereoscopic viewing is very important for visual interpretation. The two stereo-images of the same surface are always different in contrast, because they were taken from a different point of view, and sun angle. Shadows and other features are also different. CORONA stereoscopic images can be used for DEM generation and 3D analysis.

2.1.3 Applications of CORONA imagery

Despite the limitation of CORONA panchromatic images in terms of spectral signature, these valuable and unique space photographs have been used in many application and case studies in different parts of the world since 1996. Some applications in archaeology, environmental studies, and terrain analysis are discussed below:

2.1.3.1 Archaeology

Many archaeological sites have been damaged or demolished since modern land development started in the 1960s and land has been changed to agricultural and urban uses. These images can play a very significant role in identifying lost archaeological sites around ancient places in Middle Eastern countries. There is a lack of aerial photo for those historical sites due to security restrictions by most Middle Eastern countries (Kennedy 1998). CORONA images have been used in different parts of the world to identify archaeological sites by visual interpretation of the images.

An archaeological application from the Middle East (Syria) was a case study conducted by Philip (2002). During this study, CORONA imagery was used to identify an archaeological site by visual interpretation.

Challis (2002) explores the potential of CORONA imagery to identify the archaeological site of the Islamic city of al-Raqqa, Syria. Geo-referenced CORONA imagery were exported to Arc-View 3.2 GIS and the landscape features were identified and digitised on the screen, the final land cover maps were obtained as a vector dataset.

A Northern Mesopotamian (north-eastern Syria) case study was carried out by Ur (2003) to detect the ancient road network using the CORONA satellite photographs. The network and other archaeological and modern feature were identified and traced and a vector layer was created by using editing tools in ArcGIS 8.2. The final map was created based on the extracted features from the CORONA imagery.

An evaluation of CORONA and IKONOS high resolution satellite imagery for archaeological prospection in Western Syria was conducted by Beck et al. (2007). During this case study, they used visual comparison of both images to identify archaeological sites in basaltic and marl landscape. They concluded that without

CORONA and IKONOS imagery the level of understanding of those sites would be significantly reduced.

Stereo analysis, DEM extraction and ortho-rectification of CORONA satellite imagery for archaeological applications were investigated by Casana and Cothren (2008). This study presented a simple method of creating three dimensional analyses for CORONA imagery. A 10 m DEM and ortho-rectified images were created to identify archaeological sites in Syria by visual interpretation.

Hritz (2013) conducted a study of a malaria-ridden swamp in the southern Balikh valley, Syria using Google Earth Pro and CORONA. In this approach, all images were geo referenced and integrated into GIS and all archaeological sites (280 sites) were identified on each image and digitised to create a final vector dataset for each image.

The detection of remains from ancient Rome's desert frontier in Jordan was investigated by Fowler (2004). During this investigation, declassified CORONA KH-4B satellite photographs were used to identify (on the screen) the sites of Qasr Bshir, Qasr Abu el-Kharaq, and Umm er-Resas. The outcomes of this research indicated that this imagery is capable of providing the required spatial resolution to identify these remains.

Bitelli and Girelli (2009) conducted a study of the use of CORONA satellite imagery for an area of archaeological interest in Turkey. The study area was the Tilmen Hoyuk archaeological site located in the city of Gaziantep in the south-east of Turkey. They were able to create a CORONA ortho-image by using well distributed and reliable ground control points. CORONA imagery was used with aerial and satellite imagery (high and medium resolution) to perform visual change analysis for the site to cover the dates 1968, 1984, 1989, 2000, 2003 and 2006.

A case study in the Altai republic (South Siberia) was conducted by Gheyle et al. (2004) for evaluating the use of CORONA imagery to identify archaeological sites. A morphographic map was created using the conventional photogrammetric method with a Wild stereoscope. In the resulting stereo-model, they were able to identify different type of slope, mountain range and plateau. A final topographic map was obtained including the archaeological sites. The summary of this study concluded that CORONA has provided the valuable capability of generating topographic and digital terrain maps.

Goossens et al. (2006) investigated the advantage of using the dual panoramic capability of the CORONA imagery on a further case study in the Altai Mountains. During this study, they suggested that, creating ortho images and using them for digitising or interpretation or even creating a Digital Surface Model is more realistic than using only one of the two images from the same spot captured by CORONA missions.

Wilkinson et al. (2006) conducted a study in central Syria by using CORONA to identify non-tell archaeological sites (the remains of archaeological sites). The study used CORONA imagery to identify four sites on the screen visually. And later a profile or transect were created on those site and surface soil samples were collected with interval 10 to 30 m and later tested in the laboratory. The result showed from those samples contained brick material (which was used to build those sites) and they concluded that those sites are non-tell archaeological sites and CORONA imagery proved to be the major source to identifying those sites.

2.1.3.2 Environmental and land use studies

CORONA images have been used for many other applications for different parts around the world to extend the historic map of LULC change maps by manual digitising. The sections below show some of those applications which were carried out by different researchers using different methods for creating a final LULC map.

Tappan et al. (2000) conducted a case study assessing 30 years of land resource changes in west-central Senegal. The study concluded that photographic visual interpretation method would provide a better result than performing a digital image classification due to the spectral signature limitation. Land cover features were delineated from CORONA and then digitised and a vector data layer was obtained.

A case study was conducted by (Sohn et al. 2002) for monitoring the urban growth and water areas for the Han river, Seoul. This study used CORONA KH-4B imagery to create a DEM and ortho-image and then extract the urban and water areas by a manual digitising process on the screen.

The integration of CORONA KH-4A and Landsat 5 TM datasets to create bedrock geological maps in the Russian high arctic (The Severnaya Zemlya Archipelago) was carried out by Lorenz (2004). The panchromatic single layer of CORONA was used to enhance the image spatial resolution of a composite image created from Landsat

TM7, TM4, and TM3. The new dataset provided the basis for visual interpretation to create the final geological map for this area. Lithological contacts were traced from the multilayer image using GIS to create a final vector dataset.

Detection of trees in the eastern desert of Egypt using CORONA images was studied by (Andersen 2006). He adopted visual image interpretation since human vision is well adapted to pattern recognition. Each tree was digitised manually and the final vector layer was created using ArcGIS. The vector dataset of CORONA image was compared with individual trees collected during field data collection in (2003). This study indicated that more than 95% of the population of the tree mapped in 2003 was already present in 1965 CORONA images. The percentage of recognised trees (spatial accuracy) ranged from 45 to 91% for the 20 different sites of the study area. This study concluded that CORONA imagery offered a spatial and temporal dimension for this study which other data sources could not provide same information at comparable cost, coverage, and accessibility.

Patterns and dynamics of land-cover changes since the 1960s over three experimental areas in Mali were investigated by Ruelland et al. (2010). CORONA, Landsat and SPOT satellite images were used during this work. Significant land cover changes since the 1960s were identified by visual interpretation of all images and later all images were classified manually using GIS based on a grid based visual interpretation method by assigning one of the land cover classes to each 60 m square grid cells. They concluded from the multi-source time series image analysis that a grid based method is more reliable than either automatic pixel based or object oriented classification methods.

Ruelland et al. (2011) compared different methods of LUCC for the Kouonbaka catchment in the Sahel by using aerial imagery and CORONA, Landsat and SPOT satellite images. Three classification methods were tested (pixel based classification, vector grid based on screen interpretation, and object oriented classification). The final result for this analysis again confirmed that on-screen interpretation is the most suitable approach for multi-source images including CORONA satellite imagery.

Brinkmann et al. (2012) conducted an analysis of landscape transformation processes in four West African cities over the last 50 years. A common automatic classification scheme was used for Landsat imagery to obtain final LULC maps. For CORONA

imagery visual interpretation was used and they combined visual interpretation with a preliminary object based image segmentation technique using GIS.

Coskun Hepcan (2013) carried out a case study on the quantification of landscape pattern and connectivity in a Mediterranean coastal settlement. Working in the Urla district of Turkey, the main aim of this study was to analyse and interpret landscape changes for the study area by using CORONA and ASTER satellite imagery from 1963 and 2005 respectively. The land use map was derived from CORONA image using ArcGIS 9.2 and an on-screen digitising process, whilst for the ASTER image supervised classification was used to obtain a final land use map.

2.1.3.3 Terrain analysis

In addition to the different fields that CORONA images were used, also those images have been used to create DEM by taking the advantages of the dual panoramic capability of those unique images. The section below show some case studies that have been conducted by some researchers for a different part of the Globe.

Sohn et al. (2004) carried out mathematical modelling on CORONA KH-4B imagery by using different methods (traditional photogrammetric methods and mathematical modelling for geometric correction and creation of a DEM from CORONA imagery) by taking advantage of the system's dual panoramic camera capability for those historical datasets using the OrthoBASE module of ERDAS IMAGINE software. The study concluded that data from the CORONA imagery can be used in change detection applications, creating thematic maps and land use classification maps after performing mathematical processing to remove distortion.

Galiatsatos et al. (2008) carried out a case study of high resolution elevation data derived from CORONA stereoscopic images for the Orontes Valley west of Homs, Syria. A high-resolution elevation dataset was created from the stereoscopic CORONA imagery by using horizontal ground control points derived from the IKONOS imagery and vertical control points obtained from map-based contour lines. The DEM dataset was created without any field measurement as the accurate horizontal ground control and vertical ground control were derived from IKONOS image and map-based contour lines, respectively.

Digital terrain modelling using CORONA and ALOS PRISM data to investigate the remote part of the Imja Glacier, Khumbu Himal, Nepal was carried out by (Lamsal 2011). This study used CORONA KH-4A and Advanced Land Observation Satellite (ALOS) PRISM images to generate digital terrain models of part of the Glacier. Topographic maps and contour lines at 1m intervals were generated using the Lecia Photogrammetric Suite (LPS) in ERDAS software. They concluded that CORONA imagery can be used for the investigation of the surface changes of glaciers by taking the advantages of the dual panchromatic images.

2.1.3.4 Potential use of CORONA images

Based on the case studies above these images have been used extensively for creating land cover and land use thematic maps using on-screen digitising (Tappan 2000; Ur 2003; Lorenz 2004; Andersen 2006; Ruelland 2011; Coskun Hepcan 2013), and visual interpretation (Challis 2002; Philip 2002; Rigina 2003; Fowler 2004; Gheyle 2004; Wilkinson 2006; Beck 2007; Bitelli and Girelli 2009; Hritz 2013). Some case studies have carried out Stereo analysis and DEM creation (Goossens et al. 2006; Casana 2008; Lamsal 2011). Based on the literature reviewed, not a single study has been recorded or even demonstrated of using CORONA images for texture calculation. The main objective of this study is to use texture information with an original grey level of CORONA to investigate and develop a new approach of using these images for semi-automatic classification. Combining the single grayscale image and the result of texture calculation in multiband images, it is possible to create an input of CORONA images to be used in auto image classification process to create a final LULC map for 1969 for Iraqi Kurdistan.

2.2 Landsat satellite imagery

2.2.1 Background

The idea of a remote sensing satellite program (Landsat) to collect facts and information about the natural resources of the planet was first suggested in 1965 by William Pecora. It took several years to make this happen due to budgetary constraints and sensor disagreements between the Department of Agriculture, Department of Interior, and NASA which led to a delay in the satellite construction process. Another reason for delaying this program was that the

Department of Defence feared that a civilian program such as Landsat would compromise the secrecy of their reconnaissance missions (Rocchio et al. 2005). In 1970, NASA received approval to build a satellite, and after only two years, Landsat 1 was launched successfully on 23 July 1972, to start a new age of remote sensing of land from space with almost total coverage of global landmass.

Table 2.2 illustrates the performance of the Landsat series of satellites from the early seventies until today.

Table 2.2: Landsat satellites series operational time.

Satellite	Start of operation	End of performance
Landsat1	July 23, 1972	January 6, 1978
Landsat2	January 22, 1975	February 25, 1982
Landsat3	March 5, 1978	March 31, 1983
Landsat4	July 16, 1982	June 15, 2001
Landsat5	March 1, 1984	June 5, 2013
Landsat6	October, 1993	Destroyed during the launch
Landsat7	May, 1999	SLC Malfunctioning since 31/05/2003
Landsat8	February 11, 2013	Operational

2.2.2 Characteristics of Landsat series

The characteristics of a satellite in terms of spatial and spectral resolution are the most important elements while choosing the type of remote sensing platform. The Landsat satellites series have carried three instruments during their life; the Multispectral Scanner (MSS), the Thematic Mapper (TM) and the Enhanced Thematic Mapper+ (ETM+). Landsat satellite 1 carried only the Multi-Spectral Scanner (MSS), but has been out of service since 1978. This satellite is a great source of historical imagery, because it goes back to the early seventies (Jia and Richards 1999). The MSS Landsat satellite images are currently available as resampled data with a pixel size 60 m from USGS, but the original spatial resolution for the MSS is 79 m GIFOV (Ground Projected Instantaneous Field of View). In simple terms the GIFOV is the size on the ground of each image pixel, this is one of other factors which govern the size of the smallest feature that can be distinguished by the sensor. It is the main component of Spatial Resolution. Landsat 1 had four spectral bands which means it can be regarded as a low spectral resolution satellite Table 2.3.

Table 2.3: Landsat Multi-Spectral Scanner (MSS) characteristics.

Landsat MSS 1, 2, 3 Spectral Bands	Landsat MSS 4, 5 Spectral Bands	Wavelength	Pixel size	Useful for mapping
Band 4 Green	Band 1 Green	0.5-0.6	60 m	Delineates areas of shallow water, Sediment-laden water.
Band 5 Red	Band 2 Red	0.6-0.7	60 m	Cultural feature.
Band 6 Near Infrared	Band 3 Near Infrared	0.7-0.8	60 m	Vegetation boundary between land and water, and landforms.
Band 7 Near Infrared	Band 4 Near Infrared	0.8-1.1	60 m	Penetrates atmospheric haze best, emphasises vegetation, boundary between land and water, and landforms.

The Landsat Thematic Mapper was carried on Landsat's 2-5, and the Enhanced Thematic Mapper plus (ETM+) was carried on Landsat 7, and it is similar to the TM but has eight spectral bands and a higher spatial resolution (Jia and Richards 1999). The characteristics of both TM and ETM+ in terms of spatial and spectral resolution can be seen in the Table 2.4.

Table 2.4: Landsat TM and ETM+ characteristics.

Band	Spectral Bands	Wavelength	Pixel size	Useful for mapping
B1	Blue	0.45-0.52	30 m	Bathymetric mapping distinguishing soil from vegetation and deciduous from coniferous vegetation.
B2	Green	0.52-0.60	30 m	Emphasises peak vegetation, which is useful for assessing plant vigour.
B3	Red	0.63-0.69	30 m	Discrimination vegetation slopes.
B4	Near infrared	0.77-0.90	30 m	Emphasises biomass content and shorelines.
B5	Short wave infrared 1	1.55-1.75	30 m	Discriminates moisture content of soil and vegetation; penetrates thin clouds.
B6	Thermal infrared	10.40-12.50	120 m TM, and 60 m ETM+	Thermal mapping and estimated soil moisture.
B7	Short wave infrared 2	2.09-2.35	30 m	Hydrothermally altered rocks associated with mineral deposits.
B8	Panchromatic (Landsat 7 only)	0.52-0.90	15 m	15 metre resolution, sharper image definition.

The Landsat Data Continuity Mission (LDCM) was launched on 11 February 2013 by NASA and USGS. This satellite officially began normal operations on May 30, 2013, when the responsibility for satellite operations transferred from NASA to the USGS, at which stage it was named Landsat 8. The USGS now manages the satellite flight operations team within the Mission Operations Centre, which remains located at NASA's Goddard Space Flight Centre in Greenbelt, Md. (NASA 2016). The altitude of this satellite is 438 miles (705 kilometres) and it carries two sensors on-board, the

Operational Land Imager (OLI) and the Thermal Infrared Sensor (TIRS). The characteristics of this latest satellite in this series are summarised in Table 2.5.

Table 2.5: Landsat 8 (Landsat Data Continuity Mission) characteristics.

Bands	Spectral Bands	Wavelength	Pixel size	Useful for mapping
B1	Coastal Aerosol	0.43-0.45	30 m	Coastal and aerosol studies.
B2	Blue	0.45-0.51	30 m	Bathymetric mapping distinguishing soil from vegetation and deciduous from coniferous vegetation.
B3	Green	0.53-0.59	30 m	Emphasises peak vegetation, which is useful for assessing plant vigour.
B4	Red	0.64-0.67	30 m	Discrimination vegetation slopes.
B5	Near infrared	0.85-0.88	30 m	Emphasises biomass content and shorelines.
B6	Short wave infrared 1	1.57-1.65	30 m	Discriminates moisture content of soil and vegetation; penetrates thin clouds.
B7	Short wave infrared 2	2.11-2.29	30 m	Improved moisture content of soil and vegetation and thin cloud penetration.
B8	Panchromatic	0.50-0.68	15 m	15 metre resolution, sharper image definition.
B9	Cirrus	1.36-1.38	30 m	Improved detection of cirrus cloud contamination.
B10	TIRS 1	10.60-11.19	100 m	100 metres resolution, Thermal mapping and estimated soil moisture.
B11	TIRS 2	11.5-12.51	100 m	100 metres resolution, improved thermal mapping and estimated soil moisture.

2.2.3 Application of Landsat imagery

Landsat imagery provides valuable data for many researchers around the globe. The Landsat images have the potential to significantly improve the characterization of landscape element. In many studies, it has been shown that Landsat imagery is a powerful tool for providing accurate and timely geospatial information regarding changes in the Earth's landscape.

Since 2008 this imagery has been readily accessible at no cost. This makes it a very important instrument collecting information regarding the status of the landscape when there is no other accurate way of mapping and detecting change due to cost, time and access constraints.

Remotely sensed Landsat images data are not just a simple photograph taken from space, but containing many layers of data collected throughout the visible and invisible light spectrum. The Landsat system collects multi-spectral, multi-resolution, and multi-temporal images that are vital information for understanding and monitoring human activities on the planet over time. Also, those remotely sensed datasets can be used to measure changes in the landscape pattern as well as changes in the condition over time. Since changes in the landscape are dynamic, Landsat imagery

can be used to study and capture at large scale extent. Without Landsat data, the task of capturing and mapping the changes in the landscape would be much more difficult.

Landsat imagery has been used in many land use and land cover change studies because of its long-term digital archive with medium spatial resolution and relatively consistent spectral and radiometric resolution (Jensen et al. 1995). Over the past 44 years there have been countless case studies. Landsat imagery has been used for agriculture forecasting, and agriculture management purposes (production and conservation) (Kauth and Thomas 1976; Richardson and Wiegand 1977; Kauth et al. 1979; Stow et al. 1980; Lenney et al. 1996; Peterson and Aunap 1998; González-Sanpedro et al. 2008).

These images have also been used for environmental sciences and management including biodiversity conservation (Sesnie et al. 2008), climate change (Masek 2001), coastal science (Zainal et al. 1993), ecosystem science (Cohen and Goward 2004), geology (Francis and Rothery 1987; Arnell 1999), forest science (Royle and Lathrop 1997; Cohen et al. 1998; Cohen et al. 2002; Masek et al. 2008) and water resources (Jackson et al. 1977; Carpenter and Carpenter 1983; Anderson et al. 2012). Planning and development studies applications include rural planning, urban planning and urbanisation (Carlson and Arthur 2000; Masek et al. 2000; Weber and Puissant 2003; Yang et al. 2003; Xian and Crane 2005; Pham et al. 2011). The oil, gas and mineral extraction sectors (Halbouty 1976, 1980; Philp and Crisp 1982; Brame 1989) also use Landsat images in applications which include the extraction and exploration of minerals and creating final thematic maps for those areas to quantifying those resources for the better management and usages.

In spite of the vast numbers of applications that have used Landsat data for final products (thematic maps) for many purposes, there are some limitations of those products which may reduce the final outcomes for instance these images are coming from a range of different sensors (e.g. MSS, TM, ETM+, and OLI). Also there are some other issues with Landsat data which are related to atmosphere effects, noise, cloud and shadows. Also when performing some image processing the product may not always be ready for feature extraction and final analysis (e.g. if the results of the atmospheric correction are not within expected reflectance values between 0 and 1, therefore more pre-processing is required to normalise the data to be with required range of reflectance.

To be able use Landsat products with high level of accuracy, some serious of image pre-processing techniques are required to make sure the input data is suitable for further processing and obtain final outcomes. In Chapter 4, which deals with data preparation all those issues are highlighted and has been fixed as needed and required.

2.3 Chapter summary

This chapter has covered the background to the CORONA and Landsat satellite platforms. It has discussed the characteristics of each platform and applications that involved the use of those images for different parts of the world. This chapter also highlighted the potential of using the CORONA data with cross-referencing to Landsat data to extend the timeline of land use and land cover changes. For CORONA images, a limitation of use has been discussed as well as the possible solution which takes advantage of the high spatial information in the original CORONA images (Gray level) by combining with the calculation of the texture descriptive measurements layers.

3 Study area and data description

3.1 Study area and geographical location

Iraqi Kurdistan is located in the north of Iraq. It shares borders with Syria in the west, Turkey in the north, Iran in the east, and the middle Governorates of Federal Iraq in the south. South Kurdistan consists of the governorates of Duhok, Erbil, Sulamani, Kirkuk, with parts of Diyala and Nineveh and has a total area of 80,000 km². Three Governorates (Duhok, Erbil, and Sulamani) constitute the Kurdistan Regional Government (KRG 2013) in the northern region of Iraq as approved by the Iraqi Federal Government in 2005. The geographical setting for the region (Figure 3.1) is between latitudes 34° 42' N and 37° 22' N and between longitudes 42° 25' and 46° 15' east (KRG 2013) . This forms the study area for this research with a total area of 44957.06 km² which is shown in (Figure 3.2).

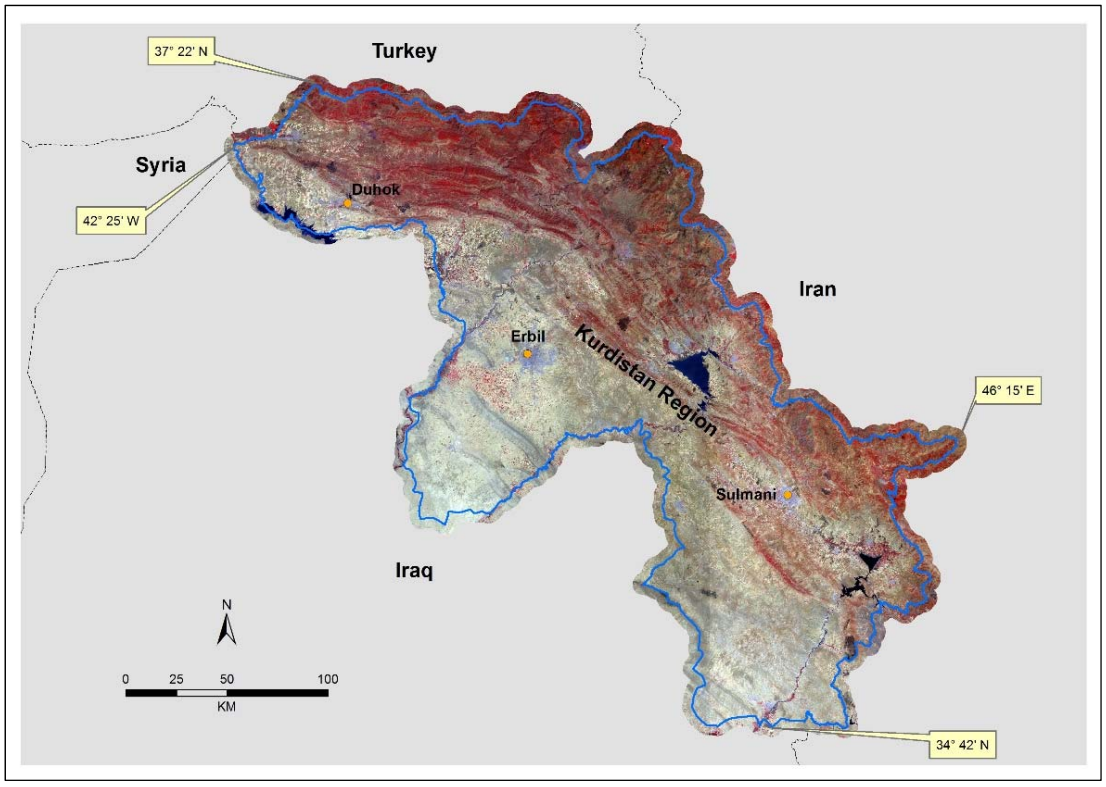

Figure 3.1: Map of the geographical setting of the study area.

Base map Sentinel-2 2016 from: United State Geological Survey (USGS).

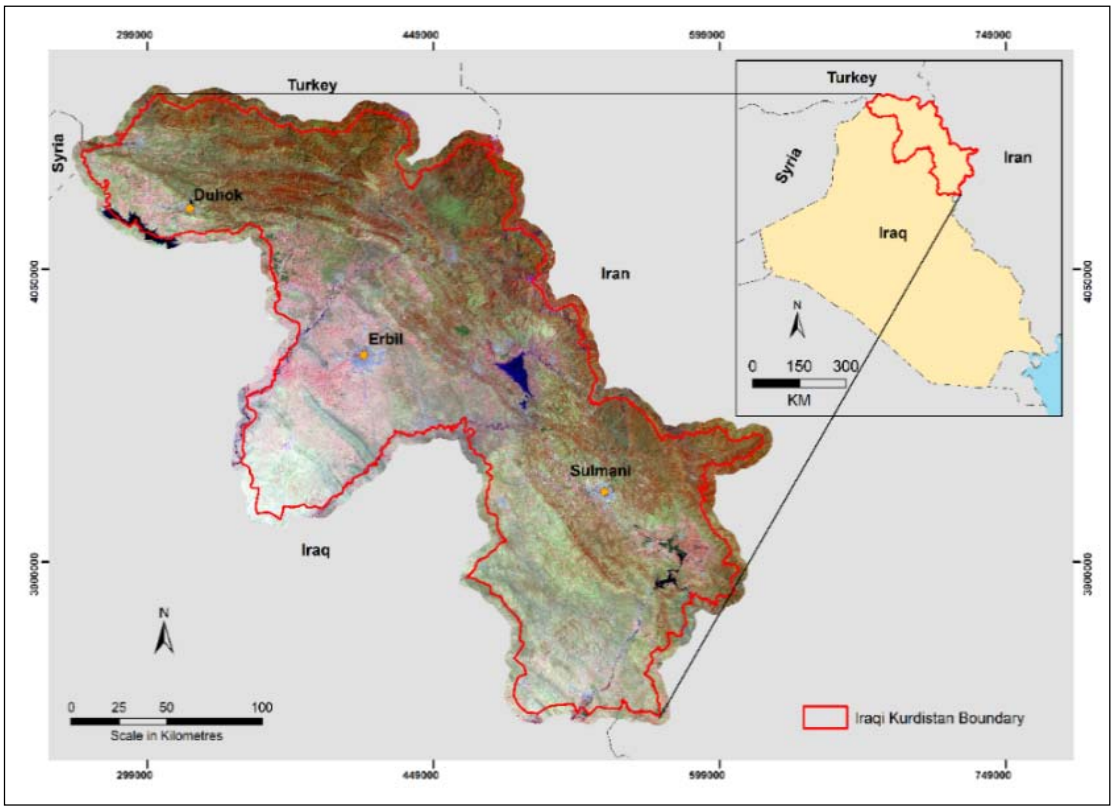

Figure 3.2: Map of study area Landsat 8 (2014) base map.

Base map Landsat 8 2014 from: United State Geological Survey (USGS).

3.1.1 Description of the study area

3.1.1.1 Historical context

Although it was once the homeland of the world's oldest civilised settlements in agriculture and livestock breeding, Kurdistan (Figure 3.3) disappeared from the world map after World War I. When the Allied Powers divided the Middle East, they denied the Kurds their dream of a Kurdish homeland as an independent nation. The Kurds were left without a country and the nation was divided between Iran, Iraq, Turkey and Syria as a penalty for the Kurds contribution against the United Kingdom and France in World War I. Throughout the 20th century the Kurdish people have struggled to regain their political and cultural autonomy which has always been rejected by the region's countries (KRG 2013). The Kurdish population today is estimated to be 35-40 million with the majority living in Turkey, Iran, and Iraq. There are also Kurds in Syria, Armenia and Azerbaijan (KRG 2013).

Figure 3.3: Historical map of Greater Kurdistan.

From: http://www.jawadmella.net/id18.html/ London, England 2005-2009.

Kurdistan had been divided and re-divided many times before the First World War. The Kurds have frequently been victims of politics and have been promised the possibility of an independent state on many occasions (McDowall 1992). They have also been victims of the Great Power politics of the UK and Russia. All major Kurdish resistance in terms of cultural and political activities has been continually crushed and criminalised by Turkey, Iraq and Iran (Olson 1992). On 11 September 1961, after another refusal by the Iraqi Government of a request for Kurdish autonomy, Mulla Mustafa Barzani (the leader of The Kurdistan Democratic Party) began the Kurdish revolution which was to last for almost ten years.

By 11 March 1970 the Kurds were able to establish an agreement with the Iraqi government for autonomous Kurdistan political representation in Baghdad. The ending of this agreement in 1974 caused an armed clash between both sides because a key part of the agreement, the inclusion of Kirkuk was not achieved. In 1975, the Iraqi government signed the “Algeria Agreement” with Iran, in which Iraq ceded the Shatt al-Arab to Iran in exchange for Iran ending its support of the Kurdistan Democratic Party and other Kurdish parties. As a result of this agreement Kurdish rights in the

Iraqi Kurdistan were nullified (KNA 2013). The withdrawal of Iranian support for the Kurdish forces (Peshmerga) in Iraq led to their effective collapse. Even more damaging to the Kurds was the destruction by the Iraqi regime of some 800 Kurdish villages along Iraq's borders with Iran and Turkey in order to make a so called 'security belt' between these three countries. As a result of the creation of this 'security belt' many villages were abandoned and agricultural production in those areas was either reduced or ended. From 1974 through to 1989, it is probable that nearly 500,000 Kurds were 'resettled' to the southern part of Iraq (KNA 2013). It is hoped that the resulting land use changes can be detected and mapped using CORONA and Landsat satellite imagery.

During the war between Iraq and Iran in the 1980s the Iraqi regime increased their military operations against the Kurds in the “Anfal campaign” with more than 180,000 Kurdish civilians being executed or disappearing. Anfal campaign” was series of systematic attacks carried out by former Iraqi Baathist regime from 1986 to 1989 against Kurds using special army forces in the north region of the country. Among those who disappeared were 8000 members of the Barzani tribe. Chemical weapons were used extensively during that campaign in the city of Halabja and the operations resulted in more than 5000 people being killed and more than 4000 villages destroyed. The rural economy for the entire Kurdistan Region in terms of agriculture, forest areas and infrastructure was demolished. Iraqi Kurdistan finally became a completely autonomous region after the Gulf war of 1991 (O’Leary 2002). The Iraqi Kurdistan consisting of the governorates of Duhok, Erbil, Sulamani, Kirkuk, with parts of the governorates of Diyala and Nineveh covers an area of 80,000 km². Since 1991, the Kurds have begun rebuilding their homeland and hold parliamentary and presidential elections for the Kurdistan Regional Government which was established in 1992 (KRG 2013).

3.1.1.2 Geology

The collision between the Arabian and Iranian plates divides Iraq tectonically into the Western desert, the Mesopotamian (Unfolded Zone), Low Folded, High Folded, Imbricated and Thrust Zones from southwest toward northwest (Buday 1980). The Kurdistan region is regarded as a part of an Alpine mountain girdle (Abdula et al. 2015). This girdle has a trend from east to west in the north of the Kurdistan region

and north-west to south-east direction in the north-east of Iraqi Kurdistan (Ameen 1992). The two main zones, the thrust and high folded zones (Figure 3.4) are surrounded by the Taurus-Zagros belt in Iraqi Kurdistan (Ameen 1992). The thrust zone is located outside the South Kurdistan boundary, from the north between the Kurdistan region and North Kurdistan (Turkey), and from the northeast with East Kurdistan (Iran).

The second zone (folded) can be divided into two zones based on the spread of folding, the imbricated folds zone which is extremely distorted and the simple folded zone. The simple folded zone is also divided into two subzones: the mountainous or high folded zone and the foothills zone. For Iraqi Kurdistan, the region is divided generally to the Low folded (Foothill), high folded, imbricated and Thrust (Zagros) zones (Figure 3.4).

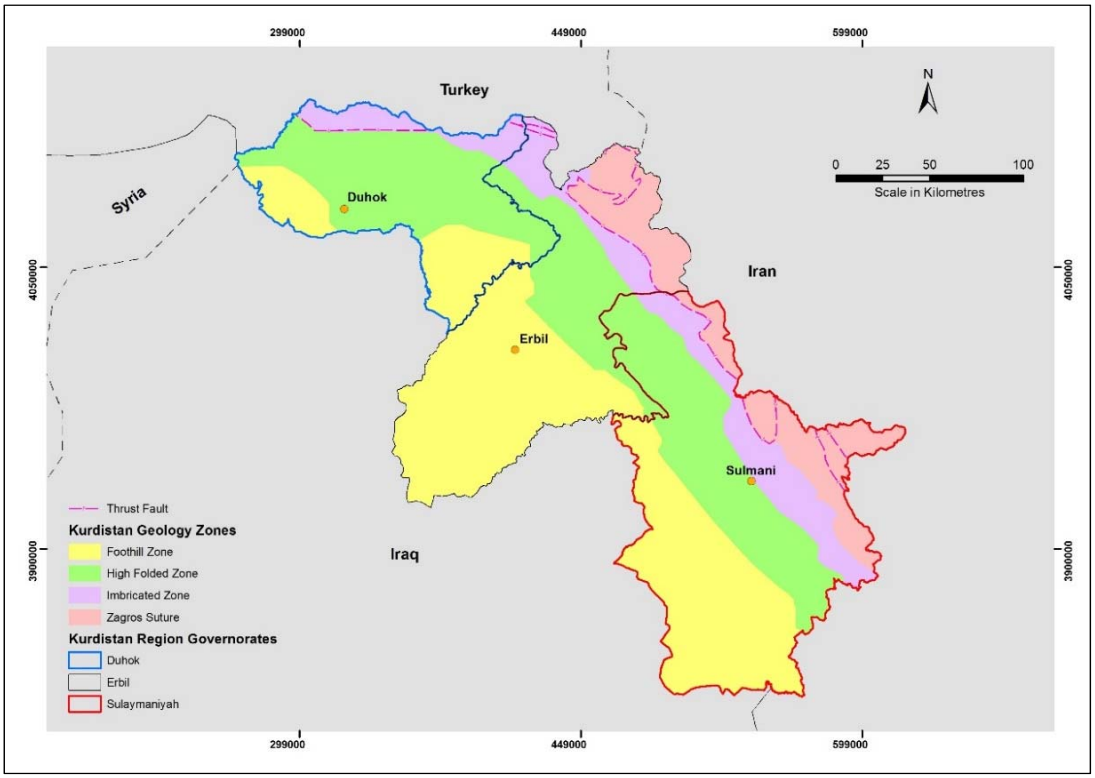

Figure 3.4: Geological map of Kurdistan region.

3.1.1.3 Topography

Most of Iraqi Kurdistan is mountainous, with the highest peak, Halgurd, being near the border with Iran and reaching 3,660 m above sea level. The mountains in Iraqi

Kurdistan are part of the larger Zagros mountain range which continues into Iran. The lowest point in the Kurdistan region is Kifri sub-district, which has an elevation of 72 m above sea level (Figure 3.5). The Kurdistan region mainly extends across the Zagros Mountain up to the Taurus Mountains in Turkey (Abdula et al. 2015).

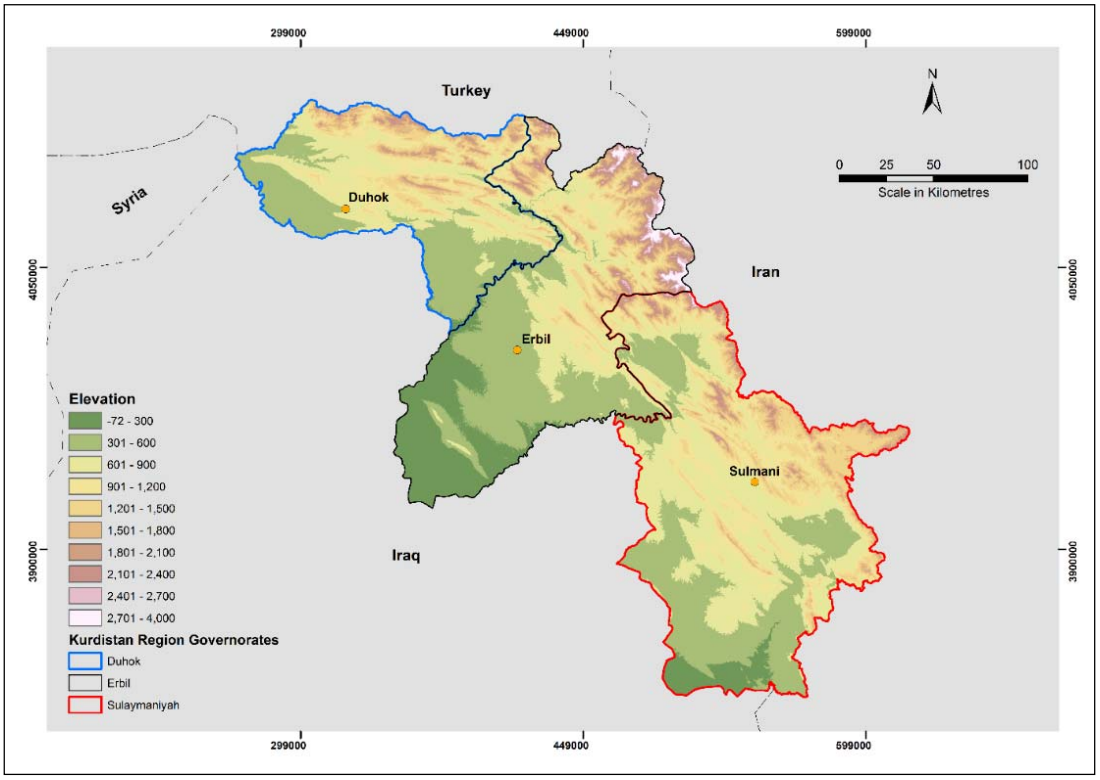

Figure 3.5: Topographical (Elevation) map of Kurdistan region.

3.1.1.4 Climate

Based on the Koppen Climate Classification System, the climate of Kurdistan can be divided into three zones as shown in Figure 3.6. The Koppen system recognises five major climatic types; each type is designated by a capital letter (Peel et al. 2007) as shown in Table 3.1.

Table 3.1: Koppen climate classification system.

Symbol	Meaning
A	Tropical Moist Climates: all months have average temperatures above 18 degrees Celsius.
B	Dry Climates: with deficient precipitation during most of the year.
C	Moist Mid-Latitude Climates with Mild Winters.
D	Moist Mid-Latitude Climates with Cold Winters.
E	Polar Climates: with extremely cold winters and summers.

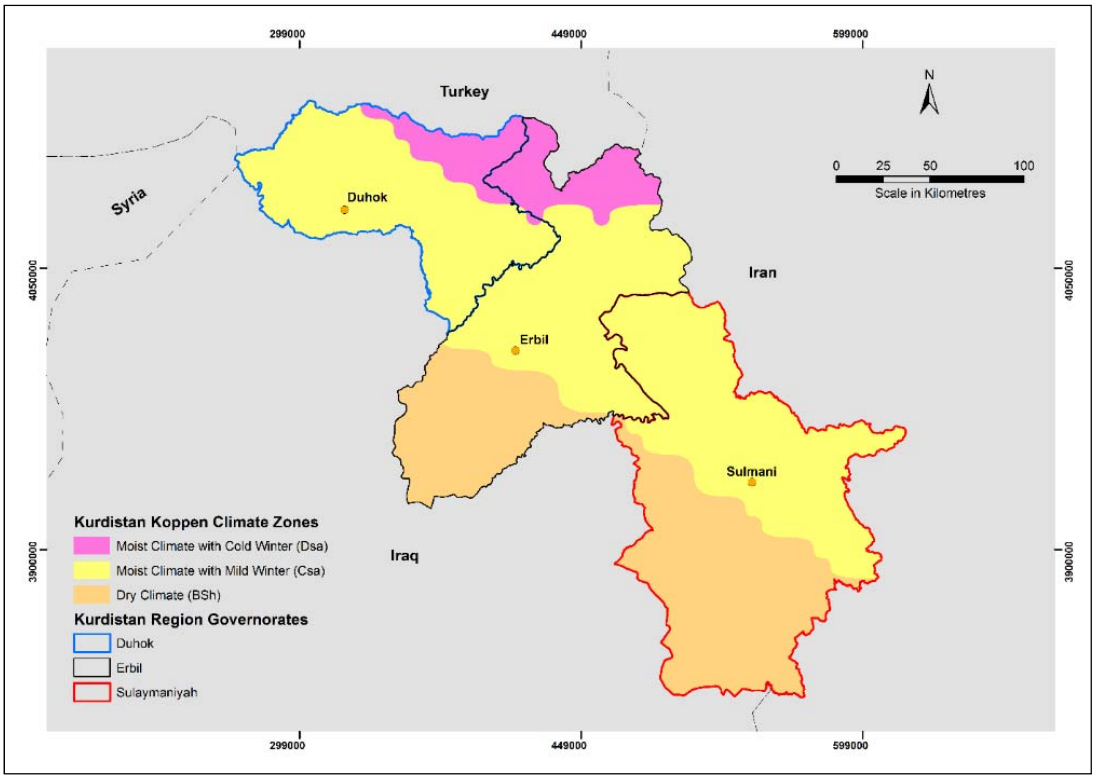

Figure 3.6: Koppen climate classification map of Kurdistan region.

The three zones are:

- A subtropical area or steppe zone (Bsh) in the south of Kurdistan Region where winter is temperate and summers intensely hot with temperatures around 40 °C. The Koppen Class description is “dry climate zone with deficient precipitation during most of the year”.
- The high plains or temperate zone (Csa), where winters are relatively severe and summers dry and hot. During the winter, snow and heavy rains fall for three months with temperature barely above freezing point. The Koppen Class description is “Moist Mid-Latitude Climates zone with Mild Winters”.
- The mountainous area Cold zone (Dsa) with extremely severe winters. Snow lie to a depth of several feet and temperatures is well below zero. In spring time, it is still cold and snow is visible on the peaks until August. The Koppen Class description is “Moist Mid-Latitude Climates zone with Cold Winters”.

Based on the three type of climate in Kurdistan region, the forest cover will be different in each zone. Natural forest covers most of the important green spaces of the area of the Kurdistan Region, located typically in mountainous and valleys areas (Csa

and Dsa zones). Under a forest areas improvement program by KRG natural forest spaces are increasing annually by 20,000 – 30,000 acres. The estimated natural forest areas in 2012 was five million acres mostly made up of oak, pine and eucalyptus trees (Resources 2012).

3.1.1.5 Hydrology

The main water resources in south Kurdistan includes both aboveground and underground water. The surface water resources in Kurdistan region consists of rivers and streams, with about 40% of the surface water for Kurdistan region (Figure 3.7) coming from the neighbouring countries of Turkey and Iran (UNDP 2011; KRG 2013).

The aboveground water consists of the major rivers of Greater Zab, Lesser Zab, Khabur, Sirwan and Awa Spi, all of which flow into the river Tigris in Federal Iraq. There are reservoirs at Dokan, Derbandikhan, and Duhok with a combined storage capacity of almost 10 billion m^3. However, the most important water resource is rainfall and snow in the Kurdistan region. The Greater Zab is one of the main branches of the Tigris and flow from its source in Lake Van (Turkey) through Erbil Governorate (Figure 3.7). It has a total length of 392 km and an annual discharge rate of 14.32 BM^3 (KRG 2013). The river enters Iraqi Kurdistan in Amedi province, and has five sub-tributaries; Shamezenan, Row Kochek in Turkey, and Rawandous, Bastourah and Khazir in the Kurdistan Autonomous Region (KAR).

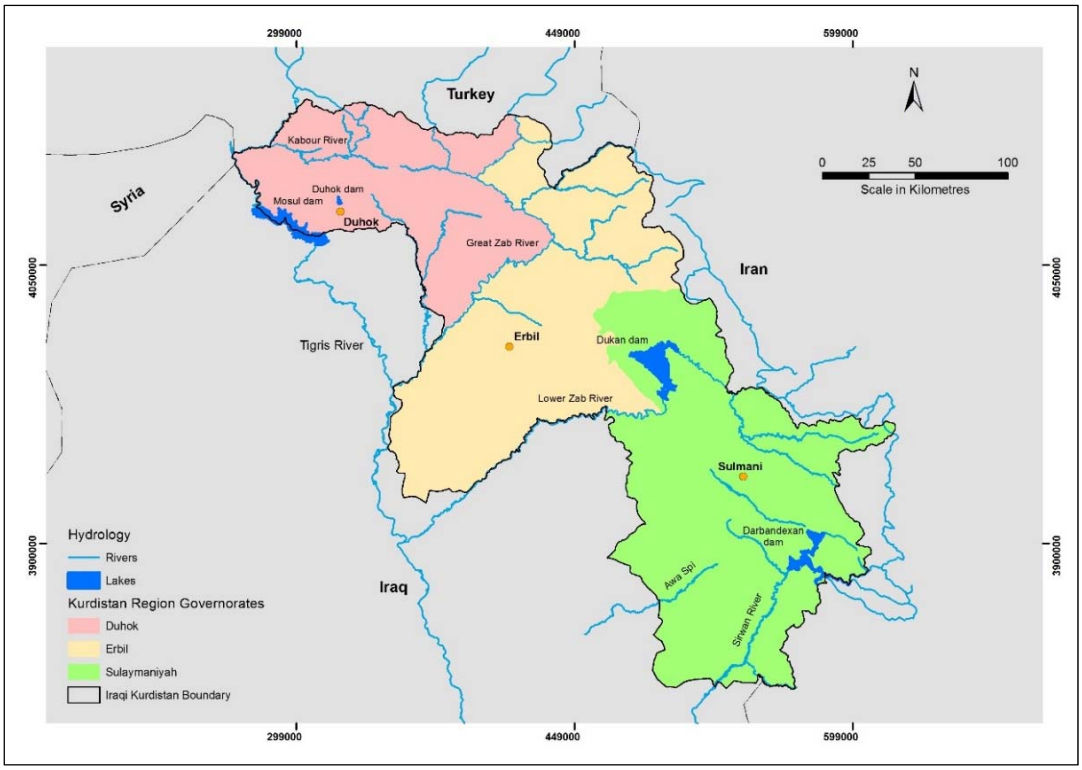

Figure 3.7: Hydrological map of Kurdistan region.

The Lesser Zab tributary passes through the Sulamani governorate. It is an international river flowing from its origin in the mountains in Iran and provides the major water supply to the Dukan Dam in Sulamani Governorate and enters the border of Iraqi Kurdistan at the Bedrazhour region. The river is 400 km in length with an annual discharge rate is 7.07 BM^3 (Billion Cubic Meters) (KRG 2013) (Table 3.2). The Khabur is also an international river flowing from Turkey and entering Kurdistan in Zakho district in Duhok governorate. It originates from the high mountains on the border of South and North Kurdistan. It has a length of is approximately 160 km with annual discharge rate of 2.20 BM^3 (KRG 2013). The final international river is the Sirwan which originates in Iran and has a length of 384 km in the Kurdistan region, with 59 % of the river length located in Iran and only 41 % is in Iraqi Kurdistan. The annual discharge of the Sirwan river is 5.86 BM^3 which is 13.5% of the total of the Tigris River discharge. The Awa Spy River which starts in Kurdistan has an annual water flow of 0.70 BM^3 and a length of 230 km. It flows into the Tigris at the city of Bald in Tikrit governorate (Hameed 2013).

Table 3.2: Annual discharge for the Kurdistan region Rivers.

Rivers	Discharge (M^3/sec)	Discharge (Billion) M^3/YEAR	Average discharge	
			In Kurdistan	Outside Kurdistan
Khabur	31	2.20	42 %	58 %
Greater Zab	421.32	14.32	58 %	42 %
Khazir	85.6	2.7	100 %	-
Leaser Zab	224	7.07	64 %	36 %
Sirwan	185	5.86	41 %	59 %
Awa Spi	27.6	0.70	100 %	-

The Kurdistan region of Iraq is also famous for springs. There are many springs supplying fresh water to the Kurdistan water resources. The sources of springs are groundwater and sub-surface water, which ultimately depend on the rain and snowfall. Figure 3.8 shows the annual mean rainfall for the Kurdistan region based on the data from 46 satiations located in different parts of the region. The rainfall data was downloaded from global weather website (https://globalweather.tamu.edu/). Any change increase in rain and snow will affect the water flow in the springs. The majority of the springs are located in the mountains areas of the three governorates of Kurdistan region Erbil, Sulamani and Duhok (KRG 2013).

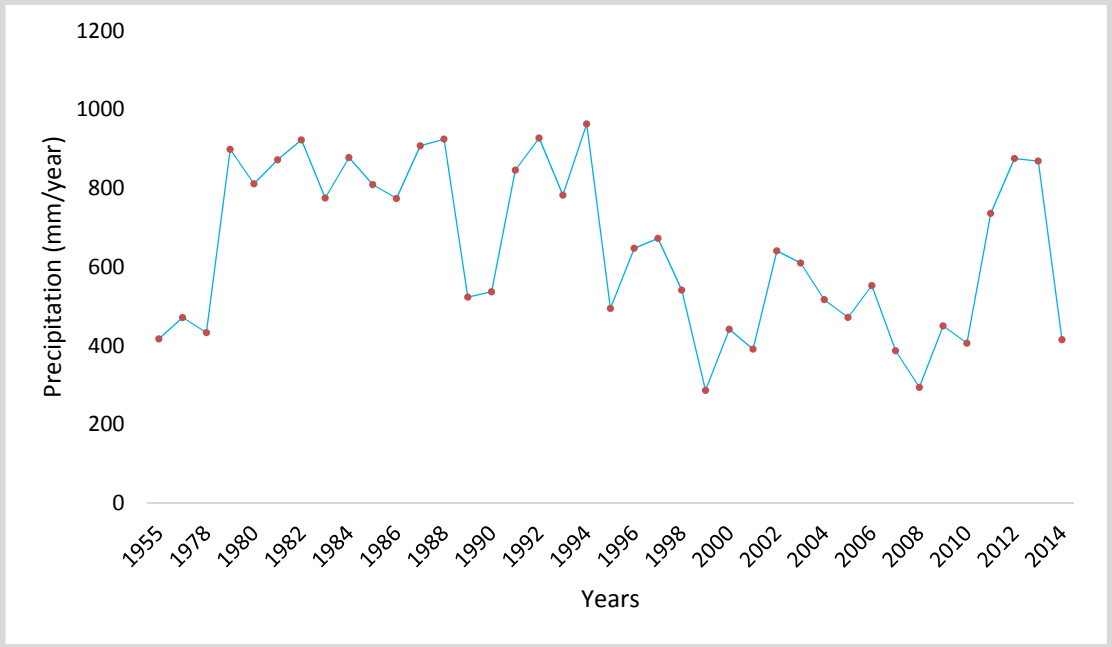

Figure 3.8: Long-term mean annual rainfall for Kurdistan region.

3.1.1.6 Natural resources

Iraqi Kurdistan is one of only ten regions in the world with over 45 billion barrels of estimated oil reserves. The first exploration wells in Iraq were drilled in the Chia Surkh region of Kurdistan by a British company in 1902. According to Jassim and Goff (2006), after the first World War appraisal drilling began in the Naft Khana area where the first oil field was found in 1923 (p. 388). In 1927, the first commercial oil strike was made in the Kirkuk structure within the Kurdistan region boundary. This led to the discovery of more oil fields in the southern part of Iraq in the late 1940s (Jassim and Goff 2006). Today the Kurdistan region is one of best places for the oil and gas companies to invest. Since 2003, as a result of new KRG policies in the oil and gas sector, the region was able to attract more than 45 companies from more than 30 countries, who are working in Kurdistan region (KRG-MNR 2013). Figure 3.9 shows areal distribution of the oil field sites with different progress stages. There are 14 sites or block with discoveries and for the rest of sites are 11, 26, 1, and 10 for the discovery with development, exploration areas, historical discovery, and open areas, respectively. In addition, the production of the oil in Kurdistan region is growing continuously as shown in Figure 3.10, especially after 2007 as the production is above millions of barrels annually. Since 2011, KRG was able to produce 200,000 barrels daily which was sent to the port of Ceyhan in Turkey. Recently the KRG increased the production to more than 500,000 barrels daily and it is aiming to increase the daily production of oil to two million barrels in the next three years (KRG-MNR 2013).

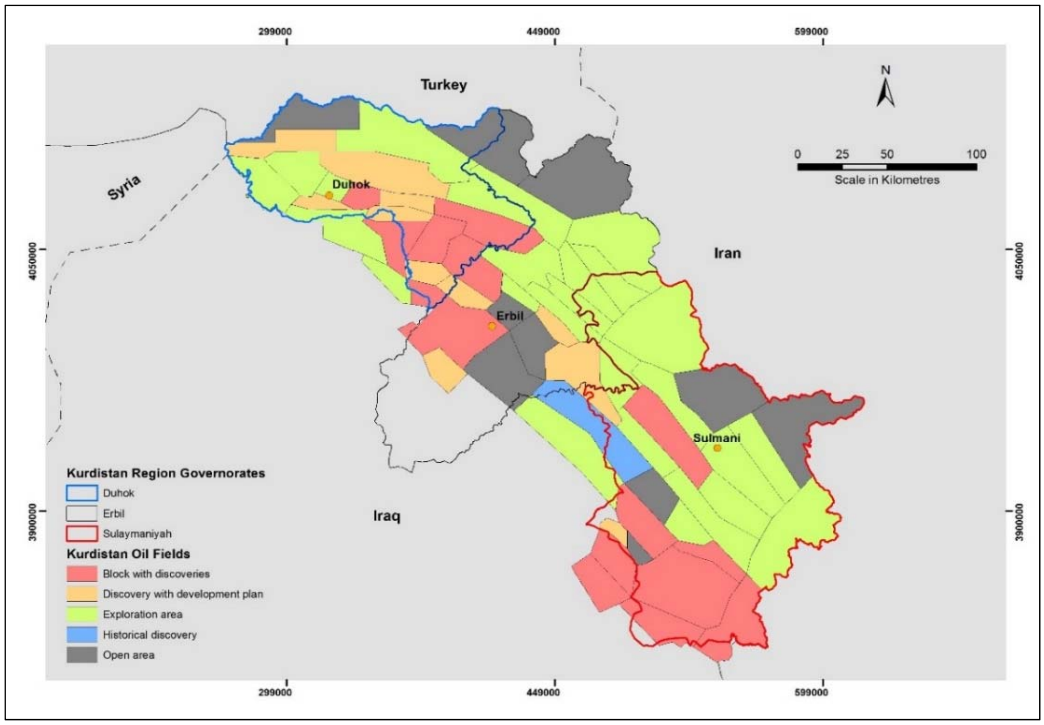

Figure 3.9: Iraqi Kurdistan Oil fields.

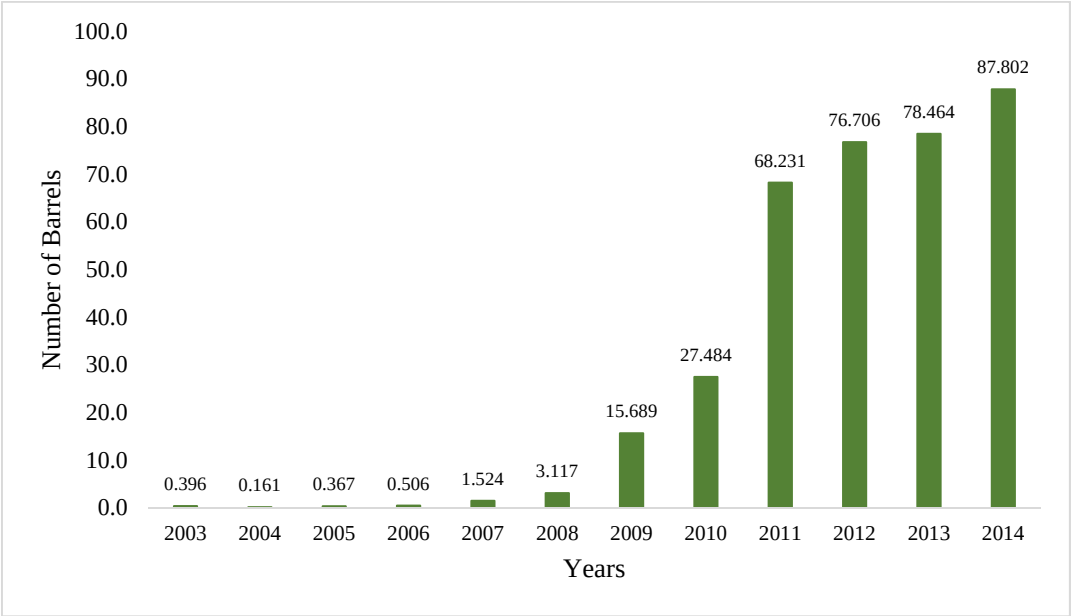

Figure 3.10: Gross Kurdistan Region oil production barrels in millions annually.

3.2 Data description

The datasets used in this project can be divided to remote sensing datasets which includes CORONA and Landsat satellite imagery, and GIS datasets which includes the Iraqi Kurdistan administrative boundaries for governorates, districts and sub-

districts level and a population dataset which was obtained from the KRG statistics agency.

3.2.1 Remote sensing data

3.2.1.1 CORONA

The study area is very large and therefore a total of 39 images were required to complete the coverage of the study area. At the start of this research, 39 CORONA images were acquired from the United States Geological Survey (USGS) website (http://edcsns17.cr.usgs.gov/ Earth Explorer). A total of 39 images were obtained (30 free of charges and 9 purchased) from the USGS to complete the areal extent of the study area of 45,000 km².

The Centre for Advanced Spatial Technologies, University of Arkansas and U.S. Geological Survey provide access to georeferenced CORONA images through the "CORONA Atlas for the Middle East" website free of charge. Thirty georeferenced images were downloaded from this website and were replaced with the thirty images downloaded at the early stage of this research. All the images from CORONA Atlas for the Middle East website were in National Imagery Transmission Format (NITF) format. Each NITF file contains one unprocessed geo-referenced CORONA image and along with RPC (Rational Polynomial Coefficients) as a replacement sensor model to be used for the ortho rectification process (CAST 2012).

Because the 30 geo-referenced images did not cover the entire study area, the 9 images purchased before were geo-referenced using the overlap area (8 % between two neighbouring images) to complete the areal extent of the study area. All these 39 images were from two missions, the first 30 images were from the mission number DS1107-2170DA and the rest of the nine images were from the mission DS1107-2154DA. The acquisition dates were August 3, 1969 for the 30 images from the CORONA Atlas and August 2, 1969 for the nine images purchased from the USGS website.

The majority of the images provided from this website (CORONA Atlas for the Middle East) are from the KH-4B satellite, which was last generation CORONA satellite. The KH-4B missions started from September 1967 through to May 1972 with sixteen successful missions capturing more than 188000 images (CAST 2012).

These satellite images have stereo viewing capabilities because of the dual panoramic cameras (one facing forwards and the other backwards with 30° angle of separation) with which the satellite was equipped. The dual stereo capability produced an approximate ground resolution of 6 feet or 1.8 m. The USGS scanned all those images at 7 microns (3600 dpi) to maintain the original spatial resolution for these unique space photographs.

3.2.1.2 Landsat

To cover the entire areal extent of the study area (Figure 3.2), five sets of Landsat images were selected for the image classification process to create land use and land cover maps for the study area. Each set of images contains at least five Landsat images. Images from Landsat-2 MSS for 1976, Landsat-4TM for 1989, Landsat-5TM for 1998, Landsat-5 for 2006 and Landsat8 for 2014 were acquired from United States Geological Survey (https://earthexplorer.usgs.gov/) as Level 1 products. Some of these images were available directly for downloading and some other were acquired by ordering them from the customer service section of the United States Geological Survey website.

The satellite data were chosen according to the following criteria:

1. A long time series of images should be available for the study area.
2. The images should be acquired in July (close anniversary dates within one month only), to increase the separation of land use classes by minimizing the seasonal variation.
3. All images should have less than 10 % cloud cover.

3.2.2 Population data (GIS data)

The population data and Kurdistan administrative boundaries shapefile were obtained from the Ministry of Planning of the KRG. The population data were obtained as multiple Excel spreadsheet files for different years and at different levels of aggregation (governorate, district and sub-district levels). Some of the population data files were not complete; there was missing data for some districts and sub-districts for some years.

3.3 Chapter summary

This chapter has outlined the study area and discussed the data collected for this research study. For the study area, geographical location and study area description were covered. The study area for this research is the Iraqi Kurdistan region which consists of three Governorates Erbil, Sulamani and Duhok with a total area of approximately 45,000 km². The description of the study area include the historical context of Kurdistan, geology, topography, climate, hydrology, and natural resources. For the data description, two types of data were included, remote sensing and GIS data. For the remote sensing data, the criteria that were used for imagery selection have been discussed as well as the number of images which were required to cover the areal extent of the study area. The GIS data, included the population data and the administrative boundaries shapefile.

4 Preparation of datasets

4.1 Image pre-processing

4.1.1 CORONA images

The 30 geo-referenced images downloaded from the CORONA Atlas for the Middle East (BETA) were in NITF format (National Imagery Transmission Format). Each NITF file contains on unprocessed geo-referenced CORONA image and along with RPC (Rational Polynomial Coefficients) as a replacement sensor model for the ortho-rectification process. The methodology suggested by CORONA Atlas for the Middle East website (Adam 2011) using ArcGIS and DEM data was adopted to obtain an ortho-rectified image for all 30 CORONA images.

All CORONA images (downloaded and purchased) were cloud free and later a number of image pre-processing steps were applied, including a colour balancing technique (Hamandawana 2007) to reduce the brightness variation between adjacent scenes. All the 39 CORONA images were resampled to have a uniform pixel size of 2.5 m. All 39 CORONA images were then mosaicked using ERDAS Imagine (Geospatial 2015) to create a blanket ortho- image completely covering the study area.

4.1.2 Landsat images

4.1.2.1 Atmospheric correction

Since remotely sensed data are influenced by a number of factors such as atmospheric effects, those datasets cannot be used directly in any image processing and analysis. The main degrading effect with Landsat image data is usually atmosphere (Tyagi and Bhosle 2011). Satellite images can only be used after performing a number of image pre-processing steps to remove or minimize these atmospheric influences to obtain correct full spectral information for each image element (pixels) (Tyagi and Bhosle 2014).

Some applications involving image classification and change detection analysis have claimed that atmospheric correction is an unnecessary step since the training data and the data to be classified are from the same source or same relative scale. Also the

correction of the image from the atmospheric scattering and absorption modified by gases and aerosols are depend on the remote sensing and atmospheric data availability (Song et al. 2001).

The raw Landsat data when received at the ground station is categorised as Level 0 data which is raw telemetry from the satellite. In order to be used for further analysis it needs to pre-processed which includes many processes such as radiometric calibration and terrain, and geographical correction (USGS 2015). Atmosphere effects can be removed or minimised using atmospheric correction techniques.

The datasets obtained from the USGS are Level 1 products and have been corrected for terrain effects and also have been calibrated radiometrically (converting from the sensor measurement radiance to a physical quantity digital number) and geo-referenced geographically (USGS 2015). These products have digital number expressed by 8-bits with range from 0 to 255. Comparing the digital numbers acquired by the Landsat satellite without correction for the atmosphere and solar angle effect can lead to misleading result. Even when the DNs for Landsat product have been calibrated, they still do not represent the actual surface reflectance from the ground that would be found when using spectrophotometry. Extracting information from a satellite image using the DNs or even Top of Atmosphere radiance may lead to wrong outcomes and conclusion. Since the Landsat images for this study are from three different sensors (MSS, TM and LC8), all dataset must be normalised radiometrically during atmospheric correction so that genuine changes are seen (Yang and Lo 2000; Paolini et al. 2006). The atmosphere correction process involves two steps; first converting DNs back to TOA radiance and then subtracting from the values for each pixel in the image the values from dark objects in each band for radiometric normalisation. The main purpose of atmospheric correction is to estimate and normalise the absolute values of below atmosphere (BOA reflectance), which refers to top of canopy reflectance (El Hajj et al. 2008).

The radiance from the remotely sensed dataset is a combination of two sets of radiances: one from the target or landscape surface categories and the other one from the sunlight which never reached the earth surface called path radiance (Figure 4.1). The path radiance has been captured by the satellite sensor during the satellite overflight. Atmospheric correction essentially the process of removing the path radiance from the remotely sensed image.

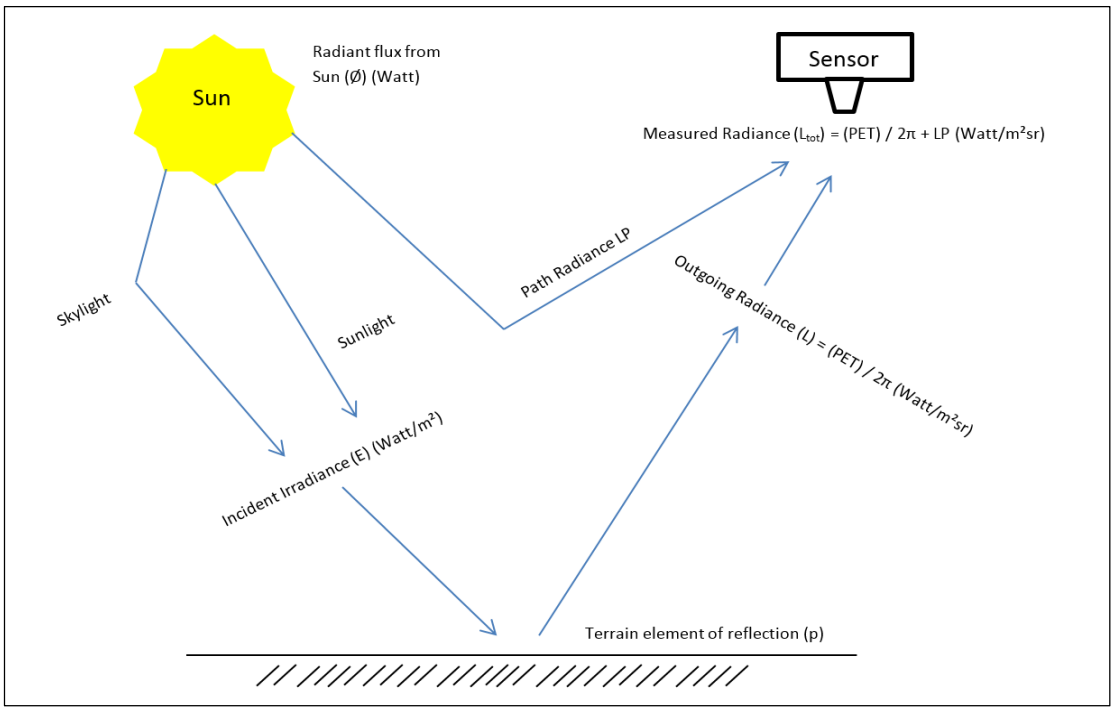

Figure 4.1: The path radiance from the sunlight which never reached the earth.

Atmospheric correction methods can be divided into two approaches; physical based and image based approaches (Lu et al. 2002). Since the physical based correction procedure method requires atmospheric measurement from the field during the satellite overflight, this method cannot be used with historical Landsat dataset because there is a lack of historical climate information for the study area.

Image based procedures are based only in the digital image information and field measurements are not required during the satellite overflight. Dark object subtraction (DOS) is an ideal method because is strictly based on image information (Chavez 1996). Since this study will not integrate any ground-based data to be mapped and compared with satellite image information (land surface temperature) and will not measure and model any variable which has direct effect in the environmental and ecological studies, therefore the DOS method can correct Landsat image radiance differences which are due to variations in solar illumination, sensor viewing geometry, and seasonality (Earth-Sun distance). DOS which is based on the following principle:

1. Define the darkest object in the image.

2. Assume the spectral reflectance for those dark objects are zero (target radiance).
3. The measured value above zero is assumed to be the atmospheric noise or path radiance for each pixel in the entire image.
4. Subtracting the path radiance from each pixel in the image will result in a relatively clean image from the atmospheric effect and the outcome will be an image with minimum effect of atmosphere.

The dark objects usually are the water bodies (Chavez Jr 1988) and they have very low reflectance and high absorption in the most of spectrum and especially beyond 0.75um. The atmospheric corrections for all Landsat images (MSS, TM, and Landsat 8) were carried out in two steps using the DOS Model in ENVI software 5.1 which is based on Chavez (1996). The output images should have reflectance values ranging from 0 to 1.

4.1.2.2 Image registration

After performing the atmospheric correction for all Landsat imageries, all five Landsat images for each date (1976, 1989, 1998, 2006 and 2014) were mosaicked to cover the entire study area of 45,000 km². The mosaic process was performed using the mosaic tool in ERDAS Imagine 2014. Since the CORONA mosaic image is an ortho-image, this image was therefore used as a reference to geo-reference and register the Landsat TM 1989 image. The selection of GCPs was based on permanent features which represent road intersections, historical sites and landmarks. A total of 100 GCPs were used, well distributed throughout the Landsat 1989 image, and the registration process yielded a Root Mean Square Error (RMSE) of <0.5 pixel. A first-order polynomial fit was applied for Landsat 1989 image with nearest neighbour sampling method.

Since the downloaded Landsat images are Level 1 product, therefore there is no need to perform image geo-referencing as already done by the provider by using ground control points, and the only pre-processing performed after atmospheric correction and creating mosaics was the co-registration between the new reference Landsat TM 1989 (registered with CORONA ortho image) and the rest of Landsat images. For this process, two methods were used to achieve pixel by pixel matching for all Landsat

imagery and representation of the same geographical location for all pixels in each image.

To be able to obtain genuine changes between any pair images, image registration is mandatory. This process was performed using the geometric correction tool in ENVI software and this tool provide many other techniques and one of those techniques was image registration, using image registration workflow. This technique defined many tie points between reference image (Landsat 1989) and the rest of Landsat images. All the registered Landsat images with TM 1989 have the total RMSE less than 0.5 pixel (Table 4.1).

Table 4.1: Registration process results of Landsat images.

Image	Year	Number of Tie Points	Total RMSE
MSS	1976	145	0.17
TM	1989	Reference Image	Reference Image
TM	1998	453	0.26
TM	2006	450	0.15
LC8	2014	320	0.42

Before getting to the second step of image co-registration, a subset image for the Landsat TM 1989 was created using Kurdistan region boundary shapefile. The subset Landsat TM 1989 was used as clipping tool in ArcMap to subset other Landsat images. During the clipping process carried out using ArcGIS 10.3, the processing environment, was set to “snap to pixel” resulting in subset images for each Landsat images matching pixel by pixel and well aligned, and each pixel in the image represents the same geographical location. Also this process will create an output images with the same pixel size as Landsat TM 1989 (30 m pixel size). The correct matching of pixels for all images is essential for obtaining a very accurate result from the changes caused by misplaced pixels during image registration process. The outcomes for the co-registration process are five subset datasets with an area of 44957.06 km^2 and with the same number of rows (10610) and columns (11915) or pixels counts (49952). During the change detection analysis process, same numbers of pixels with same geographical location will be compared for all Landsat images.

4.1.2.3 Removing outliers from the Landsat images

The reflectance values from the atmospheric correction process should be between 0 and 1, but some negative values or saturated values may be present because of dark object pixel selection during the DOS process or detector saturation. Image statistics were calculated for all images after Atmospheric correction process. The results are presented in the (Table 4.2 to Table 4.8). Some negative values and saturated values presented in Landsat MSS 1976 and Landsat 8 2014 respectively and it may be as a result of selecting very dark pixel for the DOS process. The rest of Landsat images (1989, 1998, and 2006) they were free from the saturated or negative values. The negative values and saturated values were removed for 1976 and 2014 images by using Band math tool in ENVI software which is similar to Raster calculator in ArcGIS.

Table 4.2: Statistics table of 1976 before removing negative value.

Bands	Minimum	Maximum	Mean	Std. Dev.
Band1 - Green	0.0150	0.5080	0.1450	0.0340
Band2 - Red	0.0100	0.4520	0.1870	0.0550
Band3 - NIR1	-0.0120	0.4650	0.2220	0.0490
Band4 - NIR2	-0.0360	0.5790	0.2450	0.0520

Table 4.3: Statistics table of 1976 after removing negative value.

Bands	Minimum	Maximum	Mean	Std. Dev.
Band1 - Green	0.0000	0.5085	0.0638	0.0755
Band2 - Red	0.0000	0.4525	0.0821	0.0997
Band3 - NIR1	0.0000	0.4652	0.0974	0.1149
Band4 - NIR2	0.0000	0.5785	0.1073	0.1263

Table 4.4: Statistics table of 1989 within 0-1 reflectance range.

Bands	Minimum	Maximum	Mean	Std. Dev.
Band 1 - Blue	0.0000	0.3211	0.0654	0.0761
Band 2 - Green	0.0000	0.5166	0.0753	0.0893
Band 3 - Red	0.0000	0.5988	0.0891	0.1079
Band 4 - NIR	0.0000	0.7932	0.1232	0.1446
Band 5 - SWIR1	0.0000	0.5318	0.1340	0.1591
Band 6 - SWIR2	0.0000	0.7413	0.1022	0.1236

Table 4.5: Statistics table of 1998 within 0-1 reflectance range.

Bands	Minimum	Maximum	Mean	Std. Dev.
Band 1 - Blue	0.0000	0.3815	0.0642	0.0746
Band 2 - Green	0.0000	0.5246	0.0725	0.0859
Band 3 - Red	0.0000	0.6260	0.0857	0.1037
Band 4 - NIR	0.0000	0.8400	0.1185	0.1390
Band 5 - SWIR1	0.0000	0.5412	0.1227	0.1460
Band 6 - SWIR2	0.0000	0.7874	0.0941	0.1144

Table 4.6: Statistics table of 2006 within 0-1 reflectance range.

Bands	Minimum	Maximum	Mean	Std. Dev.
Band 1 - Blue	0.0000	0.3538	0.0678	0.0792
Band 2 - Green	0.0000	0.7385	0.0784	0.0930
Band 3 - Red	0.0000	0.6247	0.0920	0.1108
Band 4 - NIR	0.0000	0.7790	0.1263	0.1467
Band 5 - SWIR1	0.0000	0.4974	0.1273	0.1508
Band 6 - SWIR2	0.0000	0.7237	0.0992	0.1211

Table 4.7: Statistics table of 2014 with saturated values.

Bands	Minimum	Maximum	Mean	Std. Dev.
Band1 - Coastal Aerosol	0.0830	1.3160	0.1540	0.0240
Band 2 - Blue	0.0650	1.2310	0.1530	0.0310
Band 3 - Green	0.0430	1.3160	0.1700	0.0440
Band 4 - Red	0.0290	1.3280	0.2060	0.0660
Band 5 - NIR	0.0120	1.3280	0.3080	0.0630
Band 6 - SWIR1	0.0000	1.3160	0.3190	0.0800
Band 7 - SWIR2	0.0000	1.2920	0.2360	0.0700

Table 4.8: Statistics table of 2014 after removing saturated value.

Bands	Minimum	Maximum	Mean	Std. Dev.
Band1 - Coastal Aerosol	0.0000	1.0000	0.0676	0.0782
Band 2 - Blue	0.0000	1.0000	0.0671	0.0786
Band 3 - Green	0.0000	1.0000	0.0743	0.0890
Band 4 - Red	0.0000	1.0000	0.0904	0.1113
Band 5 - NIR	0.0000	1.0000	0.1348	0.1582
Band 6 - SWIR1	0.0000	1.0000	0.1399	0.1669
Band 7 - SWIR2	0.0000	1.0000	0.1036	0.1261

4.1.2.4 Noise reduction

Noise may present in Landsat data because of sensor detectors effects. To test for this, Minimum Noise Fraction (MNF) estimation noise statistics were calculated using ENVI software. When calculating the Eigenvalues for each image, the eigenvalues=<2 are dominated by noise and should be excluded from each image before using them for further analysis. As shown in the Table 4.9 for the eigenvalues calculation no images have any Eigenvalues =<2. Since all images are free from noise (Figure 4.2 to Figure 4.4), therefor they are ready to extract training samples using region growth tool in ENVI software.

Table 4.9: Estimation noise statistics result Landsat images.

Bands	1976	1989	1998	2006	2014
Coastal Aerosol	NA	NA	NA	NA	1381.660
Blue	NA	798.214	708.599	907.630	34.130
Green	1018.813	29.891	25.152	34.269	19.413
Red	84.178	21.024	20.303	22.091	16.464
NIR	39.600	13.761	11.794	10.652	12.918
NIR2	13.791	NA	NA	NA	NA
SWIR1	NA	7.309	8.078	8.875	7.241
SWIR2	NA	2.398	2.679	2.002	2.353

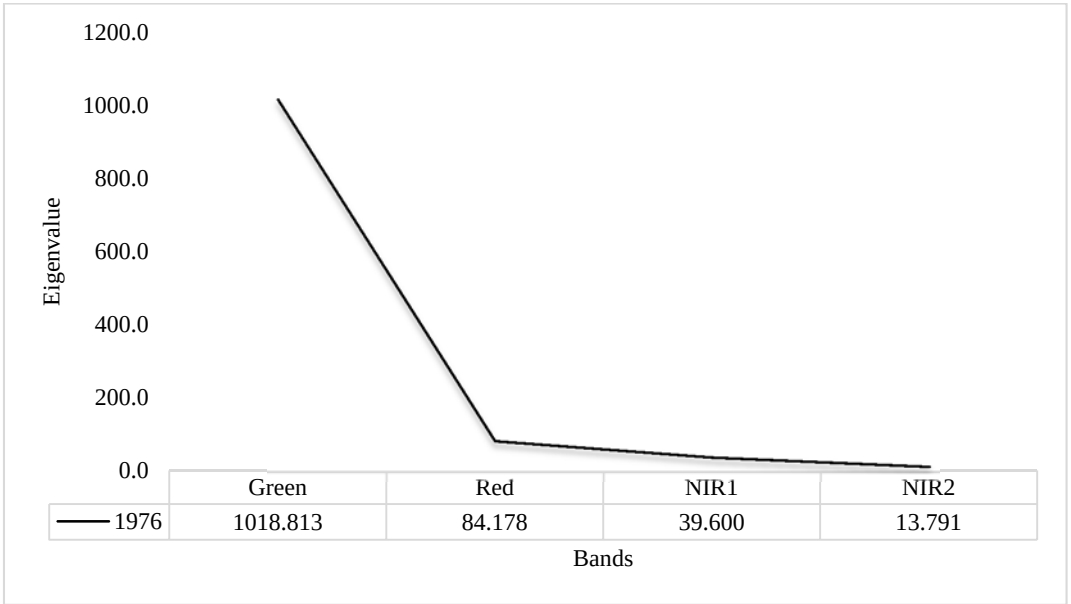

Figure 4.2: 1976 Forward MNF Estimation noise statistics.

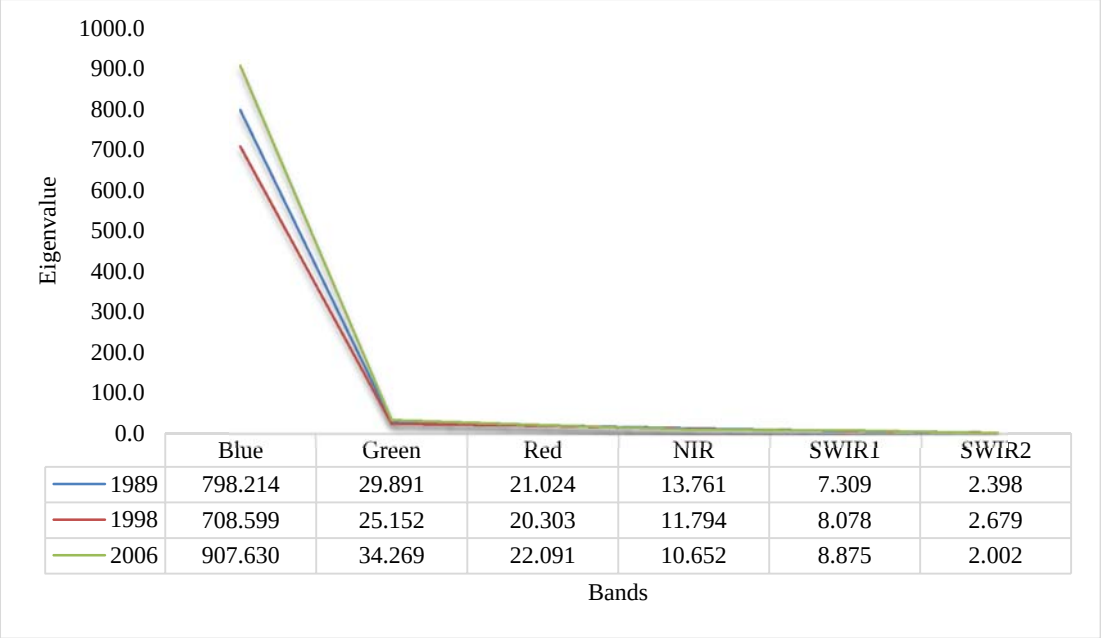

	Blue	Green	Red	NIR	SWIR1	SWIR2
1989	798.214	29.891	21.024	13.761	7.309	2.398
1998	708.599	25.152	20.303	11.794	8.078	2.679
2006	907.630	34.269	22.091	10.652	8.875	2.002

Figure 4.3: 1989, 1998 and 2006 Forward MNF Estimation noise statistics.

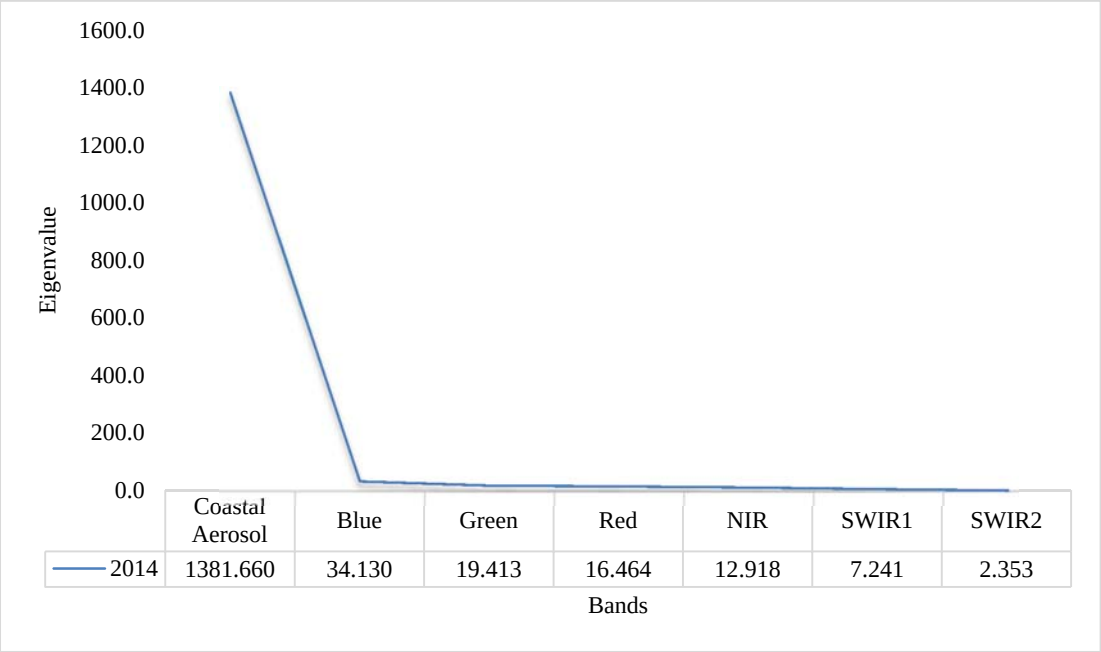

	Coastal Aerosol	Blue	Green	Red	NIR	SWIR1	SWIR2
2014	1381.660	34.130	19.413	16.464	12.918	7.241	2.353

Figure 4.4: 2014 Forward MNF Estimation noise statistics.

4.2 Population dataset

All the population spreadsheet files were compiled into a single spreadsheet to be used for further analysis. Because there were some missing data for some districts and sub-districts, therefore Formula 1 (Dewan et al. 2013) was used to estimate the population for the missing cell before and after certain date in the excel spreadsheet.

$$Pi = Pj(1 + x)^n \quad \text{(Eq. 1)}$$

$$Pj = Pi/(1 + x)^n \quad \text{(Eq. 2)}$$

Where, Pi is the population for the year of interest to be defined (new date), Pj is the population of the known year (old date), x is the annual growth rate between the two population dates (decade) and n is the number of years between both years (old and new), by inversing the formula we can get the old missing date as per formula 2.

After completing the missing data for some districts and sub-districts, the population data was encoded with a unique ID field to match the UID for the districts and sub-districts in the boundary shapefile of the Kurdistan region. The table (population file) was then joined with the spatial data (boundary polygon shapefile) using the common field (UID). The final shapefile, containing the boundary and population data will be used for further analysis to highlight relationship between the population and the land use and land cover changes for the entire Kurdistan region in districts and sub-districts levels (Figure 4.5 and Figure 4.6).

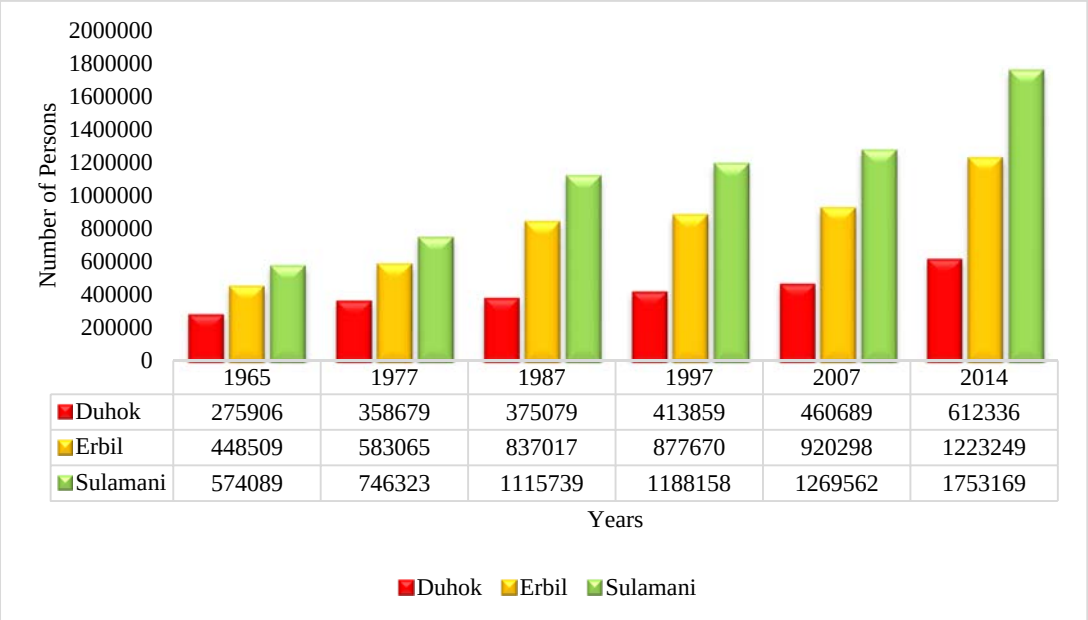

	1965	1977	1987	1997	2007	2014
Duhok	275906	358679	375079	413859	460689	612336
Erbil	448509	583065	837017	877670	920298	1223249
Sulamani	574089	746323	1115739	1188158	1269562	1753169

Figure 4.5: Kurdistan region population trend for three governorates.

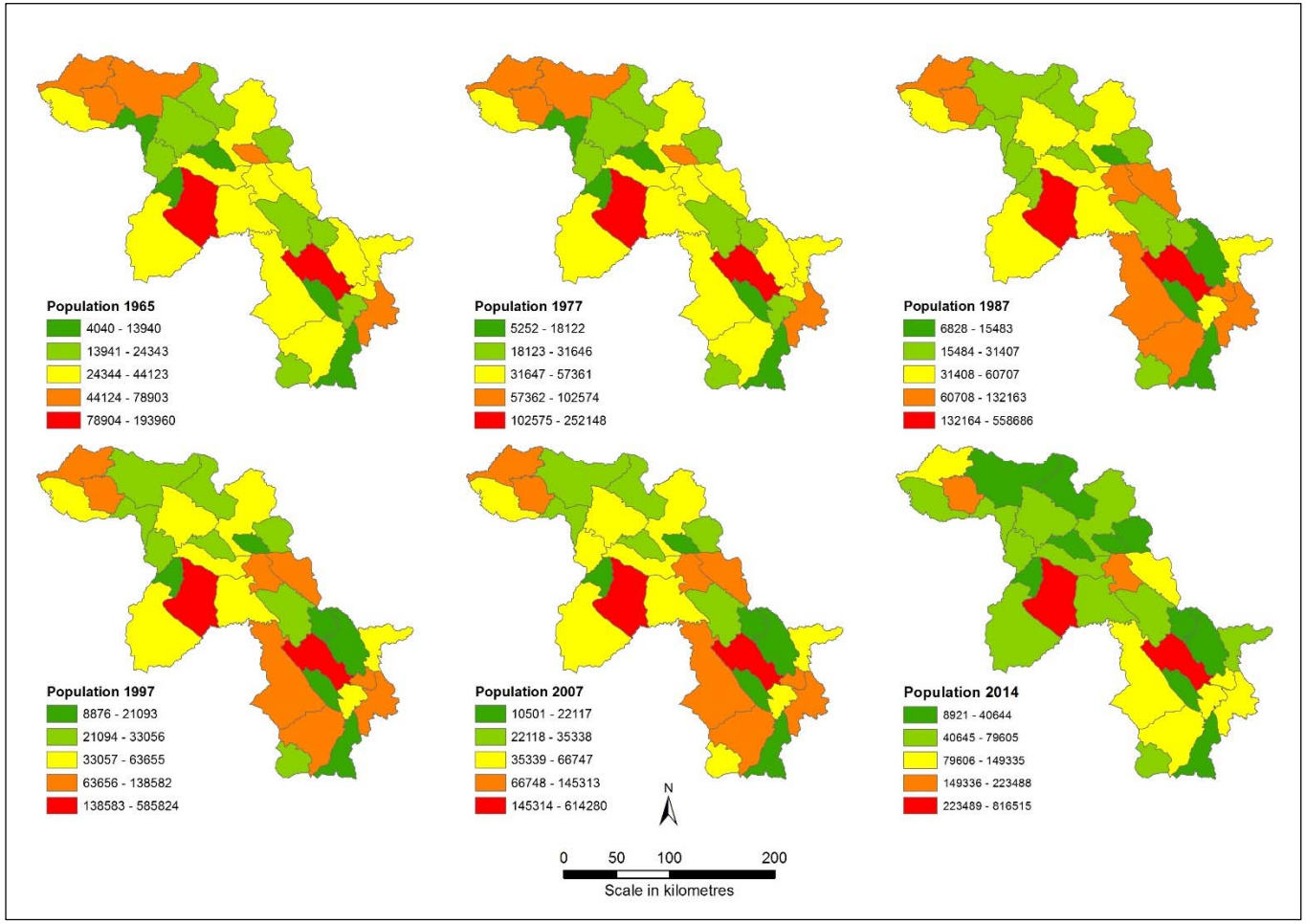

Figure 4.6: Map of Kurdistan region population in districts level.

4.3 Chapter summary

This chapter has covered all the important pre-processing steps for the CORONA and Landsat imagery to make them ready for image classification process as input data. For the CORONA images, the methodology suggested by Adam (2011) using ArcGIS and DEM data was adopted to obtain ortho-rectified images. A number of image pre-processing steps were applied, including colour balancing to reduce the brightness variation between adjacent scenes. For Landsat images, a number of image pre-processing steps were performed such as atmospheric correction, image enhancement, mosaicking, and image co-registration. Also for the Landsat datasets of 1976 and 2014, TOA reflectance correction was performed to eliminate saturated or negative values from both images. Finally, all Landsat image were tested for noise using MNF estimation noise statistics.

In addition, the population dataset was pre-processed and completed from the missing data and converted to ArcGIS shapefile dataset for further analysis with land use or cover changed maps.

5 Methodology

5.1 Classification scheme

According to the land use and land cover classification system developed by (Anderson 1976) for interpretation of remote sensing data at various scales and resolutions, Landsat images are only suitable for level I land use/land cover mapping because of pixel size restriction (Sun et al. 2009a). CORONA data can also only be classified as level one due to spectral band restriction. This study uses CORONA and Landsat data with different spatial resolution (pixel size varied started for CORONA with 2.5 m, 30 m for TM and Landsat 8 and 60 m resampled MSS), therefore, a modified of the Anderson Scheme Level I method with major land cover classes would be considered for the Kurdistan region.

The complex environment of the Kurdistan region is an additional factor for modifying the Anderson classification scheme. For instance the built area is a mixture of residential, commercial and industrial areas. It would be impossible to separate those classes using Landsat data, with its 30 m pixel size. Many studies have shown a modified Level 1 Anderson classification scheme is suitable to extract the major land cover type including water bodies, wetland, agriculture, forest, built up, and bare land areas with an acceptable level of accuracy (Yuan et al. 2005; Abdulaziz et al. 2009; Dewan and Yamaguchi 2009). The study area will therefore be classified into five major classes (water bodies, built-up, bare land, forest, and agriculture area) for the CORONA and all Landsat images. Description of these land use classes are presented in **Error! Not a valid bookmark self-reference.**.

Table 5.1: Developed Classification scheme based on Anderson System (1976).

Code	Land use/cover	Description
1	Water bodies	All areas of open water, including rivers, streams, lakes, and reservoirs
2	Built up	Urban including residential, commercial, and industrial buildings as well as open transportation facilities, airports, highways, railways, and single/multiple family houses.
3	Bare land	Uncultivated areas of sparse plant cover, including saline alkali land along river/lake beaches, barren rock or sand in sloping fields, bare land, and burned. .areas
4	Forest	Dense forest, open forest, orchards, nurseries, and all type of trees.
5	Agriculture	A cultivated with dense annual crops and vegetables, cultivated land without crops including dry land and irrigable land.

Also each land use / cover type would be coded with a number to be used during all the processes for this research including the accuracy assessment process with ground reference data as they will have same code Table 5.2.

Table 5.2: Land cover types and their unique code.

Land Use/Cover	Code
Water	1
Built up	2
Bare land	3
Forest	4
Agriculture	5

5.2 Land use and land cover overview

Land use and land cover change analysis is an important tool to map and quantify global change at various spatio–temporal scales (Lambin et al. 2000). In addition, it can measure the impact of human activities on a given environment (López et al. 2001). The processes that control land use and land cover changes are complicated, and this complexity is due to the nature of the interaction between land cover, human activities and natural processes. The land use/land cover change pattern is an outcome of natural and socio-economic factors and their utilization by humans in time and space (Torres-Vera et al. 2009). Land is becoming a scarce resource due to vast agricultural and demographic pressure.

Land cover maps document the cover classes (physical land type) of surface feature such as forests, wetlands, impervious surfaces, agriculture, and other land type such as bare land and water bodies. Land cover can be determined or classified by processing and analyzing low and medium resolution satellite and aerial imagery. Land cover maps provide information about the current landscape status in summary form. Meanwhile, the land use shows how the landscape has been used based on the human needs and it is usually the outcome of classification processes for the high-resolution imagery (satellite or aerial). Despite the difference between land use and land cover in terms of detail level, land use types in a given area are an extension of land cover categories, for instance, the built up areas can contain both residential and commercial

buildings. Both terms (LU/LC) have been used interchangeably to describe the landscape for different applications around the globe by many researchers.

Since this study implements the level one classification scheme (Anderson 1976; USGS 2015) (map five classes only), most of the time during the processing and analysis of the classified images those two terms may be used interchangeably. Since both terms refer to the relation between the landscape and human activities, both terms lead to the same meaning despite the difference in level of information extracted from the satellite images.

5.3 CORONA image classification process

5.3.1 CORONA texture calculation

In the spatial domain, each cell or pixel in the image will have a digital number or gray tone value assigned to it (Haralick et al. 1973). One of the important characteristics of a panchromatic image is the texture which can be used to identify features or regions in the image. The texture calculation normally has a set of descriptive properties that can be measured and compared through texture analysis (Haralick et al. 1973; Hudak and Hudak 2001). The output of the texture analysis is always a set of descriptive images that can be used as input for image classification process to obtain the final thematic maps. All the texture descriptors are sensitive to the orientation and directions of calculation (Haralick et al. 1973). Complex methods are required to identify all areas in the same image which have similar texture. Texture analysis relies on direction and space in the image, and therefore the locale property of any texture measure will change from one pixel to another in the same image. Since the texture is affected by direction and spacing, the analysis often requires a number of different position vectors usually oriented at 0°, 45°, 90°, and 135° (Haralick et al. 1973) as shown in Figure 5.1.

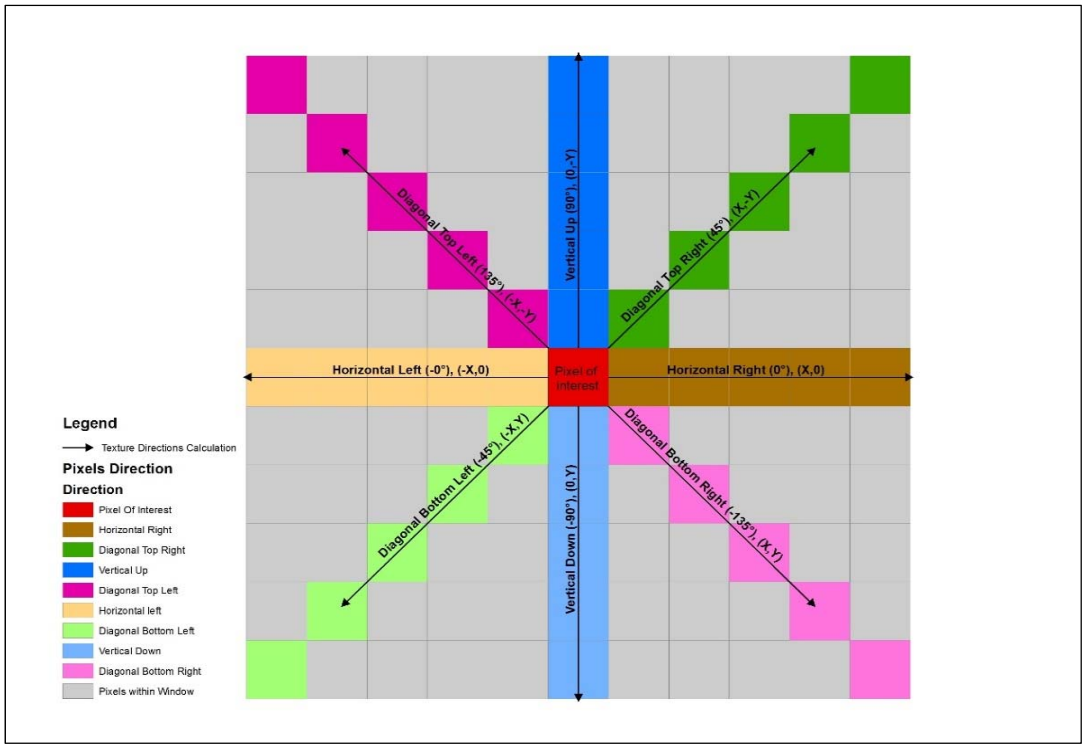

Figure 5.1: Possible texture calculation with different directions.

In texture analysis, the Gray-Level Co-occurrence Matrix is used to calculate texture values for a particular measure or descriptor. The GLCM takes into account the three important variables (difference in the gray level values, coarseness, and directionality or regular pattern) which create texture in the image. A rich texture is present in the image when there is more difference in the three variables mentioned before, especially in the gray level values. The GLCM is the function of angular relationship and the distance between every two neighbouring pixels (Haralick et al. 1973).

This matrix shows the number of occurrences of a pixel and its specified neighbour. The texture calculation is based on the Haralick method as a gray-tone spatial dependence matrix and as mentioned above the implementation considered four directions between the target pixel and the neighbouring pixels or cells separated by a certain distance in any four directions. The texture calculation is based on the geometric angles (Table 5.3) as the analysis often requires a number of different position vectors in respect to the target pixel, usually oriented in horizontal (0°), diagonal right (45°), vertical (90°), and diagonal left (135°) which refer to the geometric angles of 0°, 45°, 90°, and 135°, respectively.

The influence of those parameters on the final accuracy for classified images obtained from texture calculation has been studied. (Marceau et al. 1990) concluded that the window size has a big impact on the classification accuracy and they regarded the window size as the most important parameter in the texture classification process. (Shaban and Dikshit 2001) indicated that the best window size for extraction of the texture features are 7x7 and 9x9 and the texture measurements of contrast and mean have a high level of accuracy. The case study carried out by (Agüera et al. 2008) showed that the optimum gray level in their study was 128 while comparing the texture calculation for the Quick Bird and IKONOS satellite imagery. In addition, they found that the best results were achieved when the mean and angular second moment were used for texture classification.

Since CORONA images are single band images, selection of a spectral band is irrelevant. However since CORONA data images have never been used for texture classification before, all other parameters (size of moving window, and the quantization level) will be considered to obtain best outcome for the image classification process based on the highest level of accuracy achieved.

To test for the periodicity of the texture in CORONA data, a Fast Fourier Transform (FTT) was performed. The nature of the texture in the study area is clearly shown in Figure 5.2 to be neither periodic or aperiodic (directional) but random since the distribution of the Fourier spectra values is not restricted to any direction (Lee and Chen 2002).

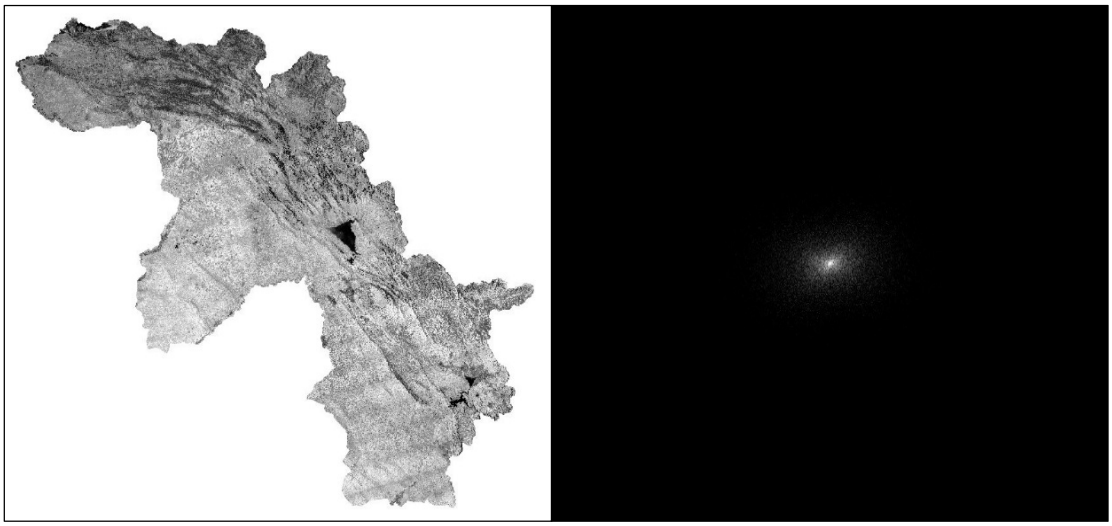

(a) CORONA panchromatic image (b) Fast Fourier Transform

Figure 5.2: Fast Fourier Transform showing the texture is random for study area.

The texture calculation uses the geometric definition of zero as its reference, whereas aspect uses geographical Azimuth as reference; for instance the geometric zero refers to zero direction (Horizontal right (0°)) which in geographical terms refers to the eastern aspect (67.5° - 112.5°). The Table 5.3 shows the possible texture orientation calculation and their corresponding Aspect angle, which are based on the Azimuth. The largest percentage of the study area is east and west aspect (36 %) in respect to Azimuth and this is matching the zero geometric orientation of 0° (Horizontal right and left direction) Figure 5.3.

Since the east and west orientation are symmetric (Haralick et al. 1973), therefore for this study the orientation of 0° (Horizontal direction, which is refers to easterly Aspect of 67.5° - 112.5°) for texture calculation would be considered with a distance metric of one pixel and a two pixels distance to target pixel. The texture calculation would include different vector sets with one pixel in horizontal (east 0°) right (1_{pixel}, 0°) and with two pixels in horizontal (east 0°) right (2_{pixel}, 0°), respectively. The calculated texture measurement would include mean, variance, homogeneity, contrast, dissimilarity, entropy, and correlation and the least correlated outputs would be used as input for the multidimensional image with CORONA original image for the image classification process.

Table 5.3: Texture directions based on geometry and corresponded Aspect

Texture direction (Uses Geometry)	Aspect (Uses Azimuth)
Horizontal Right (0°)	East (67.5° - 112.5°)
Horizontal Left (-0°)	West (247.5° - 292.5°)
Diagonal Left Top (135°)	North-West (292.5° - 337.5°)
Diagonal Right Bottom (-135°)	South-East (112.5° - 157.5°)
Diagonal Right Top (45°)	North-East (22.5° - 67.5°)
Diagonal Left Bottom (-45°)	South-West (202.5° - 247.5°)
Vertical (90°)	North (0° - 22.5°)
Vertical (90°)	North (337.5° - 360°)
Vertical (-90°)	South (157.5° - 202.5°)
NA	Flat (-1)

.

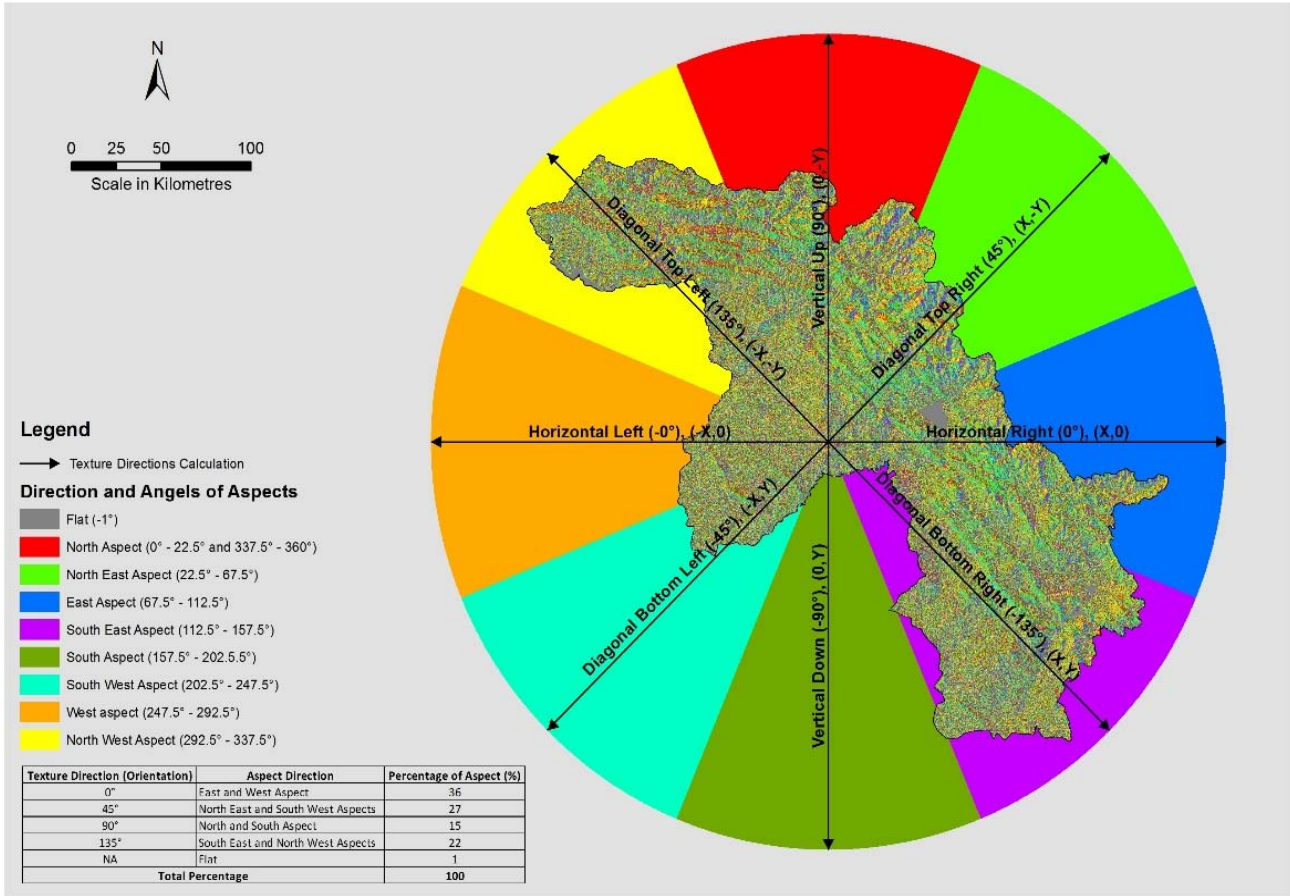

Texture Direction (Orientation)	Aspect Direction	Percentage of Aspect (%)
0°	East and West Aspect	36
45°	North East and South West Aspects	27
90°	North and South Aspect	15
135°	South East and North West Aspects	22
NA	Flat	1
Total Percentage		**100**

Figure 5.3: Texture directions (orientations) and Aspect for the study area.

5.3.2 CORONA multilayers creation

Texture measures are normally highly correlated either positive or negative (Haralick et al. 1973) (Figure 5.4). Haralick (1973) suggested the use of principle component analysis to reduce this correlation among those measures for better results. Often the selection of texture measure for image classification is based on intuition, experience, and software defaults. Based on Figure 5.4 it is possible to choose the measures with least correlation, and the Mean measure has the lowest correlation with variance and contrast among the other measurements. These least correlated texture measures can be used as an input for creating a CORONA multilayer image together with the original brightness image for the image classification process.

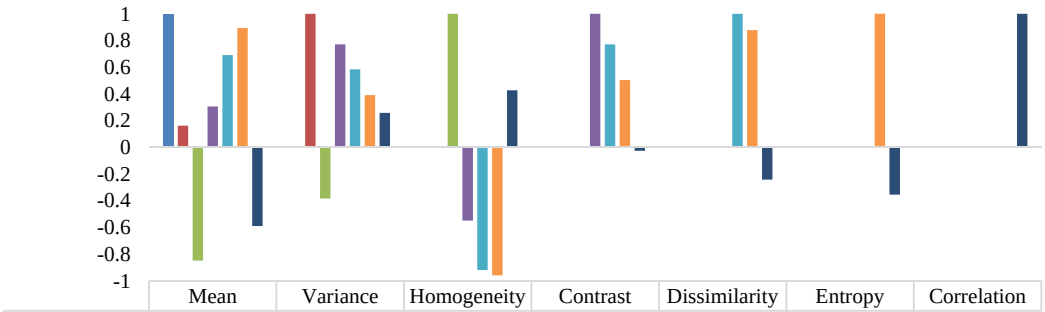

	Mean	Variance	Homogeneity	Contrast	Dissimilarity	Entropy	Correlation
Mean	1						
Variance	0.2	1					
Homogeneity	-0.8	-0.4	1				
Contrast	0.3	0.8	-0.5	1			
Dissimilarity	0.7	0.6	-0.9	0.8	1		
Entropy	0.9	0.4	-1.0	0.5	0.9	1	
Correlation	-0.6	0.3	0.4	0.0	-0.2	-0.4	1

Figure 5.4: Correlation matrix for texture measurements.

In the texture image calculations, there are three requirements for obtaining good results; connectivity, interior texture, and spatial information. After the selection of the texture descriptive measurement with minimum correlation among all texture measurements, a multilayer image was created based on the original CORONA image (gray-levels) and the least correlated texture measurements. Combining the original image with a multi-texture channel image adds a new dimension as it is spatial information which is essential for obtaining very accurate training texture regions during region growth process and good results for LULC map during the image classification process. The original image was combined with a multichannel texture

image (mean and contrast). The contrast was selected for connectivity, mean for interior texture and original image for spatial information.

5.4 Training samples extraction

5.4.1 CORONA

The selection of the training samples for a CORONA image classification process can be very challenging as the texture calculation layers look very different from the original image and require that the user to be familiar with the study area. Using the multi-channel CORONA combined image, a minimum of ten training samples or texture regions were extracted for each land cover type (bare land, built up, forest, agriculture, and water,) using a region growth method. Using the region growth tool provides statistically similar homogenous regions for the classification process (ENVI 2015). This step is very important because the outcome of image classification relies on the accuracy on those extracted regions. The best possible result for image classification is achieved when the training samples are statistically different from each other between land use or land cover types and are statistically similar within one type. The region growth tool is based on the principle of a growing function for the given region within an N dimensional array (of bands) by aggregating or grouping all pixels within the array that connect the neighbouring pixels to the seed region based on some constraints. The constraints could be a threshold value for minimum and maximum pixel value or as a multiple of the standard deviation of the pixels within a same region (Tang et al. 2002). The region growth tool is based on the seed pixels locations and spatially aggregates those pixels that meet the statistical criteria selected by the user (ENVI 2015).

The seed pixels for each land cover type were identified visually. During the region growth process, the geometry parameter was set to “point” (from a choice of region selection shapes which included polygon, rectangle, ellipse, polyline, and point). The number of rows and columns in the region selection was selected as 1 for the “brush size”, and finally, maximum growth size was set the default (1000x1000 pixels). Other parameters were a standard deviation multiplier of 1 and the number of alterations as the default (2); the eight neighbour pixels option was also selected. The main reason for setting the parameters in this way, is to obtain pure regions that have the lowest standard deviation from the mean of the selected seed pixels. Regarding

other parameters, these parameters will not affect the results for the region growth tool as the surrounding pixels will not be included in the region for the seed pixels unless their statistics are within the range of one standard deviation from the mean of the seed pixels. Even if the number of alterations increased also the size of region would not add more pixels to a region as those regions are restricted to one standard deviation rule.

The statistical separability of the resulting texture region was examined using the Jeffries-Matusita test (Jeffreys 1946). The calculated values of this statistic range between 0 and 2 and indicate how well the training samples pairs are statistically separable (ENVI 2015). The separability tool calculates or computes the spectral separability between selected regions or training samples pairs for the given input file. A higher value of Jeffries-Matusita measure indicates that the land use or cover training samples pairs are statistically separable. A value less than 1 indicates that the area should be combined with the land cover type in the same training sample pair, or it can be replaced and tool run again to improve the outcome. The training samples regions created for the CORONA image were used as input for the Jeffries-Matusita measures separability tool in ENVI software. The results for this test are shown in Table 5.4 with all pair classes being very different from each other for all land covers. Their Jeffries-Matusita statistics were within a range of 1.8 to 2 except for the water (Rivers) and agriculture specifically cultivated areas. The training pair consisting of cultivated area and water has the low Jeffries-Matusita measure value of 0.34 (ENVI 2015). This suggests that the water class cannot be accurately separated during the image classification process.

5.4.2 **Landsat**

Training samples were extracted for each Landsat image using a region growth method with similar parameters setting as used for CORONA texture region extraction. The Jeffries-Matusita test was performed for those training samples before using them in the image classification process. The Jeffries-Matusita measure values for all training samples were within range of 1.66 and 2 (Table 5.4), which indicates that training sample are statistically separable from each other and can be used for further analysis for all land use or cover types.

Table 5.4: The Jeffries-Matusita measure results for all images.

Years	Minimum	Maximum
1969	1.80	2.00
1976	1.66	2.00
1989	1.88	2.00
1998	1.78	2.00
2006	1.87	2.00
2014	1.95	2.00

5.5 Water masking

The results of the statistical separability test for CORONA image using the Jeffries-Matusita measure showed that all class pairs were very different from each other except for the water bodies (Rivers) and agriculture, and specifically cultivated areas. The training pair consisting of cultivated area and water has the low Jeffries-Matusita measure value of 0.34. This suggests that the water class cannot be accurately classified during the image classification process. Also the water areas in the image representing less than 2 % of the total study area. Excluding this class as a masked area from the image classification may increase the accuracy of the classified CORONA multiband image.

For the Landsat images, although the result of Jeffries-Matusita test showed all training samples are different statistically, those images (Landsat) were still not ready to be a direct input in the image classification process because of some artefacts. Those artefacts are referring to cloud, water bodies, and shadows in the remotely sensed data image and it may reduce the final accuracy of LULC classified image.

Since all the selected Landsat images are cloud free, there is no further pre-processing regarding cloud effect. The water bodies in the images are highly heterogeneous due mainly to differences in water clarity which will cause confusion with some of the other ground classes. It is therefore desirable to mask out all water bodies. This is also made necessary by the fact that the study area is mountainous, with a high possibility of shadows being present in the Landsat images. Confusion can occur in the image classification process between water bodies and shadow areas. The water areas also in the Landsat images representing less than 2 % of the total study area. Excluding this class as a masked area from all Landsat images could increase the final accuracy of the classified Landsat images.

The process of creating masks for all images (CORONA and Landsat) was similar and used Feature Extraction image segmentation method in ENVI software. Two different scale values were used during the segmentation process as CORONA and Landsat have different pixel sizes of 2.5 m and 30 m, respectively.

For the CORONA multiband image, the original band was used as the segment band for segment setting parameter and with edge algorithm. The scale level value of 2.5 and value of 95 merge level was used for the segment setting and merge setting parameters, respectively. The reasons for using those parameters is to obtain accurate edges for water bodies as the scale value used will effect this extraction process. Using the large scale (lower value) led to lower percentage (same as the scale value) of the gradient magnitude values being discarded from the interim gradient image during the segmentation process. By increasing the scale level, the objects (water bodies) in the image will keep most of their distinct edges. Different levels of scale were also tested during this process and the scale value of 2.5 showed better results for the segmentation process as the spatial resolution for CORONA is 2.5 m. For merge parameter, since the edge algorithm is used with high scale value and over segmentation may occur and since the merge setup is an optional parameter, using high level of merging such as 95 is useful to improve the delineation boundaries of the water bodies (Exelis 2015).

Regarding Landsat images, the NIR band was used for segmentation since the water areas would absorb the majority if not all NIR energy and it appears visually black in the image. During this process, many scale and merge levels were tested to obtain the best result for the water bodies in all Landsat images. The scale level of 30 and merge level of 95 gives best results visually, which agrees logically with 30 m spatial resolution of Landsat data.

The output for the segmentation process was raster and vector datasets, and the vector files were used in ArcGIS environment and some clean up done for both datasets (CORONA and Landsat) until the desired shapefile for the water bodies only were obtained and have been used as masks during the image classification process. For the Landsat shapefiles some editing was done because sometimes the rivers system in the Kurdistan region is less than 30 m in width and it was not possible to capture those rivers during the segmentation process. Therefore, some manual digitising was done to obtain accurate water masks for Landsat datasets.

5.6 Ground reference datasets collection

Because of the lack of historical ground reference information for the study area, the ground reference data have been collected by visual interpretation of the images themselves for each year, and this is because the field of remote sensing was restricted to military use in Iraq from 1970s till 2003. Many maps and surveys were lost during the invasion of Iraq by USA in 2003. In addition, Middle East governments are generally reluctant to supply any type of data (images or ground reference data) which in their opinion may be a threat to the security of their regime.

5.6.1 CORONA

The ground reference data for the CORONA image was collected from the image itself. Two sets of datasets (point and regions) were created based on the original image of CORONA that was used as base map layer.

For the point reference dataset, a stratified random sampling approach was adopted for each land cover type. A total of 500 random points were generated within the study area for the CORONA 1969 image. All the random points were overlaid on the original CORONA image, and 356 points were attributed (Table 5.5) to each land cover type and appropriately coded using ArcMap 10.3. Point reference datasets were converted to region of interests (ROIs) raster file with 2.5 m pixel size for the accuracy assessment process.

Table 5.5: Total number of ground reference points collected from each image.

Years	Water	Built up	Bare land	Forest	Agriculture	Number of Points
1969	108	68	60	64	60	356
1976	60	45	60	60	61	286
1989	66	64	78	64	72	344
1998	76	70	59	69	59	333
2006	65	77	72	64	96	374
2014	65	66	68	61	73	333

Five types of land cover types were generated from the random point using region growth tool for the CORONA image. A total of 140.05 km² of areas were the outcome of the region growth tool process (Table 5.6). The region raster dataset for 1969

contains all five types of land cover and they were attributed in the fields Class and Code with correct land cover type and code or value respectively.

Table 5.6: Total areas in km² extracted (each image) using regions growth tool.

Years	Water	Built up	Bare land	Forest	Agriculture	Total Area (km²)
1969	100.98	3.56	15.74	3.32	16.45	140.05
1976	4.10	1.20	12.02	7.45	3.83	28.59
1989	18.64	3.30	10.95	5.97	7.41	46.27
1998	137.71	18.01	62.94	7.95	24.49	251.09
2006	94.09	5.89	19.53	9.19	28.04	156.75
2014	166.07	37.34	107.22	7.95	21.93	340.52

5.6.2 Landsat

For the Landsat data, the ground reference data have been collected from the image itself for each year, again because of the lack of contemporary ground reference information for evaluated years (1976, 1989, 1998, 2006, and 2014) for the study areas. Two sets of reference datasets (point and regions) were created based on the original images for all Landsat data images (used Landsat as base map layer). For the point reference dataset, a stratified random sampling approach was adopted for each land cover category. A total of 400 random points for each year was generated using stratified random sampling approach. A total of 286, 344, 333, 374, and 333 random points (Table 5.5) were attributed for 1976, 1989, 1998, 2006, and 2014 with correct land use or cover types and code, respectively. The point reference dataset was converted to region of interests (ROIs) raster file with 30 m pixel size for the accuracy assessment process.

From the generated random points, five types of land cover were obtained using the region growth tool in ENVI software. A total of 823.23 km² (Table 5.6) of areas were the outcomes of the using region growth tool. The ROI raster dataset for each year contains all four types of land cover and they were attributed with correct land cover type and code respectively.

5.7 Landsat and CORONA image classification

A number of image classification techniques were performed for both datasets (CORONA and Landsat). Image classification included unsupervised (as test

technique) and supervised image classification methods. The main reason for performing unsupervised classification as a test classification is to get an idea of how many classes can be extracted from study's images.

For the supervised classification, there are a large number of image classification techniques available for instance Maximum likelihood Classifier (MLC), Minimum Distance Classifier (MDC), and Support Vector Machine Classifier (SVMC). The MLC is the most popular method and has commonly been used in image classification processes in the field of remote sensing. During this process, a pixel with maximum likelihood is classified into the corresponded class based on the posterior probability of the pixel belonging to each class (Strahler 1980; Foody et al. 1992; Gonzalez and Woods 1992; Paola and Schowengerdt 1995). Also this classifier (MLC) has been used widely because it is based on multivariate normal distribution theory (Strahler 1980).

Although MLC is a superior method and has been used by many studies (Maselli et al. 1994; Paola and Schowengerdt 1995; Frazier and Page 2000; Paul 2000; Paul et al. 2002; Erbek et al. 2004; Otukei and Blaschke 2010) because it uses the prior probabilities during classification process, and also allows the prior weighting of output classes based on their training samples sizes. However, for this research a number of supervised classifiers (MLC, MDC, and SVMC) were used and performed and the best one with the highest level of accuracy assessment will be used for the change detection and further analyses.

5.8 Accuracy assessment

Following the classification process for each individual image (Landsat and CORONA images) with different classifiers, and the generation of land use/cover classified image, the classified images (MLC, MDC, and SVMC) were re-classified to have a Code or value for each land cover type as in Table 5.2 and same as the ground reference datasets (points and regions). For the accuracy assessment process, two datasets (points and regions) were used with unfiltered classified images, and all measures of accuracy including user accuracy, procedure accuracy, overall accuracy and Kappa coefficient were calculated during this process (Congalton 1991).

5.9 Change detection

This study is using two different datasets in terms of spatial resolution (CORONA 2.5 m and Landsat 30 m) as inputs for the image classification process. Therefore, those classified images need to be uniform in pixel size for each evaluated pair classified images to perform “From-To” change detection analysis. To be able to extract pixel by pixel changes between every pair images, the pixel size for both images need to have same pixel size. Since the original spatial resolution of CORONA is 2.5 m, and therefore this spatial resolution was kept for determining an accurate land cover map for 1969 CORONA image since the Kurdish authority believes that the built up area was larger in the 1960s than 1970s and 1980s. By keeping the original spatial resolution for the CORONA imagery, it is possible to extract very accurate information for the built up areas from these unique space photographs for the land use or cover map of 1969.

Because the spatial resolution for CORONA image was higher than Landsat image, the classified Landsat images for 1976 and 2014 were resampled to 2.5 m. A test was carried out by resampling the CORONA image to 30 m pixel size and evaluating against the 30 m 2014 Landsat image using the “From-To” method. However this resampling to 30m generalised the CORONA data and much information was lost, therefore both Landsat images (1976 and 2014) were resampled to 2.5 using nearest neighbour method to provide comparison data for two epochs (1969-1976 and 1969-2014). For the remaining epochs (1976-1989, 1989-1998, 1998-2006, 2006-2014), all classified Landsat images have a uniform pixel size of 30 m (Table 5.7).

Table 5.7 : All epochs with their pixel size for change detection analysis

Image	First year	Second year	Epochs	Pixel size/m	Pixel size/m
CORONA 1969	1969	1976	1969-1976	2.5	2.5
Landsat MSS 1976	1976	1989	1976-1989	30	30
Landsat TM 1989	1989	1998	1989-1998	30	30
Landsat TM 1998	1998	2006	1998-2006	30	30
Landsat TM 2006	2006	2014	2006-2014	30	30
Landsat 8 2014	1969	2014	1969-2014	2.5	2.5

A python script was developed in the ArcGIS environment to be able to quantify and map the LULC changes by using “From-To” change detection analysis concept. This is based on a pixel-by-pixel assessment to determine the quantity of transformation from a particular LULC class to other classes and their corresponding area over the period of evaluation. Also this method captures the changes and rates between every pair of classified images. The results of this technique are a two-way cross-matrix describing all types of change in the study area.

The python script was implemented six times for the epochs (1969-1976, 1976-1989, 1989-1998, 1998-2006, 2006-2014, and 1969-2014). A new thematic change map containing different combinations of “From-To” change classes was produced for each evaluated epoch. The outcomes of this process were also included in a table of statistics showing the amount of changes in areas from one class to another.

5.10 Population mapping

Conventional population mapping methods will not show the actual distribution for the population based on the type of the land use/ cover classes. Using choropleth maps for population, the phenomena of population distribution would be shared by all the LULC types and aggregated equally with the boundary of each districts or sub-district level whose the data were collected. The choropleth method will not communicate the density of population distribution and where the people are living and their effect on the LULC types according to the population growth. In addition, relationship between the population increase and highlight their effect on the LULC changes would not be possible based on choropleth maps.

Many methods for mapping population distribution have been developed over the last few decades (USGS 2008), and one of the most widespread methods is Dasymetric population mapping. The Dasymetric mapping method has the ability to redistribute the population data according to the geographic space, for instance LULC maps. One of the most important characteristics of Dasymetric mapping is its ability to develop a relative density system to reassign the density values according to the LULC types.

Based on the Dasymetric mapping method, the water areas will always have a population density of zero as the majority of the population live on land areas and principally in built areas, with the built up areas having a high density of population. In addition, the bare areas have either zero density, or as in the Gulf countries a low

density, as some people prefer to live in desert areas. However that is not the case here for Iraqi Kurdistan region areas. The agriculture area is a second level of density after the built up areas, as the people prefer to live in those areas to take care of their crops, however it is regarded as low density area. Forest areas can be regarded as areas with very low density as they are mountainous and the accessibility is very hard and therefore not many people live there. Based on the nature of the Kurdistan region and peoples' preferred living areas, the system shown in (Table 5.8) was developed and used for the process of Dasymetric mapping. Also the reason for creating such a system (Table 5.8) is during the early 70s and late 80s, the rural areas became abandoned places by Kurdish citizens. The Iraqi regime forced the Kurdish families to leave their homes in those areas in the hope that this would reduce the support to Kurdish Peshmerga. As a result of this mistreatment by the Iraqi regime many Kurdish families migrated to big cities in the region. Also during this period during the 1980s, many villages were destroyed during the war between Iraq and Iran and in the military operations carried out by the Iraqi regime. Even today, those areas cannot be a safe place for the citizens of the Kurdistan region to live as they are within the 1050 km long war zone running from west to south with the Islamic terrorist group Daish, targeted by Turkish fighter jets in the north, and in the east by continues bombing from Iran. The ArcGIS "Dasymetric Mapping Extension" (DME) tool provided by the USGS website was implemented to create a final density map for all the corresponding years for each land use or cover map (USGS 2008).

Table 5.8: Relative density classification scheme.

Land cover type	Land cover Code	Relative Density Description	Relative Density Code (RA)
Water	1	Zero density	0
Built up	2	High density	15
Bare land	3	Zero density	0
Forest	4	Very Low density	5
Agriculture	5	Low density	10

5.11 Urban expansion analysis

Most of the urban measurement growth methods (spatial statistics, transition matrices) quantify expansion but do not describe the pattern of urban expansion types (Bhatta 2010). Also there is not any standard definition of the urban growth to quantify the

type of urban growth globally (Wilson et al. 2003). Since this study requires information to highlight the urban expansion as response to human activities including population increase and economy, therefore the type of expansion is needed for further analysis (direction or aspect analysis). An Urban sprawl model allows us to quantify and show the aerial distribution pattern for the other land classes which have been transformed to urban area (Wilson et al. 2003). Since this study has extracted all the LULC maps from the remotely sensed data (CORONA and Landsat), the use of Urban Growth Analysis Tool (UGAT) developed by (Angel et al. 2007) could define the urban expansions development types and their areal extend for the study area. UGAT is based on the same concept of the model which was developed by (Wilson et al. 2003) to provide many matrices during this approach. The python script for this tool was modified and updated to extract three types of urban growth within the study area (extension, infill, and leapfrog). The study area was divided into three sections based on the boundary shapefile at governorate level to be able to analyse the urban development for each governorate individually.

A buffer zones shapefile has been created with (1 km, 5 km, 10 km, 15 km, and 20 km) with the governorate building as the reference centre point for Duhok and Sulamani cities. For the city of Erbil, Erbil citadel was used as a reference centre point as it is exactly in the centre of the city and is close to the Erbil governorate building. In addition, the buffer zones were divided into eight directions or aspects for each buffer distance. The buffer and direction zones were used to extract the types of expansion for the three cities within each buffer zone and the direction of expansion. The definitions for the urban growth types created are based on the system described by (Angel et al. 2007) with some modification to include the definition of the input datasets (Table 5.9).

Table 5.9: Urban expansion development types for the Kurdistan region.

Development type	Description
Extension	New development which are intersecting with footprint of T1.
Infill	New development which are accruing in T1 urban open space.
Leapfrog	New development which are accruing in T2 and not intersection with footprint of T1.
New development	Sum of the all development types which are exists in the second year of epoch T2 and not existing in the first year T1.
T1	Time one or first (early) year of comparison in epoch.
T2	Time two or second (lately) year of comparison in epoch.

5.12 Chapter summary

This chapter defined the classification scheme, based on the Anderson System (1976) that was used for the image classification process. The developed system or scheme matches the objectives of this study for classifying the images (CORONA and Landsat) to the desired land use or land cover types (five classes). In addition, this chapter describes the process of ground reference datasets collection for the CORONA and Landsat satellite images that were used in the accuracy assessment process. Also, this chapter highlighted problems of missing the ground reference information for the study area.

This chapter also included comprehensive information regarding texture calculations and the possible orientations or angles to be used for this process based on the calculated aspect from the digital elevation model (DEM). The connection between texture orientation and aspect of the study area was covered and it was shown how this combination can be used as a guide for the best texture direction calculation rather than using the default parameters from the software itself. Also, this chapter defined a method for choosing the best texture combination measurements based on the correlation matrix for obtaining best possible accurate result for the single band CORONA image.

This chapter also defined the image classifier technique which was used for the image classification process after performing a training sample signature assessment test with Jeffries-Matusita measure. Also included are the reasons and technique used for creating a water mask for all the images in order to obtain accurate result for the entire

land use/cover classified images and change detection analysis using “From-To” method. In addition, this chapter described the use of an urban growth tool for delineating the areal extent and the rate of expansion for the three types of expansion that the study areas experienced during the period 1969-2014 for the three major cities for the Iraqi Kurdistan region.

6 Results

The results for this project have been broken down into sections to make it easy for readers to understand all the important steps in the entire processing sequence.

6.1 Points datasets accuracy assessment

The results for the accuracy assessment are shown in (Table 6.1). The accuracy assessment process was done twice, once without water and the other with water class. This was because the water class had been classified using a different method, as a separate step. Including water did not affect the final accuracy for each individual class, but it did increase the overall accuracy and Kappa Coefficient for all the classified images. The accuracy for the water bodies was free from the commission and omission errors as they were 100 % accurate all the time (they were excluded from image classification process). The overall accuracy (without water) for all years ranged from 79 % to 89 % and the Kappa coefficient from 0.72 to 0.86. This process showed that there is some confusion among the classes and that most of this confusion is between built up areas and bare land through both errors of omission and commission. The accuracy assessment statistics in terms of user's accuracy and producer's accuracy for each year and each class can be found in Appendix B.

For the CORONA 1969 classified land cover map, the overall accuracy of using reference points is 85 %. The Kappa coefficient of agreement for point reference datasets is 0.80.

Table 6.1: Accuracy assessment results using points reference datasets.

	Excluding water		Including water	
Years	Overall accuracy (%)	Kappa coefficient	Overall accuracy (%)	Kappa coefficient
1969	85	0.80	91	0.88
1976	79	0.72	83	0.79
1989	86	0.81	89	0.86
1998	89	0.86	92	0.90
2006	81	0.74	84	0.80
2014	88	0.85	91	0.88

For the Landsat MSS 1976 image the overall accuracy result for the point reference dataset was 79 % with a kappa coefficient of agreement of 0.72. The accuracy result

for the 1976 MSS Landsat image can be regarded as good for this type of imagery since the original spatial resolution is 79 m. For the rest of Landsat images TM 1989, TM 1998, TM 2006 and LC8 2014 the overall accuracy results for point reference dataset were 86 %, 89 %, 81 %, and 88 % and kappa coefficient were 0.81, 0.86, 0.74, and 0.85, respectively.

6.2 Regions datasets accuracy assessment

The results for the regions (polygons) datasets are shown in (Table 6.2). The same two accuracy assessments were used as for the point reference datasets. Not including water during the accuracy assessment process did not affect the final accuracy for each individual classes, the only change was an increase in the overall accuracy and Kappa Coefficient for all images when water was included. For the CORONA classified image, the overall accuracy was 84 % with kappa coefficient of 0.76. For the classified image of 1976, the overall accuracy for 1976 was increased to reach 83 % and 0.74 for the kappa coefficient. This process showed that there is some confusion among the classes because of errors of both omission and commission. The majority of this confusion is between built up areas and bare land. The detailed results for the accuracy assessment process in terms of user accuracy and procedure accuracy for each year and class can be found in Appendix B.

For the rest of the classified image (excluding water) using the regions reference datasets, the overall accuracy for all images ranged between 74 to 91 and Kappa coefficient of 0.60 and 0.88. The accuracy assessment results for each year and class can be found in Appendix B which covers user’s accuracy and producer’s accuracy.

Table 6.2: Accuracy assessment results using regions reference datasets.

	Excluding water		Including water	
Years	Overall accuracy (%)	Kappa coefficient	Overall accuracy (%)	Kappa coefficient
1969	84	0.76	96	0.90
1976	83	0.74	86	0.80
1989	91	0.88	95	0.93
1998	84	0.73	93	0.88
2006	74	0.60	90	0.82
2014	89	0.81	95	0.92

The results from the accuracy assessment for both datasets (points and polygons) excluding water for the classified images are compatible with standard accuracy for classified images to performing post classification change detection analysis. The result for both accuracy assessments complies with the standard accuracy for LULC mapping studies for the Landsat products as recommended by Anderson (1976).

6.3 Land use land cover maps

The spatial pattern and area statistics for all classified images are shown in the (Figure 6.1 to Figure 6.2) and (Table 6.3 and Table 6.4). Generally, these maps show the spatial distribution pattern of the land use/cover categories over the study area of Iraqi Kurdistan from one epoch to another. The dominant land cover classes for the classified CORONA 1969 image are bare land and agricultural areas with areas of 26749.14 km², 12187.98 km², respectively. The other land use/cover types of built up, forest and water, cover areas of 79.42 km², 5501.43 km², and 439.09 km², respectively. For the 1969 classified map bare land represents almost 60 % of the total of the study area and followed by agriculture with 27.11 %. The other land uses (built up, forest and water), occupied 0.18 %, 12.24 %, and 0.98 % respectively. As there is no information before 1969 in regards to the land use/cover map it is not possible to discuss the changes before that time. Therefore, this year is used as a base land cover map to evaluate the changes that occurred during the study period.

By examining the classified image for 1976 and the land use statistical table, it is clear that, within the study area, bare land has the largest areas of 33331.04 km² (74.14 %) followed by agriculture with an area of 5870.20 km² (13.06 %). Built up, forest and water areas are present in the study area with 53.82 km², 5194.63 km² and 507.37 km² respectively, which equate to 0.12 %, 11.55 %, and 1.13 % respectively.

On the land use/cover map for 1989, bare land remains the dominant land use/cover type with 32631.73 km² (72.58 %), followed by agriculture with an areas of 10530.59 km² (23.42 %). The built up areas cover 167.16 km² which represent 0.37 % of the total study areas. For the rest of the land use types (forest and water), the total areas are 360.20 km² (11.85 %), and 44957.1 km² (0.80 %), respectively, within the study area.

For the 1998 land use/cover map, the bare land is again dominant at 35473.14 km² (78.90 %) of the study area (Table 6.4). For this year the forest area is second in terms

of areas covered with a total of 5325.90 km² (11.85 %) followed by agriculture 3475.05 km² (7.73 %). For the rest of two classes (built up and water), the first class covers an area of 172.74 km² (0.38 %) and water with an area of 510.24 km² (1.13 %).

For the Landsat classified image of 2006, agriculture is the dominant land use/cover type occupying of 18645.42 km² (41.47 %) of the study areas followed by bare land with total area of 16758.49 km² (37.28 %). The built up areas cover a total of 219.02 km² (0.49 %). The water bodies cover an area of 444.65 km², which is 0.99 % of the total percentages of study area. Finally, the forest areas are occupying 8889.49 km² of the study area, which is equivalent to 19.77 %.

For the 2014 classified Landsat image, the major land use type for this year is bare land with areas of 32146.34 km² (71.50 %). The built up areas have reached 1254.52 km² (2.79 %) and water bodies cover an area of 416.55 km², which is 0.93 % of the study area. The last two land use types (agriculture and forest), cover a 2150 km² and 8989.60 km² of the study area which are 4.78 % and 20 %, respectively.

Table 6.3: LULC types for all years, areas in KM².

Land Cover	1969	1976	1989	1998	2006	2014
Agriculture	12187.98	5870.20	10530.59	3475.05	18645.42	2150.05
Bare land	26749.14	33331.04	32631.73	35473.14	16758.49	32146.34
Built up	79.42	53.82	167.16	172.74	219.02	1254.52
Forest	5501.43	5194.63	1267.39	5325.90	8889.49	8989.60
Water	439.09	507.37	360.20	510.24	444.65	416.55
Totals	44957.06	44957.06	44957.06	44957.06	44957.06	44957.06

Table 6.4: LULC types for all years, areas as a percentage (%) of total.

Land Cover	1969	1976	1989	1998	2006	2014
Agriculture	27.11	13.06	23.42	7.73	41.47	4.78
Bare land	59.50	74.14	72.58	78.90	37.28	71.50
Built up	0.18	0.12	0.37	0.38	0.49	2.79
Forest	12.24	11.55	2.82	11.85	19.77	20.00
Water	0.98	1.13	0.80	1.13	0.99	0.93
Totals	100.00	100.00	100.00	100.00	100.00	100.00

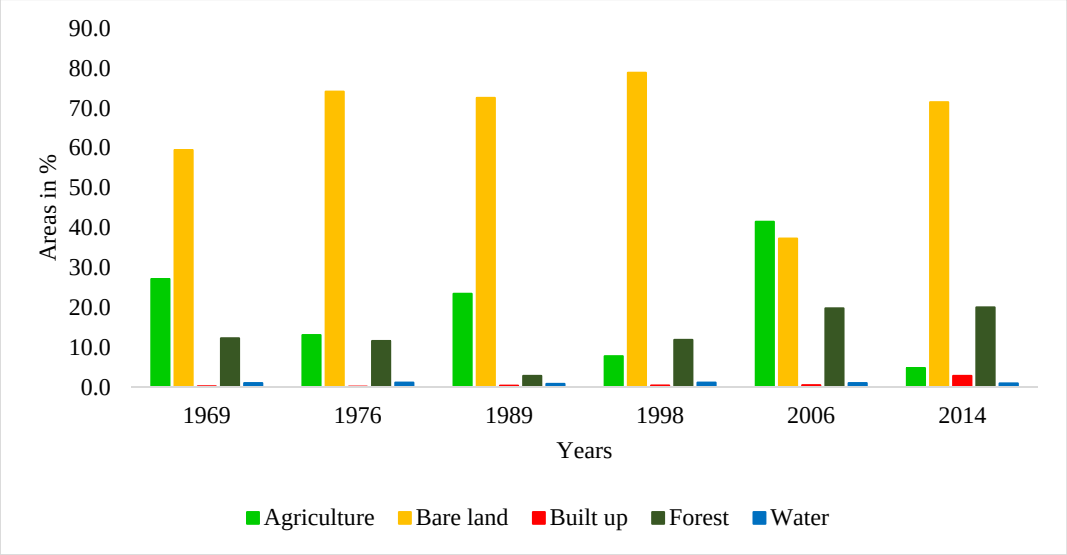

Figure 6.1: LULC types trends for all years, areas in percentages (%).

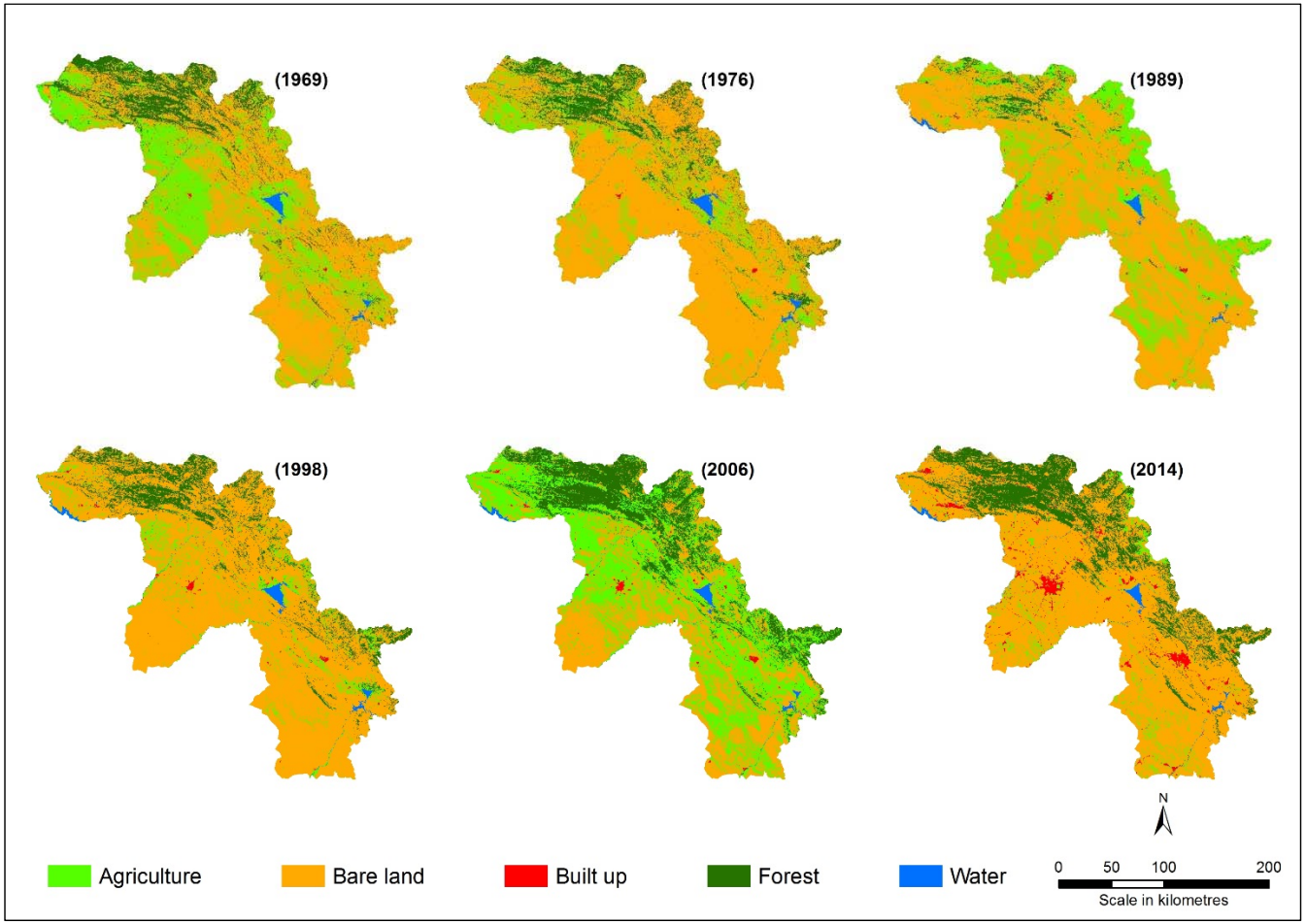

Figure 6.2: LULC final maps for all years.

6.4 "From-To" change detection analysis

6.4.1 Non-urban area

The trend of all five unchanged LULC classes, the major five LULC changed categories and net changes are shown in Figure 6.3, Figure 6.4, and Figure 6.5, respectively. All the change maps and their spatial distribution pattern changes are presented in (Figure 6.7 and Figure 6.8) and tables of statistics for the change detection are represented in (Table 6.5, Table 6.6, Table 6.7, and Table 6.8). For detailed tables of statistics for all LULC changes using the "From-To" approach in both km² and percentage (%), see Appendix C. The reasons for all the changes that occurred between every paired image (one epoch) are explained in the corresponded section in Chapter 7.

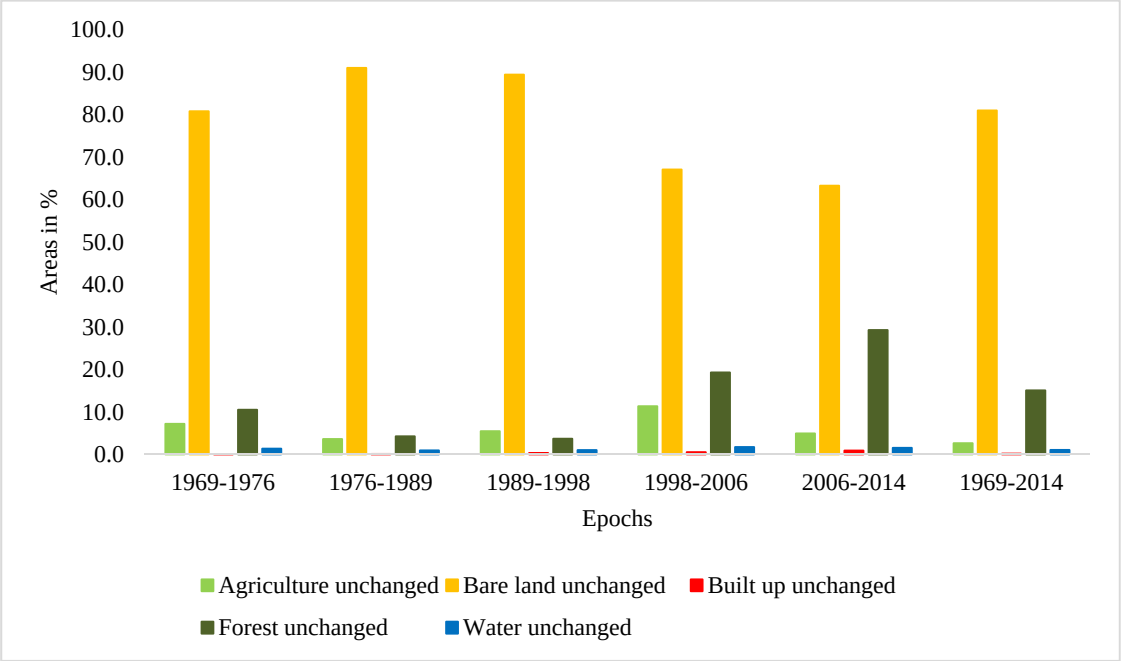

Figure 6.3: Unchanged LULC classes "From-To" in %.

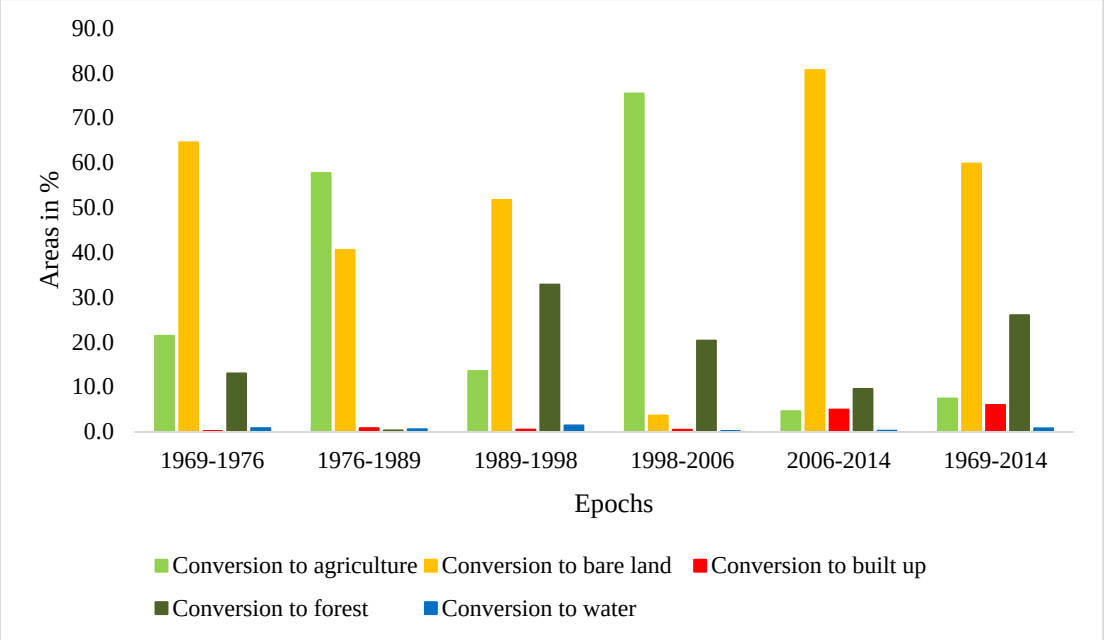

Figure 6.4: Five major changed LULC classes “From-To” in %.

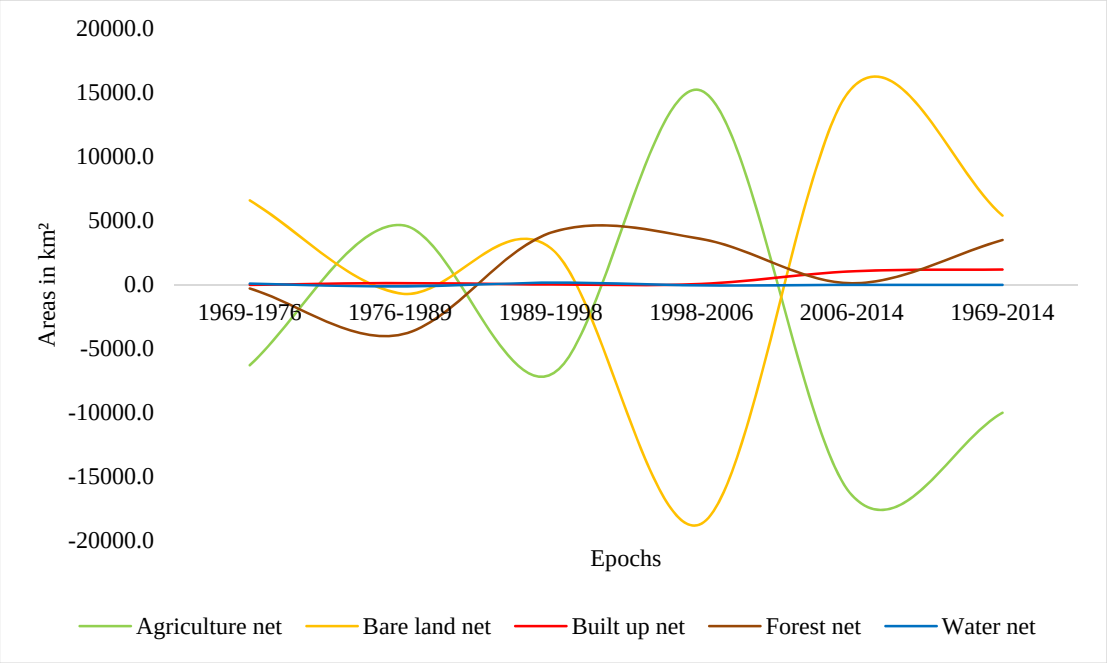

Figure 6.5: Trend of net LULC changes “From-To” method.

Table 6.5: Areas in KM² and percentage (%) in respect to total study areas.

Areas in KM² and percentage (%) in respect to total study areas						
Epochs	1969-1976	1976-1989	1989-1998	1998-2006	2006-2014	1969-2014
Unchanged	26427.9 (59)	28500.0 (63)	32351.3 (72)	23836.8 (53)	23783.7 (53)	24761.6 (55)
Changed	18529.2 (41)	16457.0 (37)	12605.7 (28)	21120.2 (47)	21173.4 (47)	20195.4 (44)
Totals	44957.1 (100)	44957.1 (100)	44957.1 (100)	44957.1 (100)	44957.1 (100)	44957.1 (100)

Table 6.6: Summary of unchanged LULC classes in %.

Change detection "From-To", areas in % in respect to unchanged areas only						
Epochs	1969-1976	1976-1989	1989-1998	1998-2006	2006-2014	1969-2014
Agriculture unchanged	7.2	3.6	5.5	11.3	4.9	2.6
Bare land unchanged	80.9	91.1	89.5	67.1	63.3	81.0
Built up unchanged	0.1	0.1	0.3	0.5	0.9	0.2
Forest unchanged	10.5	4.3	3.7	19.3	29.3	15.1
Water unchanged	1.3	0.9	1.0	1.7	1.5	1.1
Totals unchanged	100.0	100.0	100.0	100.0	100.0	100.0

Table 6.7: Summary of changed LULC classes conversion in %.

Change detection "From-To", areas in % in respect to changed areas only						
Epochs	1969-1976	1976-1989	1989-1998	1998-2006	2006-2014	1969-2014
Conversion to agriculture	21.4	57.7	13.6	75.5	4.6	7.4
Conversion to bare land	64.6	40.6	51.7	3.6	80.7	59.8
Conversion to built up	0.2	0.8	0.5	0.4	4.9	6.0
Conversion to forest	13.0	0.3	32.8	20.3	9.5	26.0
Conversion to water	0.8	0.5	1.4	0.1	0.2	0.8
Total of changed	100.0	100.0	100.0	100.0	100.0	100.0

Table 6.8: Gain, lose, and net for change detection “from-To” process.

Change detection the gain, lose, and net increase or decrease, areas in KM²						
Epochs	1969-1976	1976-1989	1989-1998	1998-2006	2006-2014	1969-2014
Agriculture gain	3966.1	9503.0	1708.2	15943.2	974.6	1496.1
Agriculture lose	10283.8	4840.7	8765.5	772.6	17469.9	11534.1
Agriculture net	-6317.8	4662.3	-7057.3	15170.5	-16495.2	-10037.9
Bare land gain	11965.3	6680.6	6519.4	762.9	17085.0	12083.2
Bare land lose	5379.4	7382.2	3677.4	19478.3	1697.3	6684.2
Bare land net	6585.9	-701.6	2842.0	-18715.4	15387.7	5399.0
Built up gain	31.4	131.9	62.6	90.7	1044.5	1209.4
Built up lose	59.5	16.4	57.0	44.4	9.2	34.7
Built up net	-28.1	115.6	5.6	46.3	1035.3	1174.7
Forest gain	2414.6	52.4	4137.8	4293.0	2021.1	5251.6
Forest lose	2722.9	3981.0	78.1	728.9	1920.9	1764.9
Forest net	-308.3	-3928.6	4059.7	3564.2	100.2	3486.7
Water gain	151.9	89.1	177.7	30.4	48.1	155.1
Water lose	83.6	236.8	27.7	96.0	76.2	177.6
Water net	68.3	-147.7	150.0	-65.6	-28.0	-22.5

The land use change maps for 1969-1976 are presented in (Figure 6.7 and Figure 6.8), and also the percentage of the five land use classes area (changed and unchanged) during this period are shown in (Table 6.5, Table 6.6, and Table 6.7). Results show that during this period 59 % (26427.9 km²) of the study area was not changed. Out of

the unchanged areas, 80.9 % (21368.0 km²) of the bare land has not changed (the largest percentage) followed by forest with 10.5 % (2780.0 km²) with the rest of the classes including agriculture, water, and built up areas having unchanged areas of 7.2 % (1904.1 km²), 1.3 % (355.5 km²), and 0.1 % (20.2 km²), respectively. Areas where LULC classes have changed cover 41 % (18529.2 km²) of the study area. Again bare land has the largest percentage of those changes (gained) with 64.6 % (11965.3 km²) and most of this transformation came from agriculture and forest with totals of 82.2 % (9836.0 km²) and 16.9 % (2019.5 km²), respectively. Also during this epoch, bare land has lost some areas with a total of 5379.4 km², which makes a total net increase in bare land area of 6585.9 km² (Table 6.8).

The land use change maps for 1976-1989 are presented in (Figure 6.7 and Figure 6.8), with changed and unchanged areas and their percentages are shown in (Table 6.5, Table 6.6, and Table 6.7). Results show that 63 % (28500.0 km²) of the study areas did not change in this period, with the changed areas being 37 % (16457.0 km²). From the unchanged areas, bare land had the largest percentage at 91.1 % (25950.1 km²) followed by forest with 4.3 % (1215.2 km²) with the rest of the classes including agriculture, water, and built up having totals of 3.6 % (1029.3 km²), 0.9 % (270.1 km²), and 0.1 % (35.2 km²), respectively. For the changed LULC classes, the largest percentage of those changes were in agriculture areas with 57.7 % (9503.0 km²) and most of this transformation came from bare land and forest with totals of 75.7 % (7191.2 km²) and 23.0 % (2184.7 km²), respectively. Agriculture has also lost some areas during this epoch; a total of 4840.7 km² of those were converted to other LULC classes which reduced the total increase for the agriculture area to net 4662.3 km² (Table 6.8).

For the period 1989-1998, the total percentage area without any change is 72 % (32351.3 km²) with the rest, a total of 28 % (12605.7 km²) regarded as changed area. The largest category for those unchanged areas is bare land with a total of 89.5 % (28953.3 km²) followed by agriculture with 5.5 % (1766.9 km²) and the rest of the classes including forest, water, and built up having totals of 3.7 % (1189.5 km²), 1.0 % (331.5 km²), and 0.3 % (110.1 km²), respectively. For the changed LULC classes, bare land areas have the largest percentage of those changes with 51.7 % (6519.4 km²) and most of this transformation coming from agriculture with a total of 98.1 %

(6397.5 km²). Also during this epoch, some 3677.4 km² of bare land was lost making the total net increase in bare land area 2842.2 km² (Table 6.8).

The period 1998-2006 can be regarded as the most significant period for the study especially after 2003 when the US and the coalition armies overthrew the Iraqi government. For this period, only 53 % (23783.7 km²) of the total area remain as unchanged areas, with the changed areas being 47 % (21173.4 km²). From the unchanged areas, bare land had the largest percentage at 67.1 % (15994.4 km²) followed by forest with 19.3 % (4598.5 km²) and the other classes including agriculture, water, and built up areas having totals of 11.3 % (2702.5 km²), 1.7 % (413.2 km²), and 0.5 % (128.3 km²), respectively. For the changed LULC classes, agriculture areas have the largest percentage of those changes with 75.5 % (15943.2 km²) most of which came from bare land and forest with total of 95.6 % (15238.1 km²) and 3.9 % (623.4 km²), respectively. During this epoch, agriculture also lost some areas with a total of 772.6 km² converted to other LULC classes which reduced the total increase for the agriculture area to net 15170.5 km² (Table 6.8).

For the period 2006-2014, results showed that 53 % (23783.7 km²) of the study areas was not changed, meanwhile the changed area was 47 % (21173.4 km²). From the unchanged areas, bare land has the largest percentage at 63.3 % (15060.1 km²) followed by forest with 29.3 % (6970.6 km²) and the remaining classes including agriculture, water, and built up areas having totals of 4.9 % (1175.8 km²), 1.5 % (367.4 km²), and 0.9 % (209.8 km²), respectively. For the changed LULC classes, bare land has the largest percentage of those changes with 80.7 % (17085.0 km²) and most of this gain coming from agriculture and forest with totals 89.4 % (15276.3 km²) and 10.2 % (1731.9 km²), respectively. Also during this epoch, a total of 1697.3 km² bare land was lost and converted to other LULC classes which led to the total net increase in bare land area to 15387.7 km² (Table 6.8).

The 1969-2014 covers all 45 years of LULC changes for the Kurdistan region. For this period, only 55 % (24761.6 km²) of the total area remains as unchanged areas with changed areas being 45 % (20195.4 km²). From the unchanged areas, bare land has the largest percentage of 81.0 % (20063.2 km²) followed by forest with 15.1 % (3738.0 km²) and the other classes including agriculture, water, and built up areas having totals of 2.6 % (653.9 km²), 1.1 % (261.5 km²), and 0.2 % (45.0 km²), respectively. For the changed classes, bare land areas have the largest percentage of

those changes with 59.9 % (12083.2 km²) with most of this transformation coming from agriculture and forest with total of 85.9 % (10374.0 km²) and 12.8 % (1541.6 km²), respectively. In general most of the built up areas was extended at the expense of bare land and agriculture with a minimum contribution from both classes of 95 % for the second epoch (1976-1989) during the evaluation from 1969 to 2014. Also during this epoch, bare land lost some areas converted to other classes, a total of 6684.2 km² which is making the total net increase in bare land area to 5399.0 km² (Table 6.8).

6.4.2 Urban area

During all epochs, the built up areas expanded, and specifically the areas surrounding the big cities of Erbil, Duhok, and Sulamani. The majority of this transition was coming from bare land followed by agriculture areas.

For the first epoch (1969-1976), built up areas gained a sum total of 31.4 km² from bare land, agriculture, forest, and water areas with total of 62.6 % (19.6 km²), 34.3 % (10.8 km²), 0.9 % (2.8 km²), and 0.3 % (0.1 km²), respectively. Also during this epoch, the built up areas also lost some areas converted to other classes, a total area of 59.5 km² has lost during this epoch which is making the total net loss of built up area to 28.1 km² (Table 6.8).

During the epoch (1976-1989), the built areas gained a total of 131.9 km², and this increase was coming from bare land, agriculture, forest and water areas with totals of 76.3 % (100.7 km²), 18.7 % (24.6 km²), 3.6 % (4.8 km²), and 1.4 % (1.8 km²), respectively. The built up also lost some areas converted to other classes, a total area of 16.4 km² was lost during this epoch making the total net increase of built up area of 115.6 km² (Table 6.8).

Built areas gained a total of 62.6 km² during the epoch (1989-1998), with this increase coming from bare land, agriculture, and water with totals of 50.0 % (31.3 km²), 48.0 % (30.0 km²), 2.0 % (1.3 km²), respectively. The built up also lost a total of 57.0 km² during this period, making a total net increase of the built up area of 5.6 km² (Table 6.8).

For the epoch (1998-2006), the built areas gained a total of 90.7 km², with this increase coming from bare land and agriculture with totals of 74.8 % (67.9 km²) and

24.5 % (22.2 km²), respectively. The built up class also lost a total area of 44.4 km² during this period, making the total net increase of built up area 46.3 km² (Table 6.8).

For the epoch (2006-2014), a total of 1044.5 km² of changed area was transformed to built up, with this gain was coming from agriculture, bare land, and forest areas with total of 59.8 % (624.1 km²), 38.7 % (404.6 km²), 1.4 % (14.9 km²), respectively. Also during this epoch, built up also lost 9.2 km² converted to other classes, making the total net increase of built up area 1035.3 km² (Table 6.8).

For the overall epoch (1969-2014), a total of 1209.4 km² of changed areas was converted to built up, and this gain was coming from agriculture, bare land, and forest areas with totals of 51.6 % (624.6 km²), 44.5 % (538.6 km²), 3.6 % (43.8 km²), respectively. Also the built up class has lost some areas with a total area of 34.7 km² converted to other classes, making the total net increase of built up area to be 1174.7 km² (Table 6.8).

According to the activities report for KRG in 2009 (Table 6.9 and Figure 6.6), the KRG distributed 68577 parcels of land to their citizens free of charges and especially in the surrounding areas of the three major cities (Erbil, Duhok, and Sulamani) to construct new buildings for residential, commercial, industrial, and others purposes (KRG, 2013). During the (2006-2014) period, the built up area increased dramatically from 219.02 km² to 1254.52 km² taking it to 2.3 % (1035.5 km²) of the total study area as a result of this new construction. Many local and foreign companies occupied the newly constructed buildings.

Table 6.9: Kurdistan Region Government 2009 annual report.

Governorates	Residential	Commercial	Industrial	Others	Parcels counts
Erbil	39430	1138	3216	590	44374
Sulamani	7645	1301	1456	171	10573
Duhok	12397	281	245	707	13630
Total	59472	2720	4917	1468	68577

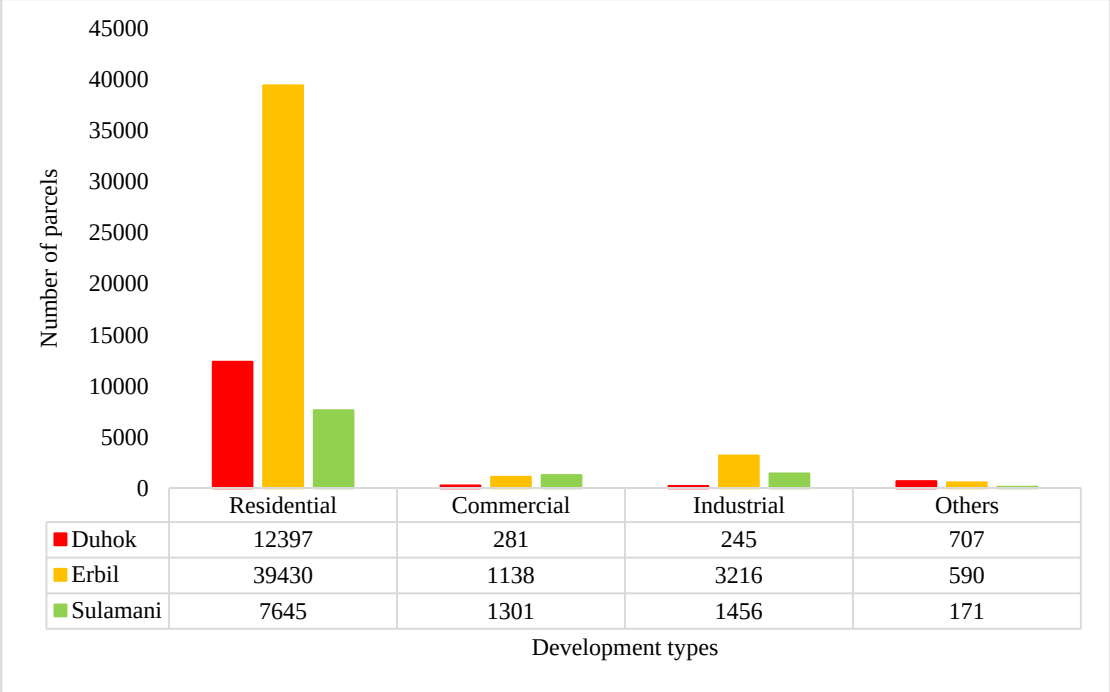

	Residential	Commercial	Industrial	Others
Duhok	12397	281	245	707
Erbil	39430	1138	3216	590
Sulamani	7645	1301	1456	171

Figure 6.6: Parcels of land for each Kurdistan region governorates.

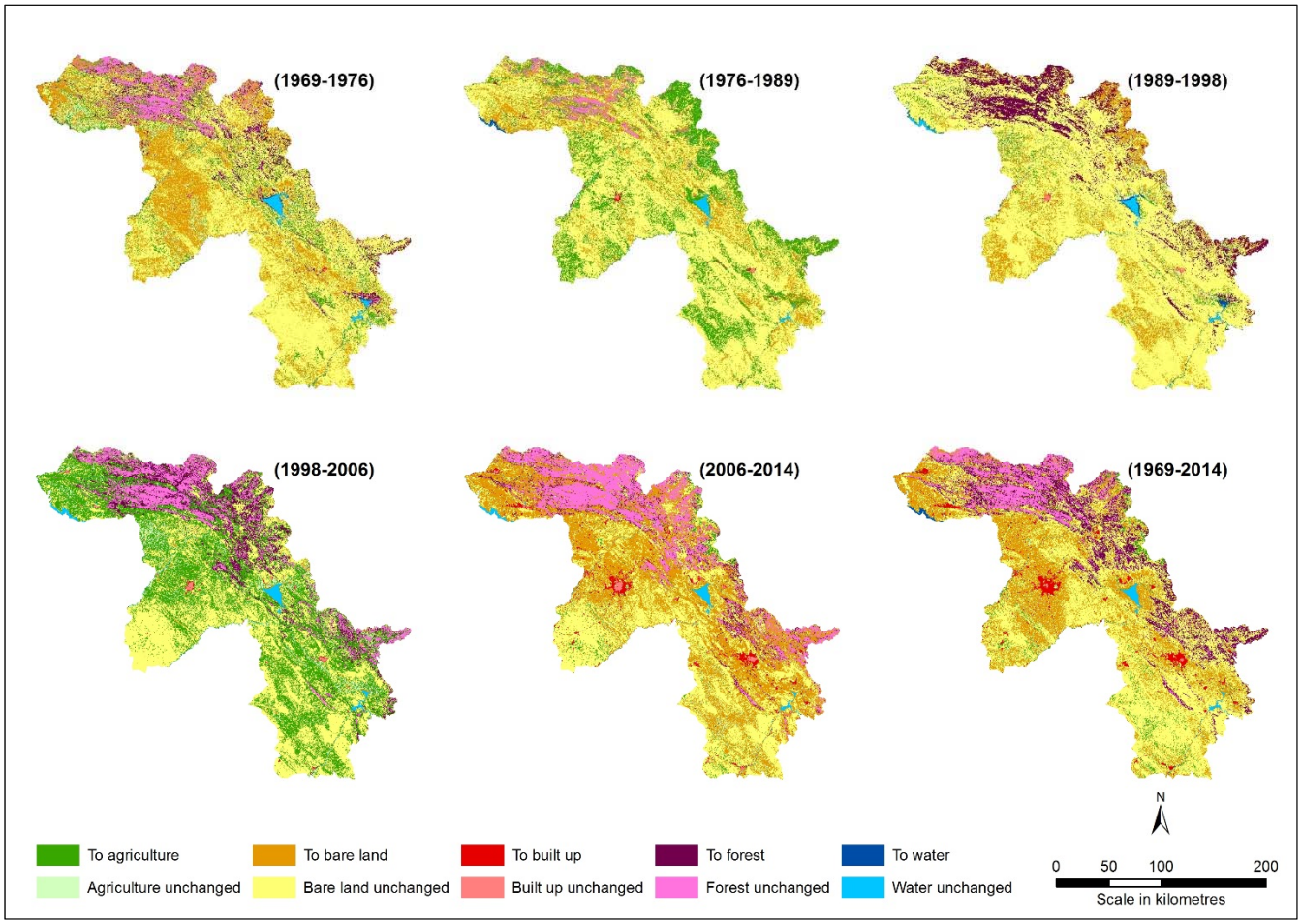

Figure 6.7: Change maps, all epochs (changed and unchanged classes).

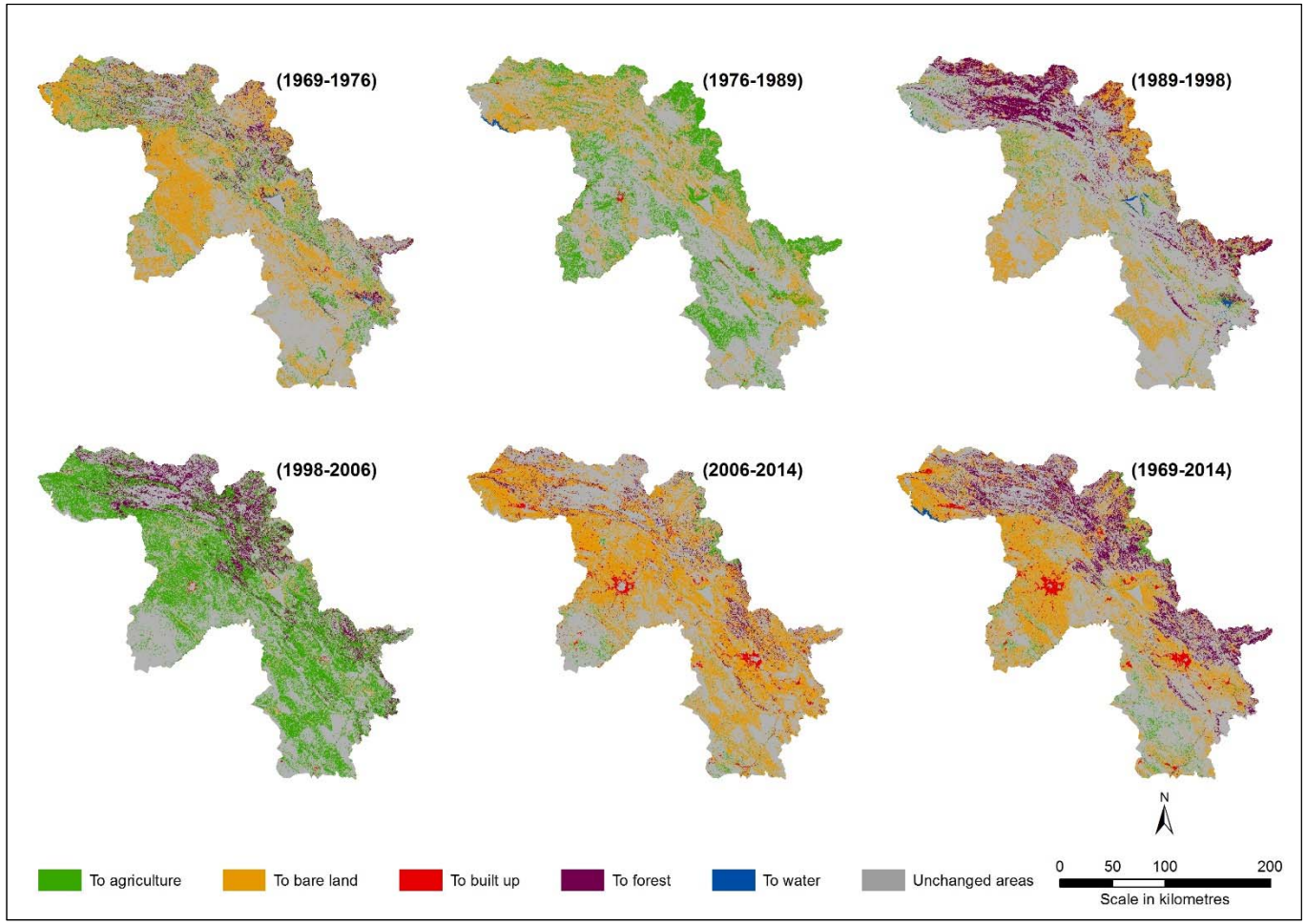

Figure 6.8: Change maps, five major conversion all epochs.

6.5 Population density and built up areas trends

The result of implementing Dasymetric population mapping can be found in the Figure 6.9. In addition, the spatial distribution of the population density data for the period 1969 to 2014 can be seen again in the same figure.

Using conventional Choropleth population mapping methods did not give the actual distribution of the population based on the type of land use or cover classes the spatial pattern of population density. Also, it did not highlight their effect on the land use or cover change according to the population growth. In addition, defining the relationship between the population increase and urban growth would not be possible based on choropleth maps.

Using choropleth maps for population, the phenomena of population distribution was evenly shared by all the land use or land cover types. Also, population data stayed aggregated evenly within the boundary of each district or sub-district level that was used for creating the choropleth population map (Figure 4.6). As is shown in the (Figure 6.9), Dasymetric mapping method has the ability to redistribute and disaggregate the population data very accurately according to the spatial geography of land use or cover maps.

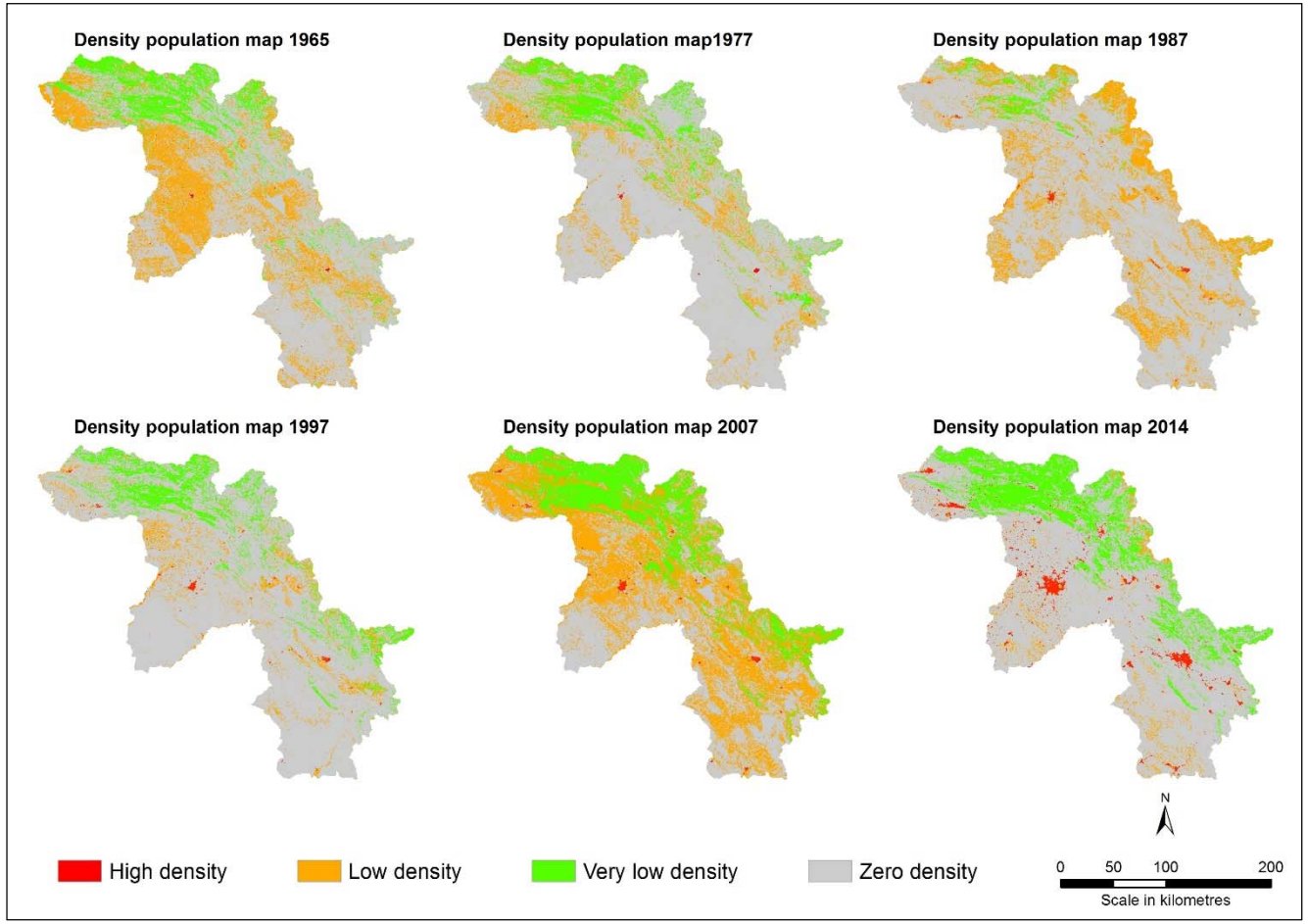

Figure 6.9: Dasymetric population density maps for Kurdistan region.

The trends of the built areas in Kurdistan can be found in the (Figure 6.10). As it shown in the figure, the built areas have increased overall for all the three Kurdistan region governorates, although there some decrease occurred after 1969 to 1976. After 1989, the negative trend was reversed specially after 1991 and really began considerable expansion after 2006. The built up areas started to increase again after 1991 when the Kurds were able to get their freedom as an autonomous from the central government in Baghdad region and they were able to rebuild their region again, but with limited capabilities.

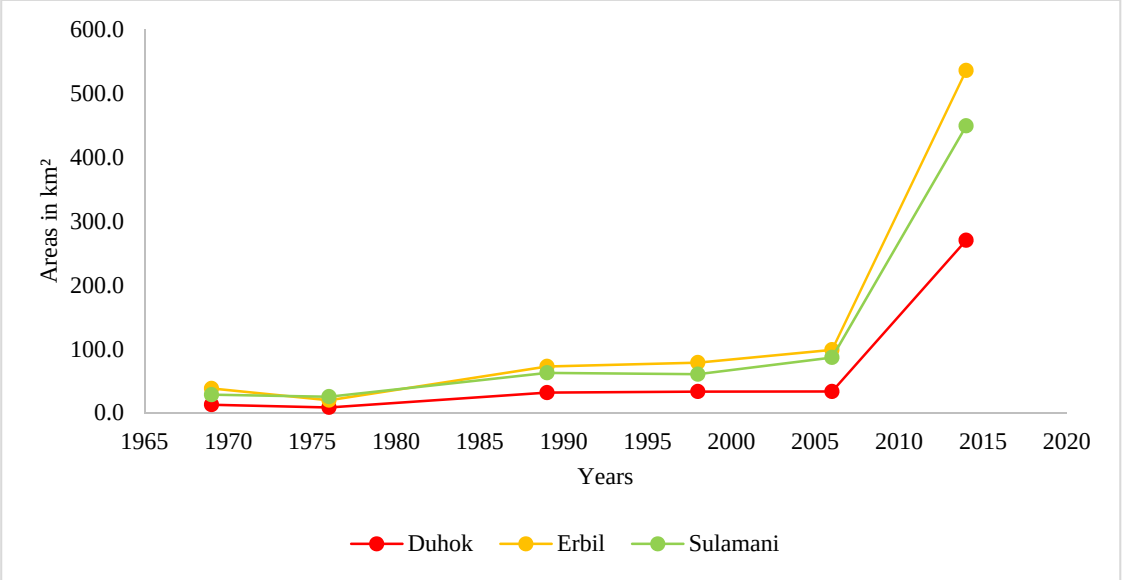

Figure 6.10: Built up trends for Kurdistan region governorates.

From (Figure 6.10) and Table 6.10, it is very clear that the built up areas have been increasing dramatically after 2006 for the Kurdistan region in general and for the capital city (Erbil) specifically.

Table 6.10: Built up areas trend for the entire Kurdistan region in km².

Years	Duhok	Erbil	Sulamani
1969	12.86	38.29	28.56
1976	8.58	19.85	25.39
1989	31.75	72.72	62.68
1998	33.42	78.70	60.60
2006	33.54	98.70	86.77
2014	270.00	535.57	448.92
Total	390.15	843.83	712.92

The average annual rates for the urban expansion for the three governorates for the last 45 years are 8.67 km², 18.75 km², and 15.84 km² for Duhok, Erbil, and Sulamani, respectively. This growth is not uniform because of the variation in the number of years between every two consecutive years. Also there is a decrease in the urban areas by 3.7 km² per year during the epoch 1969 to 1976 for the entire Kurdistan region (Table 6.11).

Table 6.11: Mean annual rates for urban expansion for Kurdistan region.

Epochs	Number of years	Duhok	Erbil	Sulamani	Total km²/year
1969-1976	7	-0.61	-2.63	-0.45	-3.70
1976-1989	13	1.78	4.07	2.87	8.72
1989-1998	9	0.19	0.66	-0.30	0.55
1998-2006	8	0.01	2.50	3.27	5.79
2006-2014	8	29.56	54.61	45.27	129.44
1969-2014	45	8.67	18.75	15.84	43.26

6.6 Population increase and urban expansion

In many countries, especially overcrowded countries such as China, India and Bangladesh, the relationship between population increase and urban expansion have been the driving factor for urban growth. Econometric model and regression analysis have been used very widely for many case studies around the globe. For this study the only data available for the analysis of the urban growth is population and therefore, the regression analysis approach was used to define the relationship between population increase and urban expansion for the Kurdistan region. The (Figure 6.11) shows the trends of population increase and urban expansion for the Kurdistan region for the period 1969 to 2014.

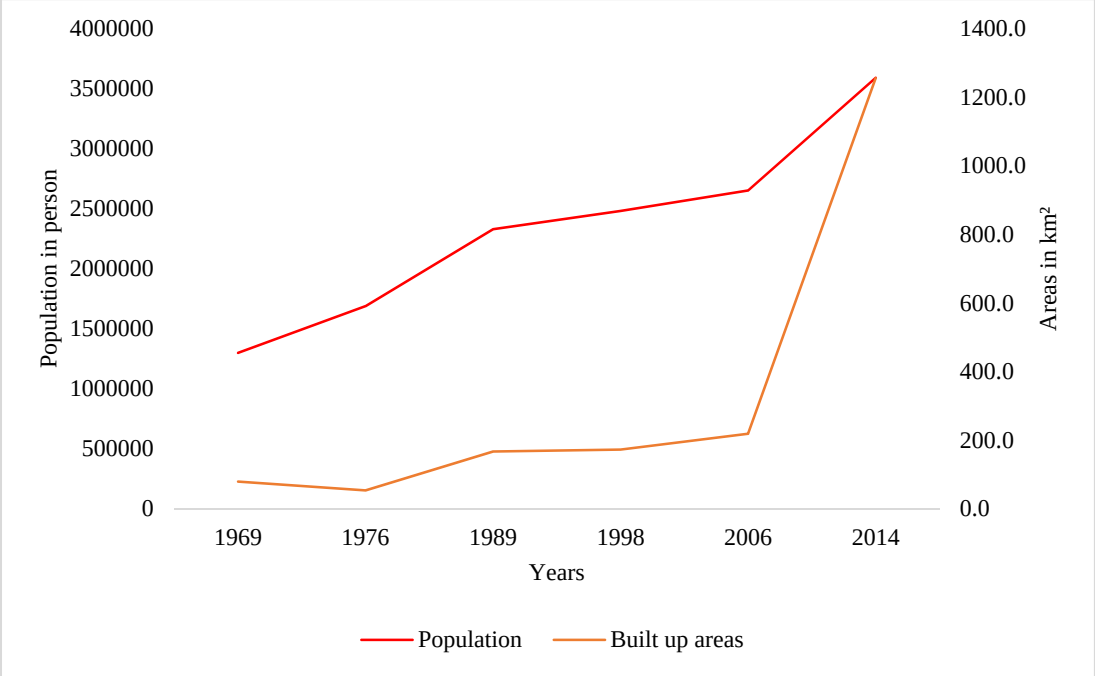

Figure 6.11: Trend of population and built up areas for the Kurdistan region.

It can be seen in Figure 6.12 and Figure 6.13 that there is positive, but nonlinear relationship between population increase and urban extension and this relationship should be continuous as the main driving factor for the urban expansion is the population increase. However there is a decrease in the built up area for the period 1969 to 1976 in spite of the population increase (refer to discussion section in Chapter 7 for more details). Also during this period, the rate of population increase was lower as many Kurdish citizens were displaced or may have been killed by Iraqi army troops during the Anfal campaign in late 1980s. However, Figure 6.12 does not show that as the annual population growth rate for Kurdistan has been almost 3 % annually. Nevertheless, population is still the main factor of urban expansion as it is the case for the parts of the world.

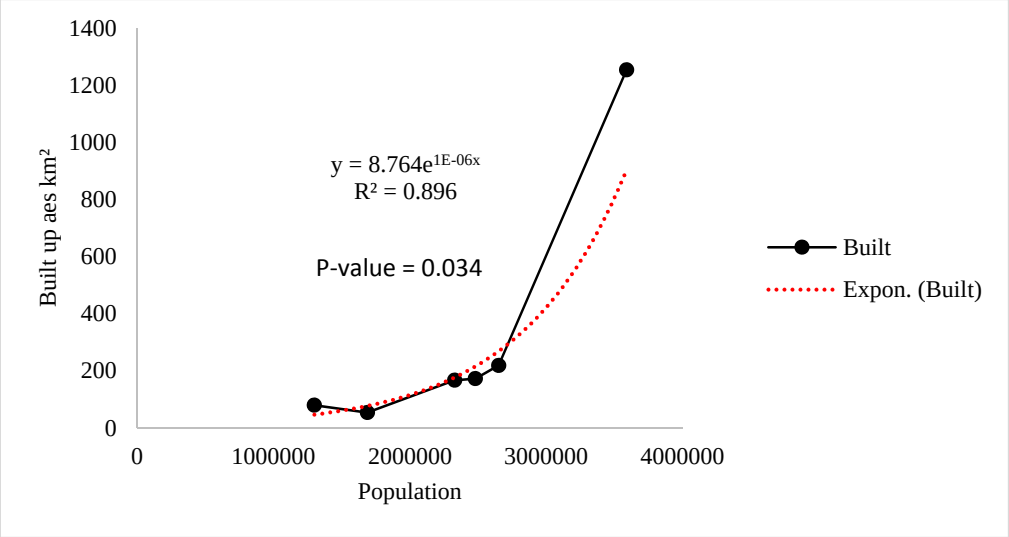

Figure 6.12: Relationship between built up areas and population increase.

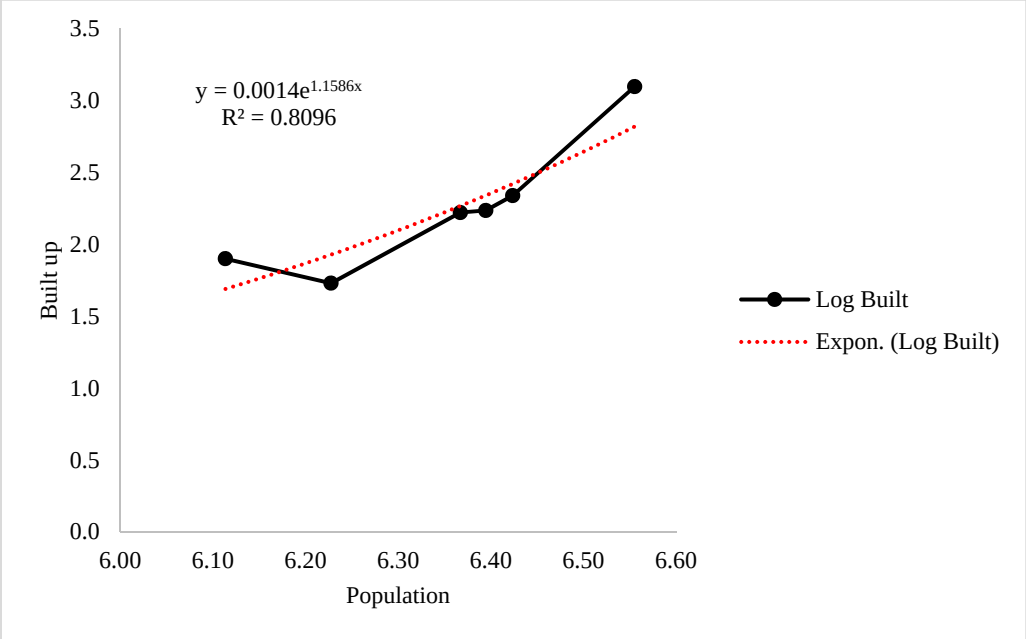

Figure 6.13: Logarithm transformation between built up areas and population.

6.7 Population density and urban expansion

Population density is another measure that can be used to define the relationship with urban growth areas beside population data. Since the density is extracted based on the Dasymetric mapping which used different levels of density, this measure may provide a better relationship with urban expansion. As shown in the (Figure 6.14) it is very

clear there is a stronger relationship between urban expansion and population density when compared with population data.

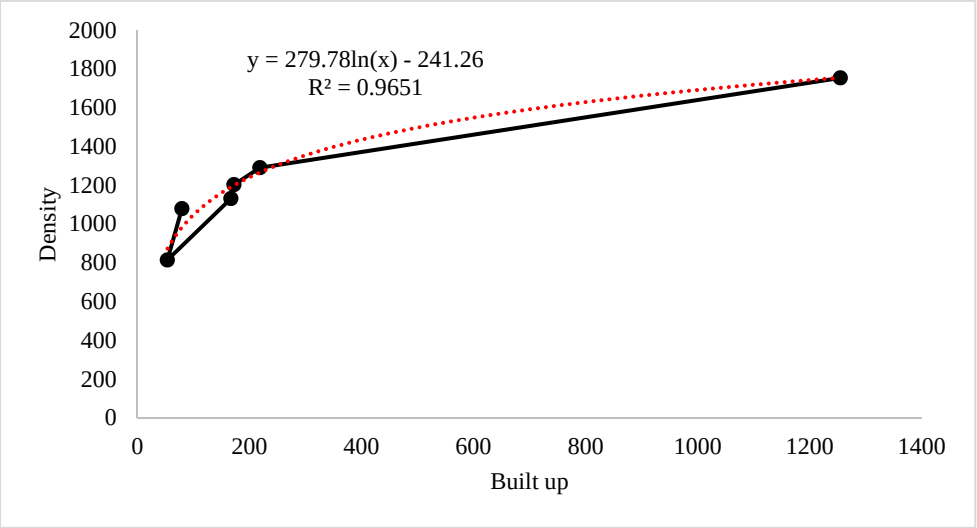

Figure 6.14: Relationship between population density and built up areas.

6.8 Urban development types for Kurdistan region

To be able to analyse the urban expansion in more detail at the local scale, individual analysis of urban expansion was carried out for the major centres of three cities of the Kurdistan region as most expansions occurred within a radius of 20 km around the centre of three cities. For detailed “from-To” change detection results statistics within 20 km radius, refer to Appendixes D and E.

6.8.1 Duhok city expansion

Duhok governorate is located in the north and northwest of the Kurdistan region with an area of 10291 km², and is third in terms of areas among the Kurdistan region governorates. Duhok consists of seven districts of which the largest one is Amedi with a total area of 2806.99 km². The total population of this governorate is about 673,264 (KRG 2013). The city of Duhok has experienced urban changes from 1969 to 2014, and Figure 6.15 shows the trends of this urban expansion. The expansion increased relatively steadily until 2006 after which, there was a significant shift in the rate of expansion.

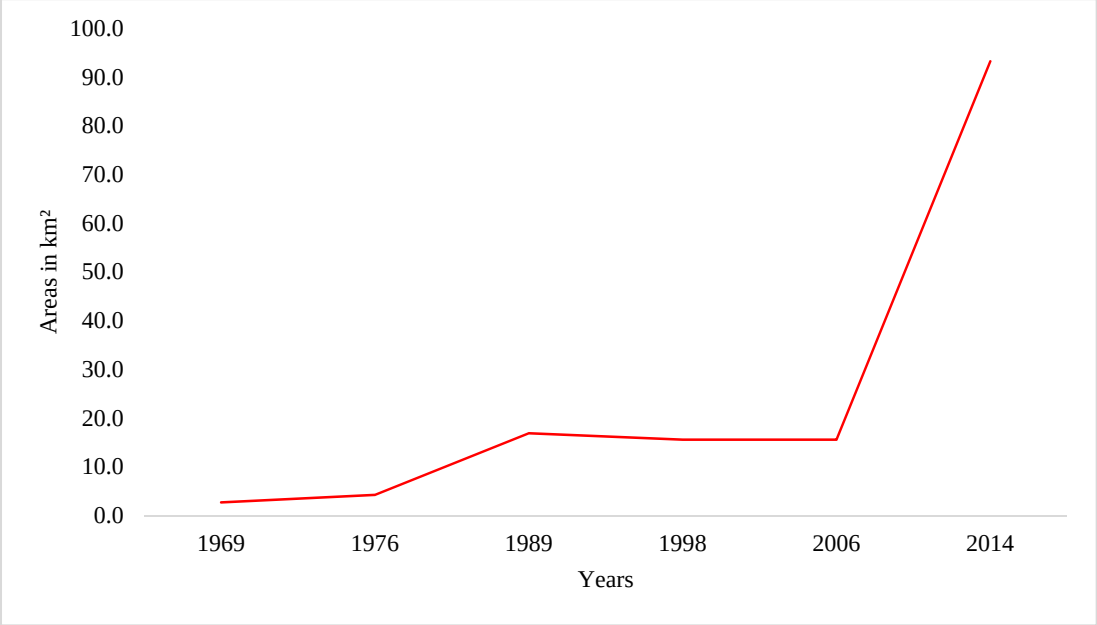

Figure 6.15: Urban areas trends for Duhok from 1969 to 2014.

The spatial pattern of the urban expansion, urban development types, and density levels for the city centre within a 20 km buffer is shown in Figure 6.16. The city has expanded dramatically since 1969 to 2014 (Figure 6.17) and experienced three types of development during this period. The density levels (Figure 6.16) support that the city has experienced big changes in the urban landscape of the city centre because of population increase.

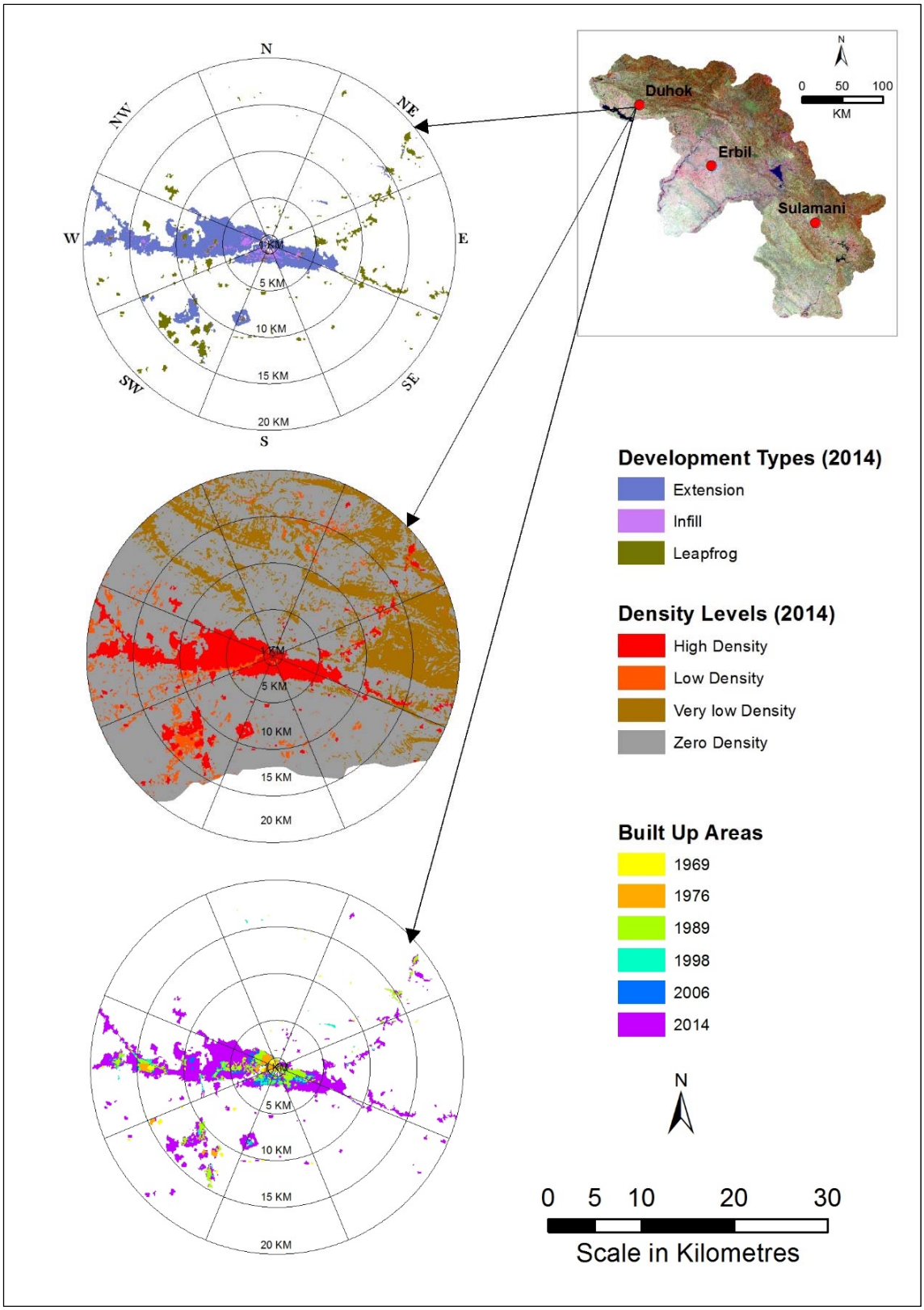

Figure 6.16: Development types, density level and urban areas for Duhok.

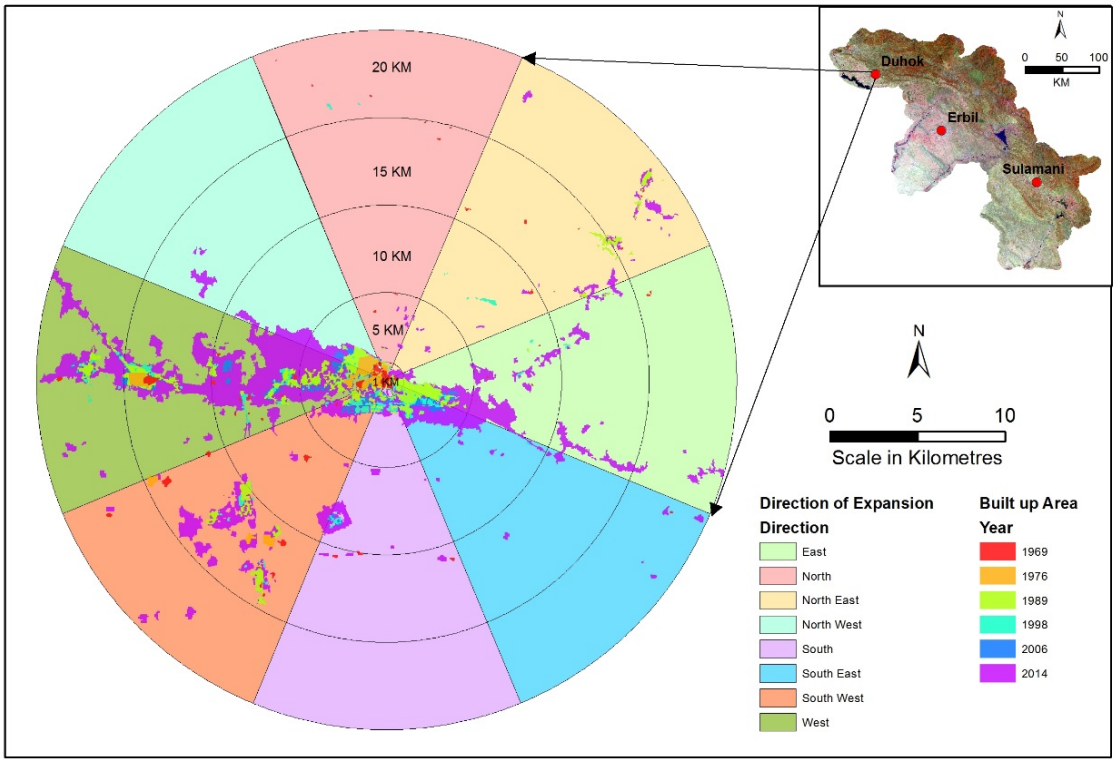

Figure 6.17: Directions of urban expansion for Duhok city.

The total expansion for the Duhok city from 1969 to 2014 within a radius of 20 km for all directions is 118.92 km², with a mean annual rate of 2.64 km² per year. Figure 6.18 shows that the city is extending in a generally westerly direction with a total expansion of 54.24 km² from 1969 to 2014.

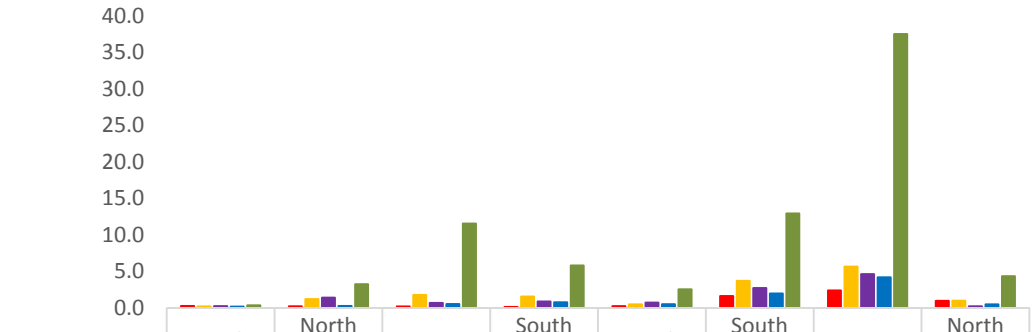

	North	North East	East	South East	South	South West	West	North West
1969 to 1976	0.23	0.18	0.16	0.09	0.20	1.58	2.35	0.94
1976 to 1989	0.16	1.18	1.75	1.51	0.45	3.67	5.63	0.95
1989 to 1998	0.21	1.38	0.64	0.84	0.70	2.69	4.59	0.18
1998 to 2006	0.14	0.22	0.48	0.72	0.47	1.93	4.16	0.45
2006 to 2014	0.32	3.21	11.53	5.78	2.52	12.91	37.51	4.32

Figure 6.18: Duhok city urban statistics to directions, areas in km².

Table 6.12 shows the three types of expansion that the city of Duhok experienced during the period 1969 to 2014. The table shows that the extension development is always the main urban development type with a minimum increase in (1969-1976) of 61 % of the total expansion that the city of Duhok experienced.

Table 6.12: Urban expansion development types for Duhok city.

	Areas in KM²			Areas in %		
Epochs	Extension	Infill	Leapfrog	Extension	Infill	Leapfrog
1969 to 1976	3.48	0.15	2.08	61	3	36
1976 to 1989	8.89	0.08	6.33	58	1	41
1989 to 1998	8.56	1.01	1.65	76	9	15
1998 to 2006	6.22	1.18	1.19	72	14	14
2006 to 2014	54.00	3.46	20.64	69	4	26

In addition, the city expansion has been examined with multiple buffers (5, 10, 15, and 20 km) and Figure 6.19 shows the types of expansion within each buffer ring and the increase in built up areas that has occurred during the study period.

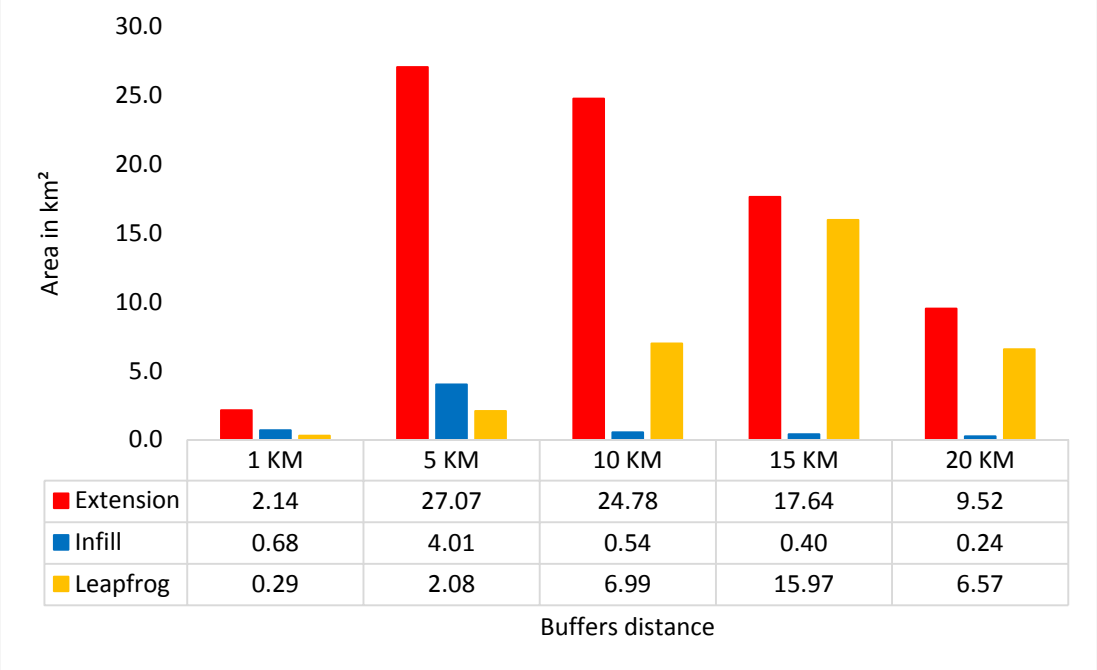

Figure 6.19: Duhok city expansion types within different buffers distance.

Also, the city of Duhok was examined and evaluated from 1969 to 2014 using direction of expansion in regards to the type of urban expansion that occurred during

this period (Table 6.13 and Figure 6.20). The table shows that the city has expanded dramatically in the westerly direction with a total of 46.00 km² as an extension.

Table 6.13: Urban development types and directions for Duhok city, areas km²

Directions	Extension	Infill	Leapfrog	Totals
North	0.50	0.04	0.53	1.07
North East	1.45	0.01	4.70	6.16
East	7.48	0.30	6.78	14.56
South East	6.45	0.98	1.51	8.95
South	2.44	0.69	1.21	4.34
South West	11.62	1.10	10.05	22.78
West	46.00	2.38	5.87	54.24
North West	5.21	0.38	1.24	6.83
Totals	81.15	5.88	31.89	118.92

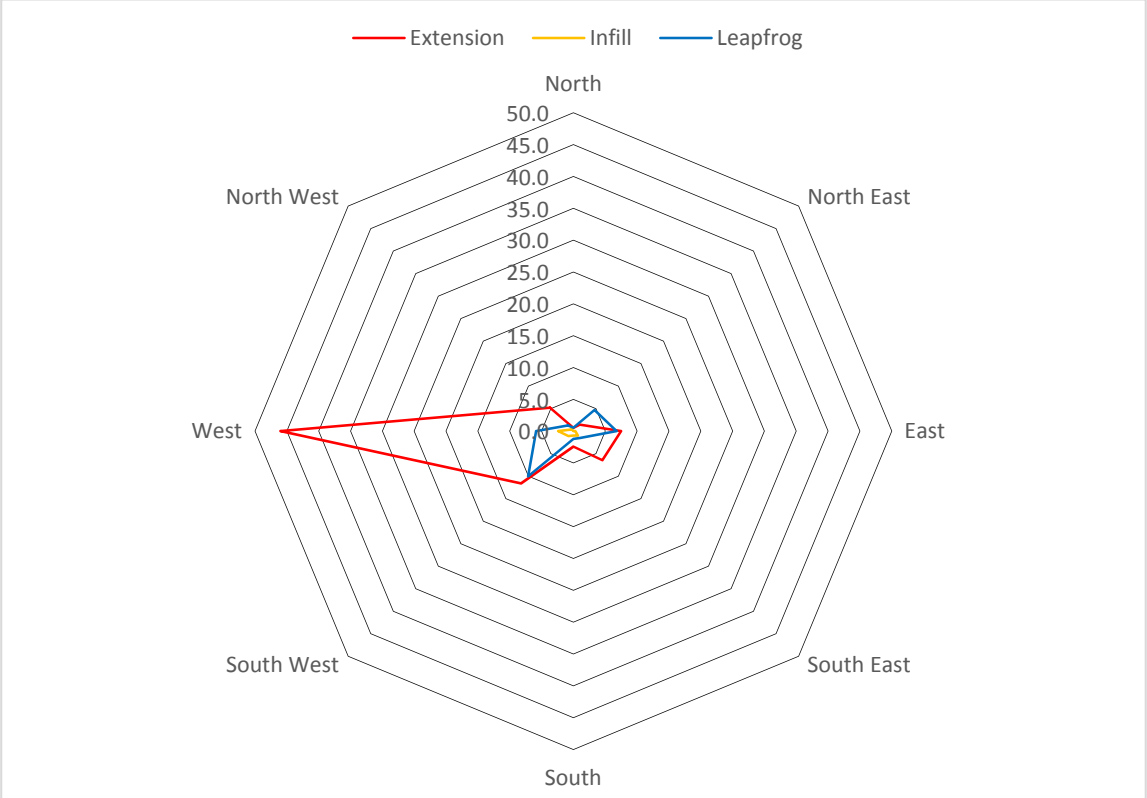

Figure 6.20: Sum area of urban expansion, Duhok city (1969 to 2014) in km².

6.8.2 Erbil city expansion

Erbil governorate is the capital city of Iraqi Kurdistan and is located in the middle of the Kurdistan region with an area of 15408.74 km², which makes it the second largest city in terms of area among the Kurdistan region governorates. Erbil consists of ten districts of which the largest one is Makhmur district with an area of 3518.31 km². The total population for the capital city is about 1,344,966 (KRG 2013). The city of Erbil has seen a massive expansion in the urban areas from 1969 to 2014. Figure 6.21 shows the urban expansion trends that occurred during the period from 1969 to 2014. As with the city of Duhok, the city has experienced dramatic changes in the built up after 2006 with previous years witnessing changes as well but at a much lower rate.

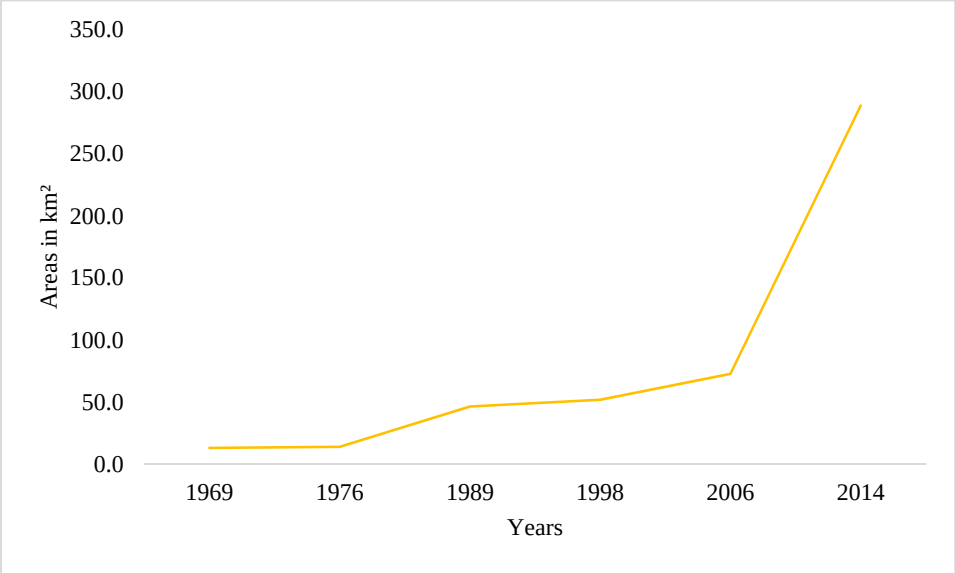

Figure 6.21: Urban areas trends for Erbil from 1969 to 2014.

The spatial pattern of the urban expansion types, density levels areas and areal extent of the built up areas for the city are shown in Figure 6.22 and Figure 6.23. For the span of 45 years the boundary of the city of Erbil has increased dramatically and all types of development have been experienced. The city has expanded in all directions, as the circular shape of the city is one of the factors which govern the direction of the city expansion.

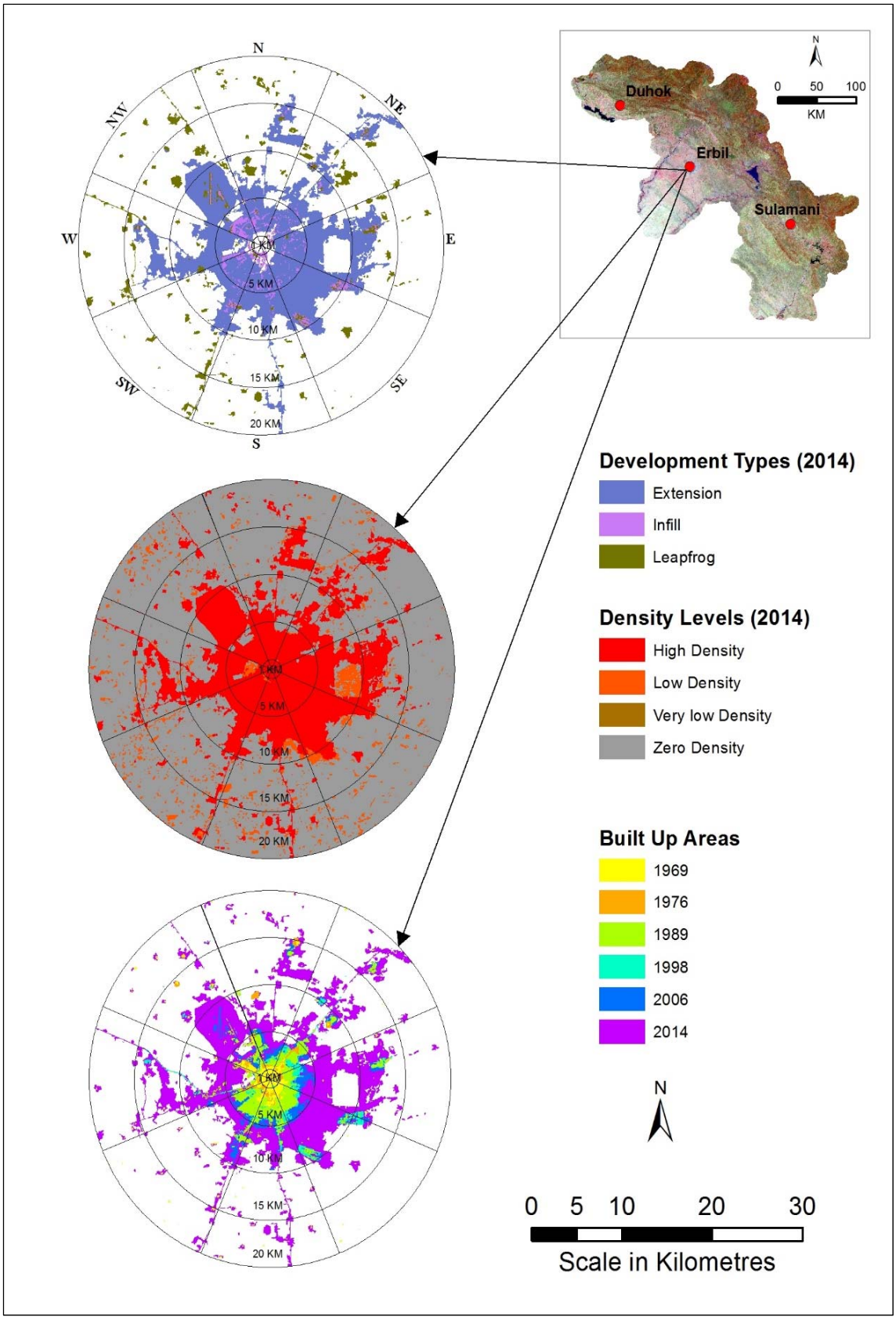

Figure 6.22: Development types, density level and urban areas for Erbil.

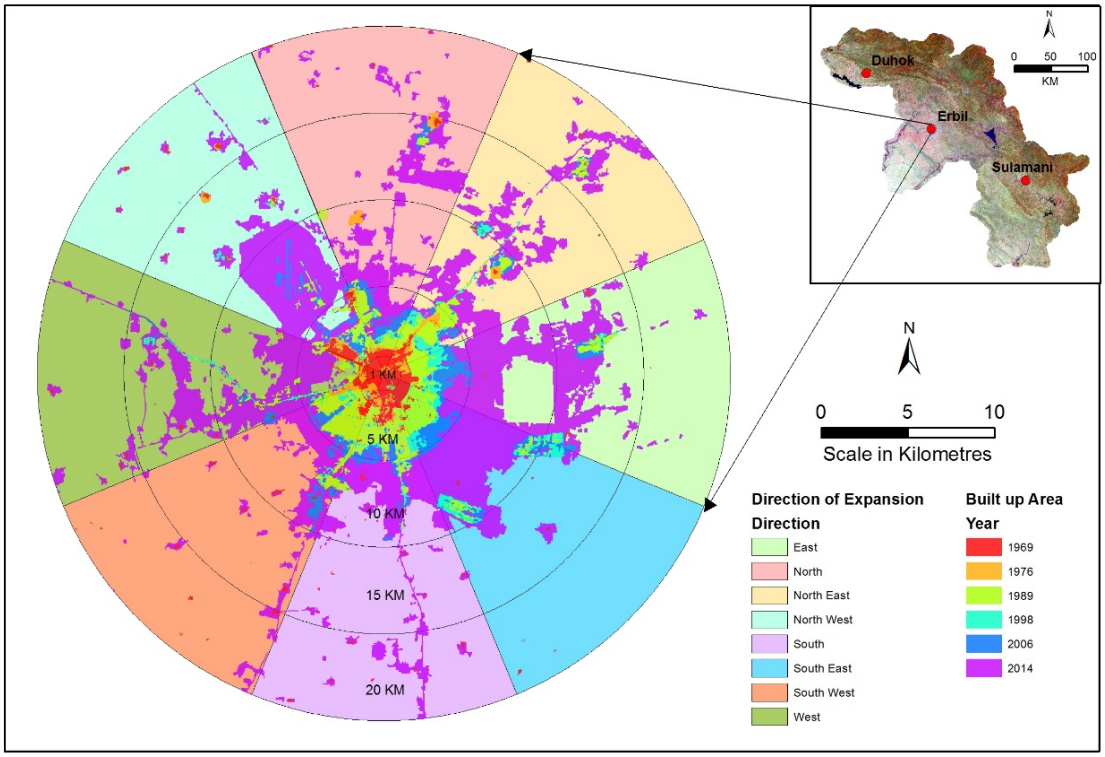

Figure 6.23: Directions of urban expansion for Erbil city.

Figure 6.24 show that the city is extending in all directions within a radius of 20 km with a total expansion of 316.20 km² from 1969 to 2014, and with an annual rate of 7.03 km² per year. The city has expanded with minimum expansion in a southwest direction with a total of 30.46 km² and maximum expansion in a northwest direction with a total of 47.74 km². As the citadel is located in the centre of the city, this circular citadel caused the city to expand in a circular pattern during the urban development. Therefore, the city has expanded in all direction with massive increase. This expansion has been at the expense of other land cover types.

	North	North East	East	South East	South	South West	West	North West
1969 to 1976	1.43	1.73	0.68	0.62	1.96	1.59	1.16	1.78
1976 to 1989	3.90	5.80	2.83	5.38	7.06	6.82	2.34	3.77
1989 to 1998	1.23	3.21	2.35	3.41	1.87	2.04	3.11	3.22
1998 to 2006	3.33	3.09	4.21	4.30	3.18	4.79	2.25	4.37
2006 to 2014	22.28	26.80	37.14	26.45	20.97	15.23	33.95	34.60

Figure 6.24: Erbil city urban statistics to directions, areas in km².

The Table 6.14 shows the three types of expansion that the city of Erbil experienced over the 45 years. The city of Erbil has experienced all three type of development with extension contributing the largest area. In recent years the city has extended in all directions in response to the developing economy and the increase in the population.

Table 6.14: Urban expansion development types for Erbil city.

	Areas in KM²			Areas in %		
Epochs	Extension	Infill	Leapfrog	Extension	Infill	Leapfrog
1969 to 1976	3.49	2.35	5.10	32	21	47
1976 to 1989	29.96	0.92	7.00	79	2	18
1989 to 1998	14.17	3.14	3.13	69	15	15
1998 to 2006	22.23	3.56	3.72	75	12	13
2006 to 2014	175.49	8.94	32.99	81	4	15

The urban expansion for the city of Erbil was examined with multiple buffers rings and Figure 6.25 showing the types of expansion within each buffer ring and the amount of areas increase within those buffer distance. Within the 1 km buffer, the city did not change as there are no spare space for new development as the city centre is

already compacted with historic citadel and buildings at the start date of this study. The citadel is in the centre of the city within the 1 km buffer and has recently been regarded as a Heritage Centre place by UNESCO World Heritage Centre. The city has expanded within the 1 km-5 km annulus and further but the biggest increase occurred within the 5 km-10 km annulus with 122.47 km² extension and followed by 1 km-5 km annulus with 62.84 km² and the 10 km-15 km annulus increased by 49.52 km² again with extension as the main development type.

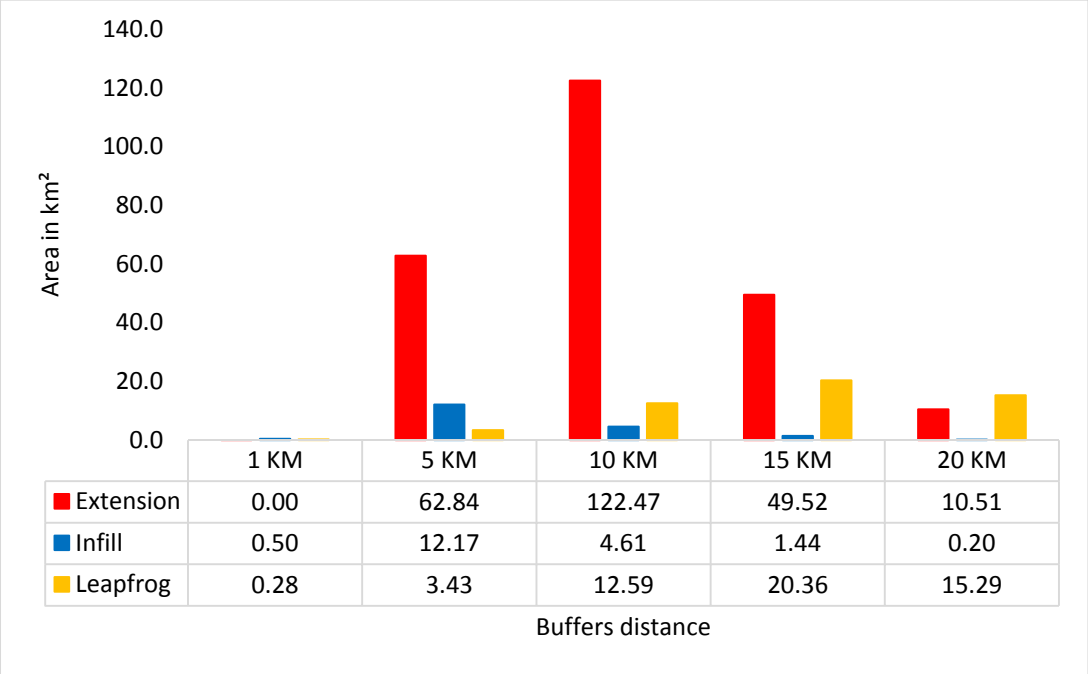

	1 KM	5 KM	10 KM	15 KM	20 KM
Extension	0.00	62.84	122.47	49.52	10.51
Infill	0.50	12.17	4.61	1.44	0.20
Leapfrog	0.28	3.43	12.59	20.36	15.29

Figure 6.25: Erbil city expansion types within different buffers distance.

The city of Erbil was examined using direction of expansion in regards to the type of urban expansion that occurred from 1969 to 2014 shown in Table 6.15 and Figure 6.26. The table shows that the city has expanded dramatically in every direction but with various amount of urban expansion. The city has expanded by 316.20 km² from 1969 to 2014 in every direction and the extension is the main development type that the city has experienced. Also, Figure 6.26 shows that the city has expanded dramatically in every direction since 1969 to 2014 with extension as the urban expansion type.

Table 6.15: Urban development types and directions for Erbil city, areas km²

Directions	Extension	Infill	Leapfrog	Totals
North	23.93	1.73	6.51	32.16
North East	31.14	1.95	7.55	40.64
East	41.16	1.70	4.36	47.22
South East	34.36	3.00	2.79	40.15
South	26.68	2.80	5.54	35.02
South West	20.65	2.97	6.83	30.46
West	33.57	1.20	8.04	42.81
North West	33.84	3.57	10.33	47.74
Totals	245.34	18.92	51.94	316.20

Figure 6.26: Sum area of urban expansion, Erbil city (1969 to 2014) in km².

6.8.3 Sulamani city expansion

Sulamani governorate is the capital city of the Kurdish culture for the Iraqi Kurdistan that is located in the south and southeast of the Kurdistan region with an area of 19257.02 km², which make it the largest governorate in terms of area. Sulamani consists of 15 districts, the largest of which is Chamchamal with an area of 3581.13 km². The total population for this governorate is about 1,927,615 (KRG 2013). The city of Sulamani has also experienced massive expansion in the urban areas from

1969 to 2014. As can be seen in Figure 6.27, the trends of the built up areas have the same pattern of increase as the other two cities. It is clear that this rapid urban expansion in the built areas has largely occurred after 2006 for the entire Kurdistan region.

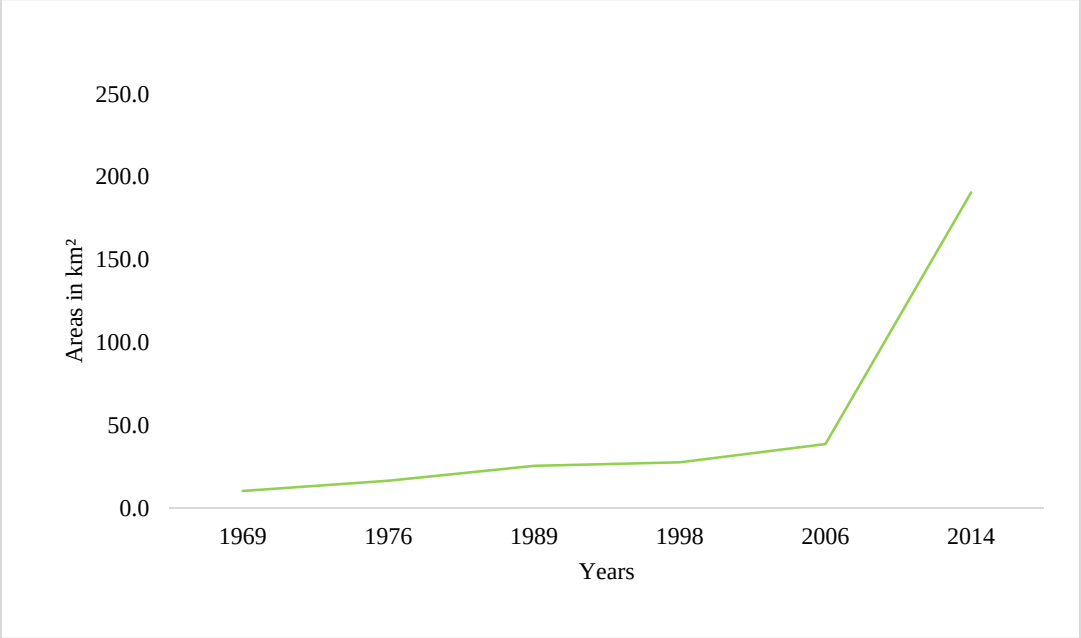

Figure 6.27: Urban areas trends for Sulamani from 1969 to 2014.

The areal extent and spatial pattern of the urban areas and their expansion in terms of development types and density levels for the city are shown in Figure 6.28 and Figure 6.29. The city of Sulamani has experienced the same dramatic increase in built area as Duhok and Erbil did since 2006. The major change in the city boundary in terms of urban areas has occurred mostly in the western direction and with extension as the major development type. As with Erbil, the city centre within the 1 km buffer distance did not change as the city centre was already built out at the start date of this study.

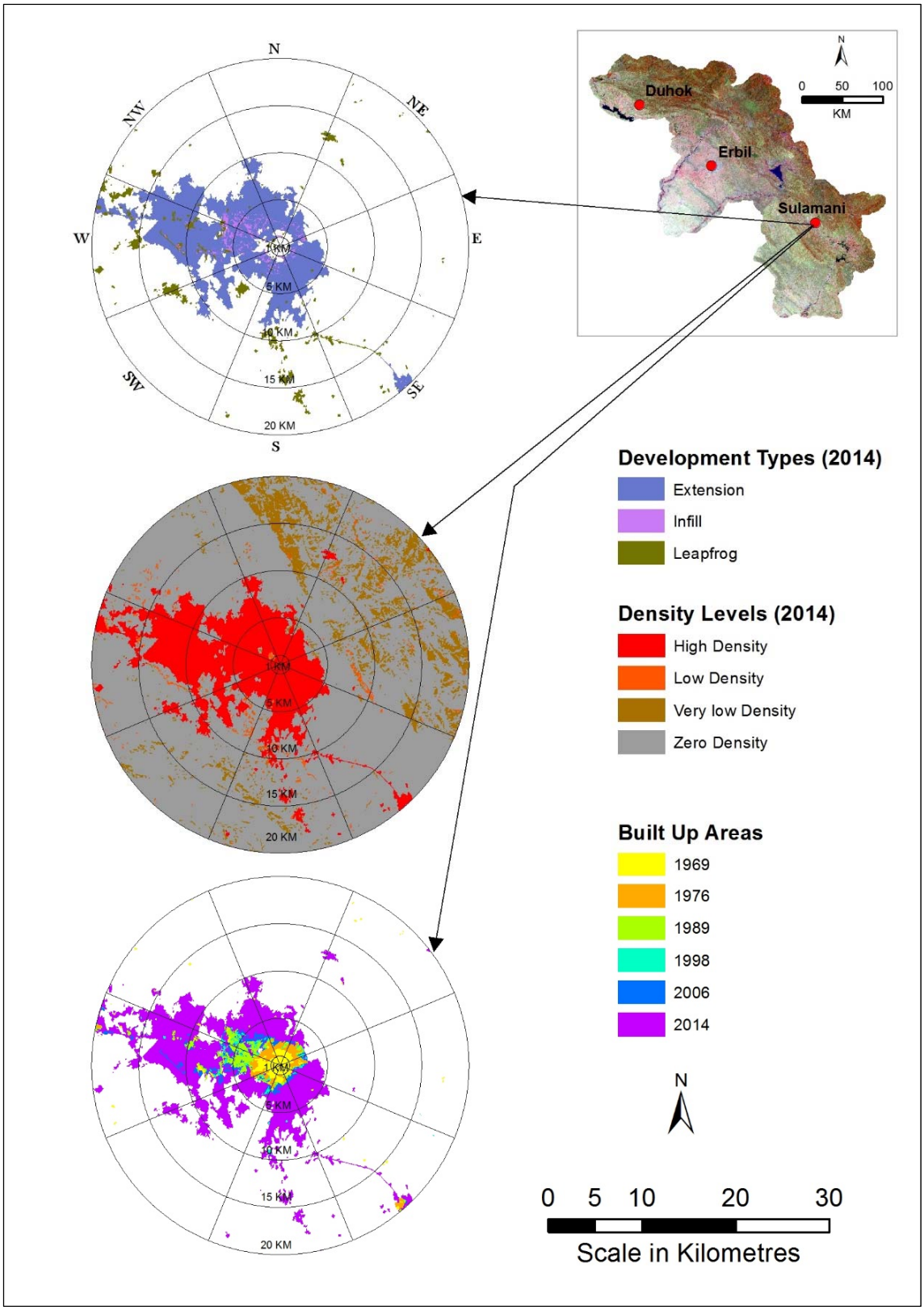

Figure 6.28: Development types, density level and urban areas for Sulamani.

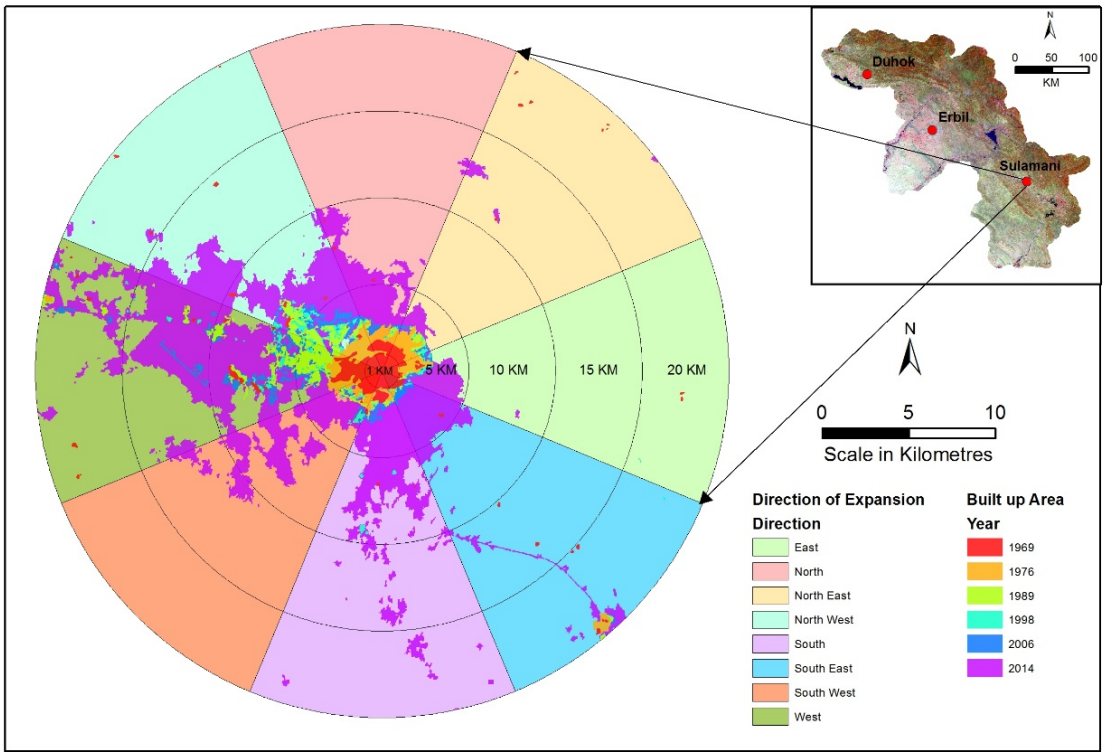

Figure 6.29: Directions of urban expansion for Sulamani city.

Figure 6.30 show a total expansion of 203.43 km² from 1969 to 2014 within the radius of 20 km, and with a mean annual rate of 4.52 km² per year. The bulk of expansion is toward the west and northwest direction from 1969 to 2014 with total expansion of 74.25 km² and 37.32 km², respectively.

	North	North East	East	South East	South	South West	West	North West
1969 to 1976	1.19	1.61	1.05	1.13	0.55	0.75	2.53	2.21
1976 to 1989	0.90	0.72	0.35	0.74	0.51	0.85	7.37	3.80
1989 to 1998	0.33	0.40	0.49	0.39	0.53	0.98	3.97	2.32
1998 to 2006	1.03	0.53	0.52	0.80	1.22	0.82	6.66	3.16
2006 to 2014	12.98	2.84	4.48	14.02	22.22	16.91	53.72	25.84

Figure 6.30: Sulamani city urban statistics to directions, areas in km².

Table 6.16 shows the three types of expansion that the city of Sulamani experienced during the 45 years. As with the other two Kurdish cities (Duhok and Erbil), extension is the main development type with minimum percentages accrued during the period 1989 to 1998 as 47 %, and for the rest of the epochs they were above 60 % of extension at the time of evaluation.

Table 6.16: Urban expansion development types for Sulamani city.

	Areas in KM²			Areas in %		
Epochs	Extension	Infill	Leapfrog	Extension	Infill	Leapfrog
1969 to 1976	8.71	0.56	1.77	79	5	16
1976 to 1989	12.48	0.51	2.26	82	3	15
1989 to 1998	4.46	2.70	2.25	47	29	24
1998 to 2006	9.12	3.51	2.10	62	24	14
2006 to 2014	129.00	5.55	18.47	84	4	12

The city was examined with multiple buffer rings and Figure 6.31 shows the types of expansion within each buffer ring and the amount of areas increased in km² for each one. As is shown in the following Figure 6.31, the city has expanded rapidly within the 1km-5 km annulus with total area of 58.11 km² and reached 63.21 km² within 5 km-10 km annulus. Extension as the development type within those buffer's distances was the predominant type of urban growth.

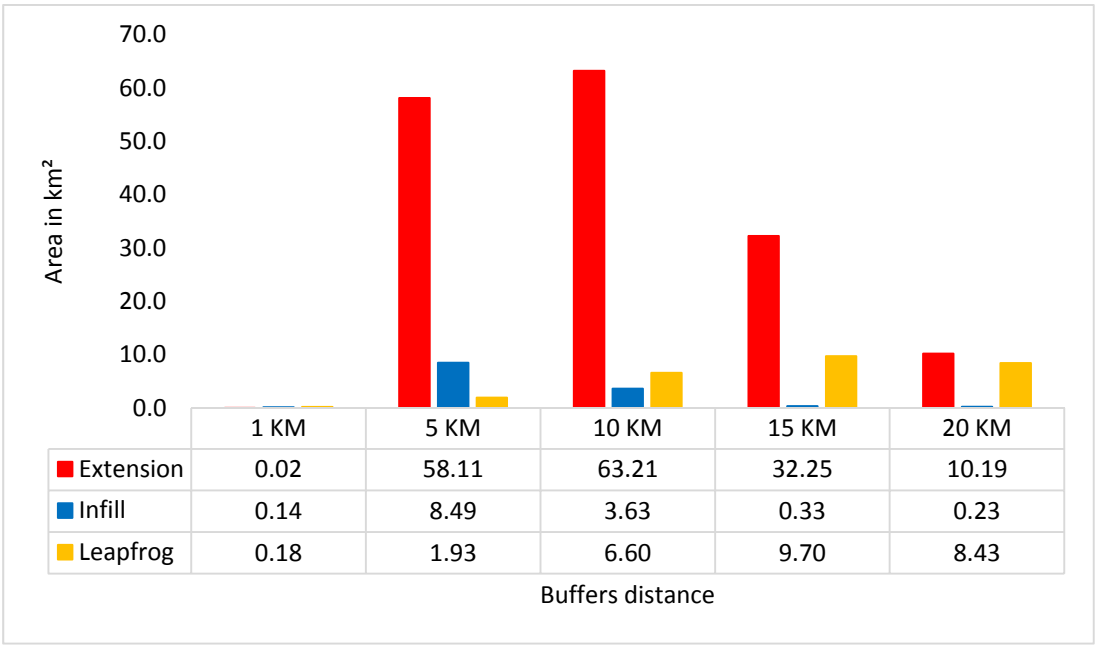

Figure 6.31: Sulamani city expansion types within different buffers distance.

Also, the city of Sulamani was examined using direction of expansion and urban development types which occurred from 1969 to 2014 (Table 6.17 and Figure 6.32). Table 6.17 shows that the city has expanded dramatically in the westerly direction with a total of 74.32 km² followed by northwest direction with a total increase of 37.32 k² and the bulk of those expansions in urban areas were an extension.

Table 6.17: Urban development types and directions for Sulamani city, areas km²

Directions	Extension	Infill	Leapfrog	Totals
North	15.26	0.63	0.54	16.43
North East	4.28	0.57	1.26	6.11
East	5.95	0.61	0.32	6.88
South East	14.65	0.48	1.96	17.09
South	17.89	0.63	6.51	25.03
South West	16.18	1.26	2.88	20.32
West	57.98	4.93	11.34	74.25
North West	31.57	3.71	2.05	37.32
Totals	163.77	12.83	26.84	203.43

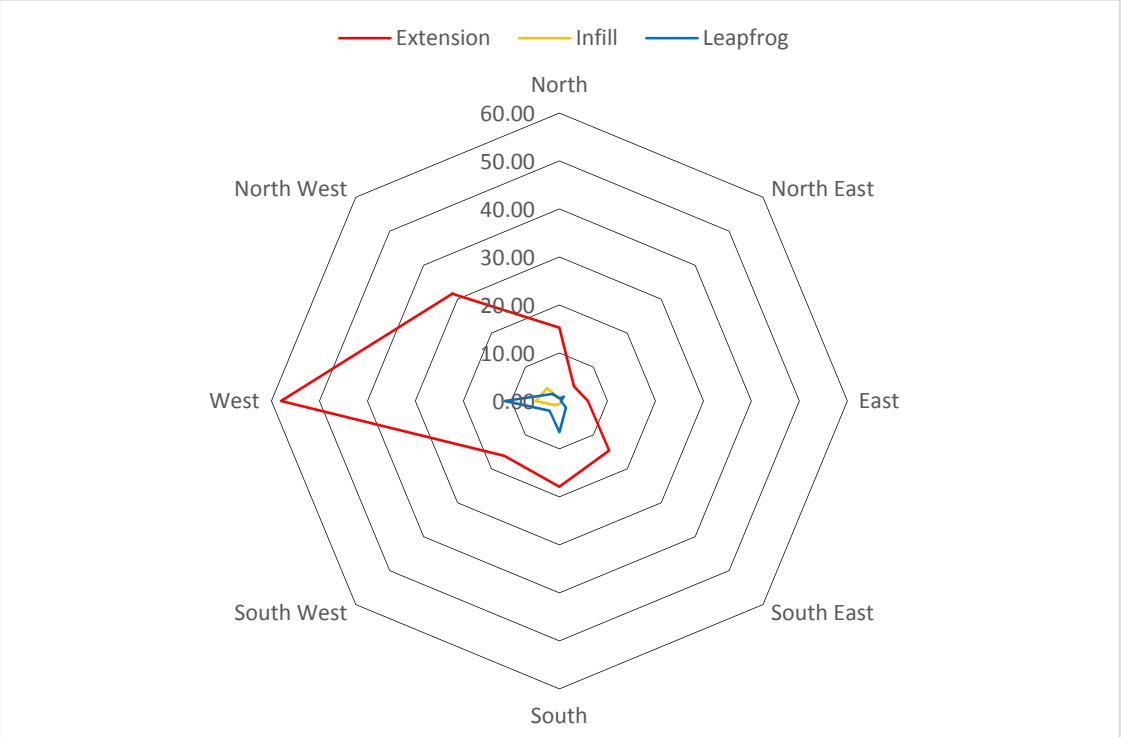

Figure 6.32: Sum area of urban expansion, Sulamani city (1969 to 2014) in km².

6.9 Chapter summary

This chapter outlined all the results for this research including the accuracy assessment, LULC maps for the classified images used during the image classification process. In addition, this chapter included the results for the change detection analysis using “From-To” approach. The relationship between population increase and urban growth has been highlighted during this chapter. The development types were highlighted using the Urban Growth Analysis Tool (UGAT). The spatial distribution of the built up areas and their pattern of the three governorates of Kurdistan region at arrange of buffer distances were covered and discussed. In addition, the direction and their expansion types in percentages for Duhok, Erbil, and Sulamani from 1969 to 2014 were reported. The totals of expansion types and their statistics in terms of areas in km² and percentages of increase were detailed in tables and figures. The results will be discussed and analysed in the following chapter.

7 Discussion

Earth's landscape is being significantly changed in different ways due to human activities which include urban expansion, population pressure, and industrial development (Ridd and Liu 1998). Major changes in the pattern of the landscape have taken place in many parts of the world because of the increase in development since the 1960s. The majority of previous land use /cover case studies have used Landsat MSS, TM and ETM+, other satellite imagery, and topographic maps to detect and map land use changes for many parts of the globe from the mid-1970s till now. The timespan of change detection has been extended to include the 1960s by cross-referencing with CORONA images. CORONA images have some limitations since they are panchromatic (signature limitation), and required geo-referencing, and colour (gray scale) balancing between adjacent scenes during the mosaicking process.

Despite the limitations of CORONA imagery, it has been used for many case studies for creating land cover and land use thematic maps. Those studies have included the identification of archaeological sites by on-screen manual digitising, and visual interpretation. Some case studies have been using those images for urban analysis and DEM generation.

However, based on the reviewed literature up to the present time, no single study has been recorded which demonstrates the use of CORONA images for texture analysis. The main objective of this study was to extend the timeline of change detection analysis and use texture information combined with the original gray levels of CORONA as input for semi-automatic classification. Combining the single grayscale image and the result of texture calculations into multiband images, it was possible to create multiband CORONA image for use in an automatic image classification process. This resulted in a final LULC map for 1969 for Iraqi Kurdistan with the same level of accuracy as that generated from Landsat images.

There was a lack of information for the study area in terms of land cover status for the early sixties and a lack of socio-economic data due to decades of political turmoil. In addition, remote sensing data was only available for military use in Iraq before 2003. Many maps and surveys were lost during the Iraq invasion by the USA led coalition in 2003. In addition, even in times of peace many Middle East governments are reluctant to provide any data, which may be a threat to the country's security. Because

of the constraints above, CORONA imagery has played a significant role in detecting and mapping the status of land cover for the Kurdistan region for 1969. The results of the accuracy assessment show that the CORONA images can be used to extend the timeline of change detection analysis with Landsat data to include the 1960s. In this case, the period of change detection for the Kurdistan region extended from 38 to 45 years by using CORONA satellite space photographs.

Visual interpretation and manual digitising may give a very accurate result as the human eyes can detect and assign correct land cover type based on the appearance and pattern of feature in the image. However those techniques are scarcely feasible (but not impossible) when the study area is very large, they are labour intensive and time consuming. The semi-automated texture analysis proposed by this research can complement visual and manual digitising with same but not less accurate outcomes. The results obtained from the studies used CORONA data for visual interpretation (Challis 2002; Philip et al. 2002; Ur 2003; Fowler 2004; Goossens et al. 2006; Wilkinson 2006; Beck 2007; Casana 2008; Bitelli and Girelli 2009; Hritz 2013) were very high in terms of accuracy and it was feasible to use manual digitising and visual interpretation for those small to medium sized study areas. However, for this research, the study area is very large and one of the objectives of this study to develop semi-automatic approach for the CORONA image classification. Also the current trend is towards automation and the approach proposed by this research may replace manual feature extraction for panchromatic images from any platforms.

The CORONA and Landsat classified datasets were analysed and quantified using the “From-To” post-classification changes detection technique, this method is more appreciated since the spatial resolution for each epoch are uniform. During this process the nature, rate, and location of changes between every two dates would be quantified and mapped.

The “From-To” method has been successfully used by a number of researchers in the urban environment (Balcik et al. 2009; Sun et al. 2009b), and has been proved to be the most effective approach for change detection, because each date is separately classified and assessed in terms of accuracy, also with this method every pair of images in single epoch have the same pixel size. Also the effect of atmospheric and sensor differences between two dates is minimised (Lu et al. 2002).

To be able to capture the changes that occurred during the study area period (1969 to 2014) for each land use/cover types accurately and efficiently, the analysis has been broken down into two separate sections, Non-urban and urban changes.

7.1 Non-urban changes

The non-urban classes here include agriculture, bare land, forest and water, all those four classes would be analysed and discussed based on the results ((Figure 6.7 and Figure 6.8), and (Table 6.5, Table 6.6, Table 6.7, and Table 6.8)) of “From-To” change detection analysis approach.

The results revealed that the study areas has preserved an unchanged area above 53 % of the total of the study areas from 1969 to 2014. The minimum unchanged area was 53 % for both epochs 1998-2006 and 2006-2014, and for the other epochs, it ranged from 55 % to 72 %. The bare land area always has the bulk of these unchanged areas in with a minimum of 63.3 % and a maximum of 91.1 % for the periods 2006-2014 and 1976-1989, respectively. Forested areas are in the second place after bare land with minimum unchanged areas of 3.7 % and a maximum of 29.3 % for the period 1989-1998 and 2006-2014, respectively. For the agriculture areas, the minimum unchanged was 2.6 % for the last epoch (1969-2014), and the maximum unchanged area was 11.3 % for the 1998-2006 period. For the water area, the unchanged areas from 1969 to2014 were under 2.0 % as the water bodies represent less than 2.0 % of the total of the study area.

The agriculture and bare land areas have an inverse relationship so that when agriculture areas have increased bare land has decreased during the study periods. The relationship between agriculture and bare land can be called interchange relation as one increased the other decreased, and therefore the analysis and discussion for both categories can be combined for all study area epochs.

The result from all figures and tables ((Figure 6.7 and Figure 6.8), and (Table 6.5, Table 6.6, Table 6.7, and Table 6.8)) for 1969-1976 epoch showed that 59 % of the study areas has not changed, meanwhile the changed area was 41 % of the total study area. From the unchanged areas, bare land has the largest percentage of just above 80 % followed by forest with just above 10 % and for the rest of classes including agriculture, water, and built up have a total of almost 10 %.

For the changed LULC classes during this epoch, bare land has experienced both gain and loss but with different rates. Bare land has increased significantly during this epoch with a total net increase of 6585.9 km² at the cost of losing an agriculture area with a total net loss of 6317.8 km². Also during this period, some forest and water areas were converted to bare land with a combined total net loss of 336.4 km². Those net gain and losses for both classes (agriculture and bare land) may be related to army operations carried out by the Iraqi regime against the Kurds during this epoch. Many agriculture and forest areas were reduced during the time those operations were carried out as those areas were burned by army troops. In addition, the increase in the bare lands and decrease in agriculture occurred in a period when thousands of Kurdish families migrated to other countries after the failure of the Kurdish revolution in 1974. As a result of this migration, the agriculture areas were abandoned by most of the farmers and the outcome of that was an increase in the bare land areas during this period.

For the 1976-1989 period, the results showed that more than 60 % of the study area has not changed, and the changed areas was just under 40 %. From the unchanged areas, bare land has the largest percentage of 91 % followed by other classes including forest , agriculture and water with a combined total of more than 8 % (Table 6.5, Table 6.6, Table 6.7, and Table 6.8).

For the changed LULC classes, agriculture areas has experienced both gain and loss in the same way as bare land from the previous epoch and with different rates. The agriculture area has gained a total net of 4662.3 km² and the majority of this transformation came from forest and bare land with a total net loss of 4630.2 km². Also during this epoch, many hectares of forest were lost during the series of attacks known as the “Anfal campaign” which was carried out from1986 to 1989 by the Iraqi army against Kurds and also by the Iraqi army burning those areas deliberately to push back the Kurdish Peshmerga forces from Iraqi soil. A total net loss of 3928.6 km² of forested areas occurred during this period. The loss of forest and bare land have contributed to increase the agriculture area during this epoch. This is due to the fact many areas surrounding big cities such Erbil and Duhok were occupied by Arab tribes from the middle and south of Iraq and they started to practise agriculture in place of the displaced Kurdish farmers. All the Kurds generally and specially those

returning from exile were disadvantaged from all the luxuries of the first-degree citizen in one of the richest countries (Iraq) in the Middle East until 2003.

For the period 1989-1998, the total areas which have not changed is above 70 % and less than 30 % within the study area underwent changes. The largest percentage for those unchanged areas were bare land with a total of 89 % followed by other classes including agriculture, forest and water with a total combined of 11 %. This period experienced little changes in the landscape although it incorporated a major changing point for the Kurdish citizens who obtained their freedom and independence from Iraq especially after the Gulf war in 1991 by the help of western countries including USA, UK, and France.

During this epoch, bare land has again experienced both gain and loss but with different rates. This class has gained the largest percentage of changes with a total net increase of 2842.0 km² and most of this gain was from agriculture which is regarded as a net loss area by 7057.3 km². Also, the forested area has gained a net total of 4059.7 km² which was mainly coming from agricultural areas. During this epoch, bare land has increased in the same way as first epoch (1969-1976) but with a lower rate. The increase in bare land areas was a result of the KRG's limited capabilities for providing the basic needs to the Kurdish farmers for increasing agriculture productions. In addition, the Kurds did not have enough funds to support the agriculture sector by converting the bare lands areas to productive agriculture areas for civilians needs in the region during this epoch. Those limitations have occurred after the Kurds got their freedom in 1991. The Kurds were living under a Humanitarian programme supported by the UN with the most distinct one being the UN Oil for Food Programme (OIP) in 1995. In addition, the rate of LULC classes transformation was less than previous epochs because the Kurdish areas were excluded from any sort of benefits from Iraqi resources and the Kurdistan people were living in a very basic lifestyle (KRG 2013).

The period 1998-2006 can be regarded as the second significant period for the study especially after 2003 when the US and the coalition armies overthrew the Iraqi government from power. For this period, only 53 % of the total areas remain as unchanged, and for the changed areas was 47 %. From the unchanged areas, bare land has the largest percentage of above 65 % followed by forest with 19 % and for agriculture, water, and built up which have a combined total of less than 14 %.

For the changed LULC classes, agricultural areas have increased by a total net gain of 15170.5 km² and most of this transformation area came from bare land with a total net loss of 18715.4 km². Also, forested areas have increased during this epoch by a total net gain of 3564.2 km² which was mainly coming from bare land areas. The dramatic decrease in the bare land areas in this epoch was a result of farmers being provided with interest-free loans for increasing the agriculture production of the Kurdistan region. The Kurds were able to get their share from the central government annual budget (11-13 %) and this gave them the ability to invest massively in the infrastructure and agriculture sectors. The increase in the agriculture areas was at the expense of the other classes, especially the bare land areas. Also during this epoch the built up areas increased significantly which is one of the other reasons behind the reduction in the bare land especially for the surrounding areas of the three major big cities in Iraqi Kurdistan.

For the period 2006-2014, results showed that 53 % of the study area has not changed, meanwhile the changed area was 47 %. From the unchanged areas, bare land has the largest percentage of above 60 % followed by forest with less than 30 % and for the other classes including agriculture, water, and built up have a combined total of less than 8 %.

This period has experienced a massive increase in the bare land with total net gain of 15387.7 km² and this increase is at the expense of losing agriculture areas on the western side of Kurdistan region by a total net loss of 16495.2 km². The western side became the front line in a war against the most barbaric terrorist group (ISIS) ever to arise for the last century. Those areas were abandoned by the Kurdish farmers and most of whom became members of the Kurdish forces (Peshmerga) in the fight against the Islamic extremist group (ISIS).

The period 2006-2014 can be regarded as the most significant period of the study as many significant events occurred after the Kurdish freedom in 1991 and especially when the Iraqi regime was wiped out by the USA and coalition troops in 2003. This event provided the best opportunity for the Kurds to seek their rights and share in the natural resources of Iraq and especially in the oil and gas sector. They also started to have their share of the Iraqi budget which ranged between 11-13 % of the total Iraqi budget (KRG 2013). With these funds, the Kurds were able to make the three major cities in Kurdistan region and especially Erbil city to one of the best places for

investments especially after implementing a liberal investment law, which was approved by the Kurdistan regional Government in July 2006. The approval of the liberal investment law offered foreign investors the freedom to expatriate profits. Also, it provided them customs relief, tax holidays, regulated banking and finance sector services (KRG 2013).

The period 1969-2014, covers the 45 years of LULC changes for the Kurdistan region. For this period, only 55 % of the total areas remain as unchanged areas and for the changed areas it was 45 %. From the unchanged areas, bare land has the largest percentage of 81 % followed by forest with 15 % and for the rest of the classes including agriculture and water they have a combined total of less than 4 %.

For the changed LULC classes, bare land areas have gained a total net increase of 5399.0 km² and most of this increase was coming from agriculture areas with a total net loss of 10037.9 km². The bare land has increased during this epoch and especially in the western side of the region, as those area became a war zone when the Islamic terrorist group appeared in the region. The increase in the bare land resulted in the decrease in other land use/cover types specially the agriculture areas. In addition, there is another factor which may be one of the reasons that the bare land has increased. The farmers of Kurdistan lost interest in growing wheat as the central government still owe the Kurdistan farmers the money for the wheat for the last two seasons 2012 and 2013. The agricultural areas was much larger in the 1960s (KRG, 2013), and those areas started to decline as many people, including farmers, were displaced by the Iraqi regime from 1974 to 1990. Also the migration of many families in the Kurdistan region to big cities or aboard after the failed 1974 revolution was driving factor for decline in those areas. Again with increasing instability in the region from 2014 onward, those areas declined again.

Regarding the forest area in Kurdistan region, it has been through a systematic decline which was caused by the Iraqi regime from mid-1970s to late 1980s. This land use/cover type has decreased during the first and second epochs (1969-1976) and (1976-1989) by a net decrease of 306.3 km² and 3928.6 km², respectively. The decrease in the forest areas may be related to the operation that was carried out during the period (1974 to 1991) by the Iraqi army. Many forested areas were burned during the war between Iraq and Iran in 1980s. Also, the Iraqi army was deliberately burning these areas to push back the Kurdish Peshmerga forces from Iraqi soil.

The forest area started increasing again during the 1989-1998 period, forested areas increased significantly by 32.8 % (4136.8 km²) of the total change because of the transition from agriculture and bare land areas to forested areas by 54.4 % (2249.8 km²) and 45.6 % (1886.2 km²), respectively. Although 78.1 km² of forest was lost, there was nevertheless a total net increase of the forest area for this period to 4059.7 km² during this period. The forested areas were continuously increased for the epochs 1998-2006 and 2006-2014, as those epochs are within the KRG programme to increase the forested areas as they have been lost during the “black era” from 1974 to early 1991. The forest areas were increased with a net gain of 3564.2 km² and 100.2 km² for the epochs, 1998-2006 and 2006-2014, respectively as some of those forest areas were lost because those areas were the targets of Turkish fighter jet and Iranian bomb attacks. Some loss of forest areas may be related to poor management skills by the people who look after these areas.

Finally, water bodies are regarded as the last non-urban land use/cover type in the study area. During the first epoch (1969-1976), water bodies increased by 68.3 km². This slight increase may be related the amount of the rainfall during this period (Figure 3.8), as the Kurdistan region depend highly (60 %) on the precipitation. For the second epoch (1976-1989), although the Iraqi regime built a new dam in the Mosul region, the water areas decreased slightly by 147.7 km². The purpose of this dam was to provide water resources and electricity to the other governorates at the expense of Kurdish land as many agricultural and built up areas were lost under the water in 1984 when the construction was completed. Another reason that the water decreased is that the Kurdistan region depends on 40 % of the water supply on the neighbouring countries, especially Iran. The decline in water area is not related to the army operations carried out by the previous regime as the Iraqi government always wanted to keep the water supply stable since the middle and south governorates depend on Kurdistan for their water supply. During the war between Iraq and Iran 1980 to 1988, the Iranian regime reduced the water which flows to the Dukan and Derbandikhan dams and this is one of the main reasons of the water surface areas decreased during the second epoch. For the third epoch (1989-1998) in the study evaluation, the water surface areas increased by 150.0 km² and this increase could be related as mentioned before to the level of precipitation received in the Kurdistan region during this period (Figure 3.8). For the rest of epochs, 1998-2006, 2006-2014

and 1969-2014, the water decreased gradually by 65.6 km², 28.0 km², and 22.5 km², respectively. This decrease may be related to the amount of rainfall received during this epoch for the Kurdistan region and the Iranian government restricting inflow again since 2006.

7.2 Urban change

Urban growth change for this study area was divided into two sections, the first section covering the regional scale for the Kurdistan region and the other is the local scale for urban expansion of the three major cities in the Kurdistan region. The reason for analysing this way is to capture the changes in the landscape for the three big cities as the bulk of those changes occurred within a radius of 20 km around those cities during the evaluated study periods. In addition, to be able to analyse those changes in more detail other approaches were implemented for instance using different analysis methods including urban development types. The regional scale shows the urban growth in less detail in contrast to the local scale which shows the extent of urban growth and also the type of urban development based on the Urban Growth Analysis tool (UGA).

7.2.1 Regional urban growth

According to the area statistics for the urban areas LULC types, the built up areas for the entire Kurdistan at regional scale (in respect to the total study area) were 0.18 % (79.42 km²), 0.12 % (53.82 km²), 0.37 % (167.16 km²), 0.38 % (172.74 km²), 0.49 % (219.02 km²), and 2.79 % (1254.52 km²) for the years 1969, 1976, 1989, 1998, 2006, and 2014, respectively. Change detection analysis revealed that the urban areas were in stable increase until 2006. The urban areas increased dramatically during the epoch 2006-2014 for the Kurdistan region as a response to firstly economic development and secondly population increase and especially Kurdistan getting a fair share from the Iraqi budget after 2003. While there was a decline in the urban area during the first period (1969-1976), it could be related to the destructive action by the Iraqi army against Kurds and their homeland. The destruction of the landscape by the army troops was the main reason for losing built up areas in the Iraqi Kurdistan. According to records held by KRG, around 4000 to 5000 villages were demolished during the period 1974 to late 1980s, many army campaigns were carried out by the Iraqi regime and many lives were lost during those operations. It is estimated more than 180,000

people disappeared and until today enormous numbers of graves were found in many parts of the middle and south of Iraq. The remainder of those graves belong to Kurds as many Human rights organisations have confirmed the existence of those graves and that the victims are Kurds (KRG 2013).

The urban areas at regional scale for the first epoch (1969-1976) both decreased and increased at the same time with a total gain of 31.4 km² and loss of 59.5 km², respectively (Table 6.8). The increased areas were around the big cities of the Kurdistan region, and the bulk of these increases were from bare land, agriculture, and forest areas with 62.6 % (19.6 km²), 34.3 % (10.8 km²), and 2.8 % (0.9 km²), respectively. The reduction in urban areas by 59.5 km² during this period may be related to army operations carried out after the downfall of the 1974 revolution. Because the Kurdistan region experienced gain and loss at the same time and this led to a total net loss of 28.1 km² of the built up areas during this epoch.

The urban areas witnessed a total gain of 131.9 km² during the second epoch (1976-1989). The increase in built up areas was coming from the transformation of bare land, agriculture, and forest areas with totals of 76.3 % (100.7 km²), 18.7 % (24.6 km²), and 3.6 % (4.8 km²), respectively. Also this increase related to that many villages in rural areas being demolished in past period 1969 to 1976 and the residents of those villages migrated to big cities and therefore the urban areas around big cities increased noticeably. Also during this epoch, a total of 16.4 km² of built up areas was lost during the construction of the Mosul dam 1981-1986, this led to a reduction in the total net increase of built up areas to 115.6 km².

For the remaining epochs, the built up areas were in steady increase till 2006. During the third epoch 1989-1998, the built up areas increased by a total of 62.6 km². This came from the transformation of bare land, agriculture, and forest areas with totals of 50.0 % (31.3 km²), 48.0 % (30.0 km²), and 2.0 % (1.3 km²), respectively. Also during this epoch many built up areas were lost due to the region’s instability including a civil war between two main Kurdish parties in 1996 and continuous bombing by Turkey and Iran to the area occupied by civilians. Also, the accuracy of the result and more than half of the built up areas were coming from bare land and there is the possibility of misclassified areas as built up during image classification. The loss of 57.0 km² of built areas led to a decrease in the total net gain of built up areas to 5.6 km² during this epoch. The reason for this slight increase may be related to the fact

that the KRG was unable to provide loans to civilians for new buildings in response to the population growth during this period.

For the fourth epoch (1998-2006), the built up areas increased by a total of 90.7 km². The increase came from transformation of bare land and agriculture with totals of 74.8 % (67.9 km²) and 24.5 % (22.2 km²), respectively. Also during this period some built up areas were lost and could be related to the accuracy of results as the bulk of those areas were coming from bare land and some confusion was noted in the accuracy assessment between bare lands and built up areas. A total loss of 44.4 km² of built up area during this epoch led to a decrease in the total net gain of the built area to 46.3 km². The increase in the built up areas related to the fact that the KRG was able to provide free loans and blocks of land to new families free to establish their dream home when the KGR was able to get Kurdistan's share from the central government budget in Baghdad.

For the fifth epoch (2006-2014), the built up area was increased by total gain of 1044.5 km². The increase in built up areas was the result of the transformation of the agriculture and bare land areas with totals of 59.8 % (624.1 km²) and 38.7 % (404.6 km²), respectively. Also during this epoch, there were some areas which have been regarded as lost built up area (may be related to misclassified pixels as built up in 2006), a total of 9.2 km² of built up areas led to decline the built up areas to total net of 1035.5 km². The dramatic increase in the built areas was a result of the amount of the funds that the KGR was injecting in the infrastructure sector. Through those massive funds, the KRG was able to provide extensive free loans to the residential sector and beyond that to include agriculture, industrial, and commercial sectors as well.

Also, for the period 2006-2014 according to the activities report for KRG in 2009, around 68577 parcels of land were distributed free of charge for people to construct new buildings for residential, commercial, industrial, and others purposes (KRG 2013). During this period, the built up area increased almost by 2.3 % of the total of the study area, and agriculture and bare land areas had converted to building to be used by many local and foreign companies. Additionally, official figures indicate that there are currently 15,000 local companies and 2,300 foreign companies from 78 countries registered in the Kurdistan Region. Based on the report from the ministry of planning there are more than 2500 companies in Erbil region only and all those

companies, of course, need a place to establish and run their business. Therefore, the built up area was the major land use/cover class to have a dramatic net increase of 1035.5 km².

Over the 45-year period (1969-2014), the built up area increased by a total of 1209.4 km². The increase was the result of transformation of agricultural, bare land, and forest areas with totals of 51.6 % (624.6 km²) and 44.5 % (538.6 km²), and 3.6 % (43.4 km²), respectively. During this epoch, also some areas which have been regarded as lost built up areas due to misclassification of pixels of bare land as built up, a total of 34.7 km² (27.4 km² coming from bare land) reduced the increase in built up areas to a total net of 1174.7 km². The dramatic increase in the built areas was obvious as the significant period (2006-2014) of the study is within this long epoch (1969-2014), and therefore the expectation of increasing built up areas would be very high as a response to long term population increase and economy development for the Kurdistan region.

7.2.2 Local urban growth

At the local scale within a 20 km radius, all the three Kurdistan cities bore their share of the systematic destruction for instance; Duhok city within 20 km radius has lost about 2.1 km² during the period (1969-1976) followed by Sulamani with a total loss of 2.4 km² and Erbil has lost almost twice as much as Duhok and Sulamani with 5.0 km². Also during this period the three cities gained built up area mostly from bare land with totals of 4.8 km², 5.9 km², and 8.7 km², respectively. The cities experienced both gain and loss during this period because of the instability of the region, but had total net gains in built up areas of 2.7 km², 0.9 km², and 6.3 km², respectively.

For the second epoch (1976-1989), the three cities (Duhok, Erbil, and Sulamani) gained a total of 13.2 km², 32.3 km², and 8.9 km², respectively. Most of this increase was coming from bare land for the three cities. The reason Erbil got the big share of expansion in the built up areas is that this city was considered the summer capital of Iraq in the late 1980s. The Iraqi regime started to expand this city to become the summer destination for many Arab people from Iraq and other neighbouring countries.

For the third epoch (1989-1998), the three cities did not gain big areas except for the city of Erbil because of the budget constraints for the KRG during this epoch. Few

parts of Kurdistan region experienced urban expansion between 1989 and the early 2000s, and this was because the Kurdistan region did not have any income to invest in the infrastructure sector and therefore, the annual urban growth was very low. Also, some built up areas were lost because of the civil war in 1996 and USA operations against Islamic groups (Ansar al-Islam) in the Sulamani region in 1998 (KRG 2013). The total net increase in the built up area for Duhok city was 0.2 km² and Erbil 5.4 km² and Sulamani 2.1 km². The bulk of this increase for the three cities came from bare land during this period.

For the period 1998-2006, the urban areas were increased for the cities of Duhok, Erbil, and Sulamani with total net gain of 8.0 km², 25.2 km², and 12.9 km², respectively. This increase in built up area was a result of population increase and economic improvement especially after getting the Kurdistan region's share from the central budget in Baghdad. The majority of this increased built up was a result of bare land transformation to new buildings for the three Kurdish major cities. In 2003 Kurdistan region could guarantee their share from the new Federal government budget after the invasion of Iraq by the USA and since then the Kurds invested a lot of funds in the Kurdistan region infrastructure and as a result of that the urban area was expanded dramatically.

For the 2006-2014 period, the three major cities of Duhok, Erbil, and Sulamani had a net increase of built up areas of 77.9 km², 216.7 km², and 152.5 km², respectively. This increase in built up areas for three cities as mentioned before is related to the economic improvement by KRG investing heavily in the infrastructure sector and also population increase. The majority of the built up areas were coming from the agriculture areas as the city boundaries reach the agriculture areas within the 20 km radius.

For the overall span of 45 years of changes, a total net gain of 90.8 km², 275.5 km², and 180.4 km² of the built up areas were increased for Duhok, Erbil and Sulamani, respectively. This increase is related to the time when the Kurdistan region in general and the three cities centre, especially, experienced a massive increase in urban expansion. The majority of those transformed areas to built up came from bare land areas for the three cities.

Except for the time period (1974 to 1989) when the Kurdistan region lost some built up areas because of the landscape destruction by army operations carried out by the previous regime, Iraqi Kurdistan have experienced definite urban expansion and especially the three major cities. The direction of expansion and the amount of expansion within certain buffer distances with regard to the city centre as a reference point will now be discussed.

7.2.2.1 Duhok city urban expansion

This city is regarded as the third of the cities in the Kurdistan region based on the total areas. This city has experienced a definite urban expansion within the buffers distance (1 km, 5 km, 10 km, 15k m, and 20 km) since 1969 to 2014. The city has expanded in all directions from 1969 till 1998 with total areas from 2.69 km² to reach 39.32 km² for the all epochs within this period. However, from 2006 until 2014, the city had enormous expansion in the western direction as a response to the population increase and dramatic improvement in the economy of the region after 2003.

Based on the annual report for the KRG in 2009, the Duhok governorate has a share of freely distributed 13630 parcels land units which has been used for many purposes such as residential, commercial, and industry. The majority of those parcel of land distributed by KRG were developed in the Duhok city surrounding areas. A total of 12397 residential units were distributed to middle and low-income residents with free interest loans which resulted in an increase to the city boundaries in dramatic ways during the period of eight years (2006 to 2014).

The city expanded by more than 50 km² of built up areas since 2006. Most of the development types for the city of Duhok is of the extension type with a minimum of 58 % for the epoch 1976 to 1989. The city experienced some leapfrogging and infill but with not the same rate when compared with extension development type. Also, the majority of the expansion from 1969 to 2014 was in buffer distances of 5, 10, and 15 km from the Governorate building centre reference point with total areas of extension of 27.07 km², 24.78 km², and 17.64 km², respectively. This indicates that as the distance from the reference point increases the development type’s rate is decreasing. Population increase is one of the main reasons of the city experiencing a dramatic expansion in urban areas.

The population has been continuously increasing since 1965, the population of the city centre was only 78903 persons in 1965 and in 2014 it reached 193151 persons with the total increase by 244.8 % or annually 5.4 % since 1965. The city may experience big changes in the next several years as the population increases, the demand on the built areas will increase. Duhok city is located in an environment that mostly consists of mountain slopes, hills and valleys, with a vast agricultural plain in the western direction. Also, the city is surrounded by natural mountain barriers on three sides, Zawa Mountain in the south toward south-east directions and Bekher Mountain in the north toward north-west directions. The city has therefore experienced an urban expansion towards the west. Further expansion for this city would mostly be in the westerly direction because of these natural barriers.

7.2.2.2 Erbil city urban expansion

The Erbil city has experienced a definite urban expansion since 1969 to 2014 in all directions, but the rate of expansion for the period 2006 and 2014 is massive. The city has expanded by almost 30 km² in south-west direction and more than 25 km² for the other directions. The east direction expanded by more than 45 km², but this expansion in the eastern direction may be prevented in the future, as the city will reach the natural barrier of Safin Mountain. This will prevent the city to expand in the eastern direction in the next few years if the city keeps growing with the same current annual rate (54.60 km² /year). Also in the north-west direction, the city will not be able to expand any more than current expansion for this direction except for the leapfrogging type as the Erbil international airport is located in the north-west of the city and acts as a natural barrier.

Regarding development types, most of the development for the city of Erbil is of the extension type with a minimum of 32 % for the epoch 1969 to 1976 and for the rest of epochs; minimum of 69 % for the period 1989 to 1998. The city experienced a maximum of 47 % of leapfrogging for the period 1969 to 1976, and in 1969 to 1976 infill had a maximum of 21 %. For most of the time extension development is the main urban growth type for the city of Erbil.

Also the majority of the expansion from 1969 to 2014 was within buffer distances of 5, 10, and 15 km from the Erbil Citadel centre reference point with total areas of extension of 62.84 km², 122.47 km², and 49.52 km², respectively. And this indicates

that beyond 10 km buffer development type's rate it decreases since the increase for 20 km buffer was only 10.51 km². Making the Erbil city the capital city of Iraqi Kurdistan, and population increase and industry development, especially in the oil and gas sector, are the main reasons for the city experiencing dramatic urban expansion. As the capital city of the region, many business persons have invested their money in a big project in the industry, tourism and infrastructure sector.

Population is another major factor of urban expansion in the city of Erbil. The total population of the Erbil city in 1965 was only 193,960 persons and in 2014 it reached 816,515 persons with a total increase of 421.0 % or annually 9.4 % since 1965. The city may experience big changes in the next several years as the population increase and improvement of the economic sector after the ending of the war against the terrorist Islamic groups. The direction of the expansion would be in mostly all directions except for the North West as the Erbil international airport would prevent the city expansion in this direction. The city of Erbil is able to accommodate all the urban development in the future because of the majority of development and big funds are implemented to this city by the Kurdistan region government.

The Erbil governorate has the largest percentages of the total number of the land units which was distributed by the KRG since 2003. According to the annual report for the KRG in 2009 (Figure 6.6 and Table 6.9), Erbil has a total of 44374 units of which 39430 were residential, 1138 commercial, 3216 industrial and 590 were parks and recreation centres. The majority of those land units were developed in the Erbil city surrounding areas. Also providing the middle and low-income residents with interest free loans resulted in an increase to the city boundaries in such a dramatic way during the eight-year period (2006 to 2014).

Since this city is located in an area of open plain, it experienced expansion in every direction. There are no natural barriers for the city of Erbil like Duhok and Sulamani, to prevent the city expansion in any direction. Since the shape of the city is a circle, there is therefore a possibility for the city to expand in the future in every direction except the North West aspect.

7.2.2.3 Sulamani city urban expansion

For the city of Sulamani, the population of the city increased by 361.3 % 177657 to 641786 during the period of 1965 to 2014. The population of the city with an annual

rate of increase of 8.0 %. The city of Sulamani has experienced a big increase in the urban areas after 2006 again as a result of KRG providing interest-free loans to people with middle and low incomes. Also, distributing 10573 land units was a major factor of the dramatic city expansion for the period 2006 to 2014. The city experienced an urban expansion in the west and northwest directions during that eight-year period. In the previous epochs, the city expanded in almost every direction until 2006. The natural barriers of Azmer, Goyija and Qaiwan mountains in the north and north east, Baranan Mountain in south directions and Tasluja Hills in the west forced the city to expand in the west and northwest directions.

The city has expanded more than 60 km² in the West direction and followed by more than 30 km² in the North West. Most of the expansion in the city of Sulamani is of extension types with a minimum 47 % for the epoch 1989 to 1998. The other two types of urban expansion are infill and leapfrogging, at lower rates of development. Regarding the buffer distance 5 km, 10 km, 15 km, and 20 km from the governorate building as a reference point, the city has expanded by 58.11 km², 63.21 km², and 32.25 km², and 10.19 km², respectively. The city within 1 km buffer distance did not experience much expansion as the city centre is already compacted with building and there is no spare space or land for development to occur there.

Generally, urban expansion in the Kurdistan region has been a result of many factors including economic development, population increase and the KRG having to rebuild the built up areas demolished by the previous regime to accommodate returning Kurdish family from exile and the population increase which has occurred in the last 45 years. Since 2003, the KRG have received annually about 11 to 13 % of the central government funds from Baghdad. Most of the time the Kurds were supposed to get 17 % based on the population of Kurds in Iraq, but always the post 2003 Iraqi government paid them less than their share. Most of the money from this budget went to education, health and other government sectors. The remaining funds were used to rebuild the Kurdistan infrastructure which was destroyed by the Baath’s regime in the past. The Kurds were able to rebuild many villages and other infrastructure, but in reality, the Kurds need more than 17 % of the Iraqi budget to be able to reconstruct the demolished urban and rural areas within the Kurdistan region boundary. As the Kurds do not have any other sort of income except their share from the central

government, therefore, the infrastructure was not increased in the same level of the economy and population increases.

Also by looking at the built up trend for the Kurdistan region from 1969 until 1998, the urban growth rate was very small when compared with the rate of population growth. There is one reason only for this, as the Kurdistan region was left behind by the Iraqi regime during this period. Most of the Iraqi budget was used in the military sector and only a little portion of the total budget was used for the civilians and in infrastructure areas. Therefore, the majority of the Iraqi cities in general, and particularly the Kurdistan region, did not increase at the same rate of the population increase in whole Iraq. Since 2013, the built up sector in Kurdistan region has not increased as a result of the war against Islamic groups in the region. Cities or villages close to the front line were abandoned by civilians in those areas to save their lives from those barbarous groups. Since the arrival of this Islamic terrorist group (ISIS) in the region, many people were displaced from their territories and went toward big cities such as Duhok, Erbil, and Sulamani.

8 Conclusions and recommendations

8.1 Conclusion

In this research, a new approach of classifying CORONA images with a high level of accuracy was proposed and carried out. Although there are some limitations of using CORONA single band images directly in the image classification process, the methodology described and used by this research overcame those limitations. Creating a multiband image for CORONA from the original brightness values and texture information and using this image directly as an input in the auto classification process, achieved a high level of overall accuracy (85 %) and kappa coefficient (0.80). Water was classified by a separate image segmentation process.

In addition, this approach was capable of extending the time-line of change detection analysis for the Kurdistan region by cross-reference between CORONA space photographs and Landsat data. Most modern developments started in the early 1960s, so by using CORONA images it was possible to start the change detection analysis in the 1960s.

Kurdistan region has experienced many periods that almost erased the Kurds from Iraq completely and from the international family. The Iraqi regime practised genocide against Kurds when they were seeking their rights in the country of Iraq. Because of the United States of America and their allies, the Kurds were able to establish a new era to overcome all the organised army campaigns they experienced between 1974 and 1991. The Kurds were able to stand against all those systematic army operations and were even able to survive chemical weapons attacks on 16 and 17 March 1988 in the city of Halabja.

The changes in the landscape in Kurdistan region have been massive in terms of land use and land cover. These changes can be broken down into three phases: destruction and demolition of the landscape era, which started from 1974 to 1991, this stage included burning forest and agricultural lands. These demolitions went beyond that to include built up areas and more than four thousand (4000-5000) villages destroyed from 1974 to 1991. These systematic operations led to decrease in the agricultural, forest, and built up areas resulting in migration and displacement of thousands of Kurds to other places such as local big cities or abroad.

The second period can be regarded as a stage of freedom with relatively little changes in the landscape that started from 1992 until 2002, especially when the Kurdish got their freedom and became an autonomous region from Iraq and Kurdish people returned from exile to their Motherland to rebuild the devastated region. The Kurdistan region during the period of 1992 to 2002 was a region of relatively little changes in the landscape and massive population increase. The land use and land cover patterns remained static with minor changes for forest, water and built up areas. The little increase in the built up areas during this period was not enough to accommodate the population increase. Most of the Kurdish families were living together under the same roof and the newly married couple were unable to build their own home as the economy was in the lowest level for the Kurdistan region during this period.

There was an interchange between agriculture areas and bare land, as those two categories were changing when there was a war in the region. The land in the Kurdistan region has always been suitable for agriculture practices. Those areas became a bare land when they were abandoned by the people. The eastern side of Kurdistan became bare land because of the Iraqi war against Iran between 1980 and 1988. The satellite images provide a solid evidence that those areas became bare land when they became the front line war zones for almost ten years. Also recently, this pattern is appearing again but in the opposite direction (western) which has become a war zone, also with a different enemy (Islamic terrorist group). In addition, the Landsat image for 2014 provides concrete evidence that the agriculture areas have been abandoned by the local Kurdish farmers in those areas.

The third phase runs from 2003 until 2013, the Kurds were able to guarantee their rights in the post 2003 Iraq government and specially getting their own budget from the central government. The economic growth in the oil and gas sector was the main factor of the remarkable changes in the Kurdistan landscape. Having a direct impact on the urban growth, and improved the living standards for most of the middle and low-income citizens in the Kurdistan region. Also by implementing a liberal investment law in July 2006, the KRG offered foreign investors a big opportunity to invest their funds in a new dynamic region in the Middle East. The Kurdistan region became an attractive “business hot spot” when the KRG provided to the investors

freedom to expatriate profits, customs relief, tax holidays, regulated banking and finance sector services.

In addition, the KRG was able to boost the infrastructure sector by providing the low and middle income population in Kurdistan region with a free parcel of land. Based on information released in the activities report for KRG in 2009, there were around 68577 units of land distributed after 2003 which included parcels for residential, commercial, industrial, and others purposes. Based on the 2009 KRG report, a total of 59472 residential units were distributed to citizens of Kurdistan region, also the KRG provided those citizens interest free loans to build on their land units and, therefore, the urban areas were increased during the period 2006-2014. The other sectors such as commercial, industrial and others purposes (parks and recreation centres) all have their share of those units. For commercial, industrial, and others purposes, 2720, 4917, and 1468 units were distributed, respectively.

The interpretation and classification of CORONA and Landsat satellite imagery was advantageous for estimating the rate and spatial patterns of the urban expansion in the Iraqi Kurdistan region for the period 1969 to 2014. The use of remote sensing technology is becoming increasingly important in land use changes because large areas can be classified quickly and at low cost. By integrating remote sensing and GIS, the final maps for the land use changes were obtainable. The results of this study demonstrate the potential of using multi-temporal Landsat data to provide accurate and economical ways of mapping and analysing the land use changes which occurred during the study period. The result of this research can provide to authorities in KRG with highly accurate outcomes and so that they can use that accurate information where needed for land management and policy decisions.

This study showed that the combination of CORONA, Landsat MSS, TM, and LC8 data was extremely well suited to detect the changes in the urban development for the Kurdistan region. The spatial resolution of Landsat imagery was sufficient to capture and classify the characteristics of human activities. In addition, the spectral resolution of this series was suitable to distinguish urban areas from other types of land cover. Several changes of land use patterns were observed and quantified between 1969 and 2014. The most visible changes occurred in the study area is the remarkable expansion of the urban areas which can be explained by the increase of the high-speed economic development and population increase.

Also this study revealed that normal human activities are not only the factors making the changes in the landscape, but also organised army operations are another factor for making negative change, especially in the demolition and destruction of landscape. The use of CORONA imagery was a considerable help in creating a baseline land use map for the study area because the accurate information was required for the time before the Kurds were downgraded by the Iraqi regime to third class citizens. Also CORONA images are the only available images that can provide useful digital information for the 1960s. By the use of CORONA images, the timeline of the study period was extended to include 1960s. The methodology used in this study for the CORONA image can be regarded as a new approach to classify those images with a high level of accuracy.

8.2 Recommendations

A further study would be to implement the suggested methodology to others part of divided Kurdistan. Since other parts experienced a similar, if not worse, situation to Iraqi Kurdistan, it is possible to capture and map the human activities that are the main reason of change in the Kurdistan landscape for more than half a century.

Since Iraqi Kurdistan has experienced a dramatic change in the landscape for the last eight years with high urban growth rate, it is suggested a national land use development policy is established in the Kurdistan region for planning and development purposes. In addition, it is suggested a continuous monitoring system for the Kurdistan region is established since the rates of urban growth is significant. Also, this continuous monitoring system allows the authorities in the Kurdistan region to be informed of those changes in the landscape and the reasons behind those changes.

Based on the methodology used by this research for CORONA panchromatic image classification, using this new approach is recommended to classify a panchromatic image by combining gray levels with the texture calculation measures to obtain an input to be used directly in the image classification process. This study proved that a classified image with high level of accuracy could be achieved by implementing the suggested methodology. In addition, calculating the aspect of the study area using DEM dataset provides a solid decision of selection the best direction for texture calculation.

The study area has experienced dramatic changes in the landscape and especially in urban environment with a massive urban expansion during long-term evaluation. It is highly recommended that future studies in the Kurdistan region go one step further to capture the relationship between land use/cover changes and environmental issues, the most common one in the urban areas being surface urban heat islands. Land use/cover changes is one of the main factors increasing the land surface temperature in the urban areas. The impervious areas in the urban environment are increasing when the mixed urban pattern converting to pure urban at the expense of green areas in the same environment which may lead to increase in local increase heat.

References

Abdula, R.A., Balaky, S.M., Nourmohamadi, M.S., & Piroui, M. (2015). Microfacies Analysis and Depositional Environment of the Sargelu Formation (Middle Jurassic) from Kurdistan Region, Northern Iraq

Abdulaziz, A.M., Hurtado, J.M., & Al-Douri, R. (2009). Application of multitemporal Landsat data to monitor land cover changes in the Eastern Nile Delta region, Egypt. *International Journal of Remote Sensing, 30*, 2977-2996

Adam, B. (2011). On the fly and Permanent Orthorectification of NITF Images in ArcGIS

Agüera, F., Aguilar, F.J., & Aguilar, M.A. (2008). Using texture analysis to improve per-pixel classification of very high resolution images for mapping plastic greenhouses. *ISPRS Journal of Photogrammetry and Remote Sensing, 63*, 635-646

Alphan, H., Doygun, H., & Unlukaplan, Y.I. (2009). Post-classification comparison of land cover using multitemporal Landsat and ASTER imagery: the case of Kahramanmara angstrom, Turkey. *Environmental Monitoring and Assessment, 151*, 327-336

Ameen, M. (1992). Effect of Basement Tectonics on Hydrocarbon Generation, Migration, and Accumulation in Northern Iraq (1). *AAPG Bulletin, 76*, 356-370

Andersen, G.L. (2006). How to detect desert trees using corona images: Discovering historical ecological data. *Journal of arid environments, 65*, 491-511

Anderson, J.R. (1976). *A Land use and land cover classification system for use with remote sensor data*. Washington: U.S. Govt. Print. Off.

Anderson, M.C., Allen, R.G., Morse, A., & Kustas, W.P. (2012). Use of Landsat thermal imagery in monitoring evapotranspiration and managing water resources. *Remote sensing of environment, 122*, 50-65

Angel, S., Parent, J., & Civco, D. (2007). Urban sprawl metrics: an analysis of global urban expansion using GIS. In, *Proceedings of ASPRS 2007 Annual Conference, Tampa, Florida May*: Citeseer

Arnell, N.W. (1999). Climate change and global water resources. *Global Environmental Change, 9*, S31-S49

Balcik, F., Sanli, F., Goksel, C., Ulugtekin, N., & Dogru, A. (2009). a change detection analysis in the izmir bird paradise: integration of remote sensing and geographic information system. *Fresenius environmental bulletin, 18*, 51-56

Beck, A. (2007). Evaluation of Corona and Ikonos high resolution satellite imagery for archaeological prospection in western Syria.(Method). *Antiquity, 81*, 161

Bhatta, B. (2010). *Analysis of urban growth and sprawl from remote sensing data*. Springer Science & Business Media

Bitelli, G., & Girelli, V.A. (2009). Metrical use of declassified satellite imagery for an area of archaeological interest in Turkey. *Journal of Cultural Heritage, 10, Supplement 1*, e35-e40

Brame, D.B. (1989). Earth surface hydrocarbon gas cloud detection by use of landsat data. In: Google Patents

Buday, T. (1980). *The regional geology of Iraq: stratigraphy and paleogeography*. State Organization

Carlson, T.N., & Arthur, S.T. (2000). The impact of land use—land cover changes due to urbanization on surface microclimate and hydrology: a satellite perspective. *Global and Planetary Change, 25*, 49-65

Carpenter, D., & Carpenter, S. (1983). Modeling inland water quality using Landsat data. *Remote sensing of environment, 13*, 345-352

Casana, J. (2008). Stereo analysis, DEM extraction and orthorectification of CORONA satellite imagery: archaeological applications from the Near East. *Antiquity, 82*, 732-749

CAST (2012). CORONA Atlas of the Middle East (BETA) , Center for Advanced Spatial Technologies (CAST), University of Arkansas/U.S. Geological Survey. In

Challis, K. (2002). Corona remotely-sensed imagery in dryland archaeology: the Islamic City of al-Raqqa, Syria. *Journal of field archaeology, 29*, 139

Chavez Jr, P.S. (1988). An improved dark-object subtraction technique for atmospheric scattering correction of multispectral data. *Remote sensing of environment, 24*, 459-479

Chavez, P.S. (1996). Image-based atmospheric corrections-revisited and improved. *Photogrammetric engineering and remote sensing, 62*, 1025-1035

Cohen, W.B., Fiorella, M., Gray, J., Helmer, E., & Anderson, K. (1998). An efficient and accurate method for mapping forest clearcuts in the Pacific Northwest using Landsat imagery. *Photogrammetric engineering and remote sensing, 64*, 293-299

Cohen, W.B., & Goward, S.N. (2004). Landsat's role in ecological applications of remote sensing. *Bioscience, 54*, 535-545

Cohen, W.B., Spies, T.A., Alig, R.J., Oetter, D.R., Maiersperger, T.K., & Fiorella, M. (2002). Characterizing 23 years (1972–95) of stand replacement disturbance in western Oregon forests with Landsat imagery. *Ecosystems, 5*, 122-137

Congalton, R.G. (1991). A review of assessing the accuracy of classifications of remotely sensed data. *Remote sensing of environment, 37*, 35-46

Coskun Hepcan, C. (2013). Quantifying landscape pattern and connectivity in a Mediterranean coastal settlement: the case of the Urla district, Turkey. *Environmental Monitoring and Assessment, 185*, 143-155

Deng, J.S., Wang, K., Hong, Y., & Qi, J.G. (2009a). Spatio-temporal dynamics and evolution of land use change and landscape pattern in response to rapid urbanization. *Landscape and Urban Planning, 92*, 187-198

Deng, J.S., Wang, K., Li, J., & Deng, Y.H. (2009b). Urban Land Use Change Detection Using Multisensor Satellite Images. *Pedosphere, 19*, 96-103

Dewan, A.M., Corner, R., Hashizume, M., & Ongee, E.T. (2013). Typhoid Fever and its association with environmental factors in the Dhaka Metropolitan Area of Bangladesh: a spatial and time-series approach. *PLoS Negl Trop Dis, 7*, e1998

Dewan, A.M., & Yamaguchi, Y. (2009). Land use and land cover change in Greater Dhaka, Bangladesh: Using remote sensing to promote sustainable urbanization. *Applied Geography, 29*, 390-401

El Hajj, M., Bégué, A., Lafrance, B., Hagolle, O., Dedieu, G., & Rumeau, M. (2008). Relative radiometric normalization and atmospheric correction of a SPOT 5 time series. *Sensors, 8*, 2774-2791

ENVI (2015). ENvironment for Visualizing Images. In. USA: Harris Geospatial Solutions

Erbek, F.S., Özkan, C., & Taberner, M. (2004). Comparison of maximum likelihood classification method with supervised artificial neural network algorithms for land use activities. *International Journal of Remote Sensing, 25*, 1733-1748

Exelis (2015). Feature Extraction Module. In, *Exelis Visual Information Solutions* (p. Image segmentation). Colorado: Exelis Visual Information Solutions

Foody, G.M., Campbell, N., Trodd, N., & Wood, T. (1992). Derivation and applications of probabilistic measures of class membership from the maximum-likelihood classification. *Photogrammetric engineering and remote sensing, 58*, 1335-1341

Fowler (2004). Cover: Declassified CORONA KH-4B satellite photography of remains from Rome's desert frontier. *International Journal of Remote Sensing, 25*,

3549-3554

Francis, P., & Rothery, D. (1987). Using the Landsat Thematic Mapper to detect and monitor active volcanoes: An example from Lascar volcano, northern Chile. *Geology, 15*, 614-617

Frazier, P.S., & Page, K.J. (2000). Water body detection and delineation with Landsat TM data. *Photogrammetric engineering and remote sensing, 66*, 1461-1468

Geospatial, H. (2015). Erdas Imagine. In. USA: Hexagon Geospatial

Gheyle, W. (2004). Evaluating CORONA: a case study in the Altai Republic (South Siberia).(Method). *Antiquity, 78*, 391

González-Sanpedro, M., Le Toan, T., Moreno, J., Kergoat, L., & Rubio, E. (2008). Seasonal variations of leaf area index of agricultural fields retrieved from Landsat data. *Remote sensing of environment, 112*, 810-824

Gonzalez, R.C., & Woods, R. (1992). E.(1992): Digital Image Processing. *Addison-Wesley, 5*, 11-15

Goossens, R., De Wulf, A., Bourgeois, J., Gheyle, W., & Willems, T. (2006). Satellite imagery and archaeology: the example of CORONA in the Altai Mountains. *Journal of Archaeological Science, 33*, 745-755

Halbouty, M.T. (1976). Application of Landsat imagery to petroleum and mineral exploration. *AAPG Bulletin, 60*, 745-793

Halbouty, M.T. (1980). Geologic significance of Landsat data for 15 giant oil and gas fields. *AAPG Bulletin, 64*, 8-36

Hamandawana, H. (2007). Proposed methodology for georeferencing and mosaicking Corona photographs. *International Journal of Remote Sensing, 28*, 5-22

Hameed, H. (2013). Water harvesting in Erbil Governorate, Kurdistan region, Iraq: detection of suitable sites using geographic information system and remote sensing. *Student thesis series INES*

Haralick, R.M., Shanmugam, K., & Dinstein, I.H. (1973). Textural Features for Image Classification. *Systems, Man and Cybernetics, IEEE Transactions on, SMC-3*, 610-621

Hritz, C. (2013). A malarial-ridden swamp: using Google Earth Pro and Corona to access the southern Balikh valley, Syria. *Journal of Archaeological Science, 40*, 1975-1987

Hudak, A.T., & Hudak, C.A. (2001). Textural analysis of high resolution imagery to quantify bush encroachment in Madikwe Game Reserve, South Africa, 1955-1996. *International Journal of Remote Sensing, 22*, 2731-2740

Jackson, T.J., Ragan, R.M., & Fitch, W.N. (1977). Test of Landsat-based urban hydrologic modeling

Jassim, S.Z., & Goff, J.C. (2006). *Geology of Iraq*. DOLIN, sro, distributed by Geological Society of London

Jeffreys, H. (1946). An Invariant Form for the Prior Probability in Estimation Problems. *Proceedings of the Royal Society of London. Series A, Mathematical and Physical Sciences, 186*, 453-461

Jensen, J.R., Rutchey, K., Koch, M.S., & Narumalani, S. (1995). Inland wetland change detection in the Everglades Water Conservation Area 2A using a time series of normalized remotely sensed data. *Photogrammetric engineering and remote sensing, 61*, 199-209

Jia, X., & Richards, J.A. (1999). Segmented principal components transformation for efficient hyperspectral remote-sensing image display and classification. *IEEE Transactions on Geoscience and Remote Sensing, 37*, 538-542

Jusoff, K., & Senthavy, S. (2003). Land use change detection using remote sensing and geographical information system (GIS) in Gua Musang district, Kelantan, Malaysia. *Journal of Tropical Forest Science, 15*, 303-312

Kauth, R., Lambeck, P., Richardson, W., Thomas, G., & Pentland, A. (1979). Feature extraction applied to agricultural crops as seen by Landsat

Kauth, R.J., & Thomas, G. (1976). The tasselled cap--a graphic description of the spectral-temporal development of agricultural crops as seen by Landsat. In, *LARS Symposia* (p. 159)

Kavzoglu, T. (2008). Determination of environmental degradation due to urbanization and industrialization in Gebze, Turkey. *Environmental Engineering Science, 25*, 429-438

Kennedy, D. (1998). Declassified satellite photographs and archaeology in the Middle East: Case studies from Turkey. Antiquity 72 (277): 553-561.

Kesgin, B., & Nurlu, E. (2009). Land cover changes on the coastal zone of Candarli Bay, Turkey using remotely sensed data. *Environmental Monitoring and Assessment, 157*, 89-96

KNA (2013). About Kurdistan. In: Kurdistan National Assembly

Kostka, R. (2002). The world mountain Damavand: documentation and monitoring of human activities using remote sensing data. *ISPRS Journal of Photogrammetry and Remote Sensing, 57*, 5-12

KRG-MNR (2013). Oil production in Kurdistan region. In. Kurdistan region: Ministry of Natural Resources

KRG (2013). Kurdistan"s geography and climate. In: Kurdistan Regional Government

Lambin, E.F., Rounsevell, M., & Geist, H. (2000). Are agricultural land-use models able to predict changes in land-use intensity? *Agriculture, Ecosystems & Environment, 82*, 321-331

Lamsal, D. (2011). Digital terrain modelling using Corona and ALOS PRISM data to investigate the distal part of Imja Glacier, Khumbu Himal, Nepal. *Journal of Mountain Science, 8*, 390-402

Leachtenauer, J.C. (1997). Digitizing CORONA imagery: Quality vs. cost CORONA: Between the Sun and the Earth, the First NRO Reconnaissance Eye in Space.

Lee, K.-L., & Chen, L.-H. (2002). A new method for coarse classification of textures and class weight estimation for texture retrieval. *PATTERN RECOGNITION AND IMAGE ANALYSIS C/C OF RASPOZNAVANIYE OBRAZOV I ANALIZ IZOBRAZHENII, 12*, 400-410

Lenney, M.P., Woodcock, C.E., Collins, J.B., & Hamdi, H. (1996). The status of agricultural lands in Egypt: the use of multitemporal NDVI features derived from Landsat TM. *Remote sensing of environment, 56*, 8-20

López, E., Bocco, G., Mendoza, M., & Duhau, E. (2001). Predicting land-cover and land-use change in the urban fringe: a case in Morelia city, Mexico. *Landscape and Urban Planning, 55*, 271-285

Lorenz, H. (2004). Integration of Corona and Landsat Thematic Mapper data for bedrock geological studies in the high Arctic. *International Journal of Remote Sensing, 25*, 5143-5162

Lu, D., Mausel, P., Brondizio, E., & Moran, E. (2002). Assessment of atmospheric correction methods for Landsat TM data applicable to Amazon basin LBA research. *International Journal of Remote Sensing, 23*, 2651-2671

MacDonald, R.A. (1995). Opening the Cold War Sky to the Public: Declassifying Satellite Reconnaissance Imagery. Photogrammetric Engineering b Remote Sensing, 61 (4):385-390.

Marceau, D.J., Howarth, P.J., Dubois, J.-M.M., & Gratton, D.J. (1990). Evaluation of the grey-level co-occurrence matrix method for land-cover classification using SPOT imagery. *IEEE Transactions on Geoscience and Remote Sensing, 28,* 513-519

Masek, J., Lindsay, F., & Goward, S. (2000). Dynamics of urban growth in the Washington DC metropolitan area, 1973-1996, from Landsat observations. *International Journal of Remote Sensing, 21,* 3473-3486

Masek, J.G. (2001). Stability of boreal forest stands during recent climate change: evidence from Landsat satellite imagery. *Journal of biogeography, 28,* 967-976

Masek, J.G., Huang, C., Wolfe, R., Cohen, W., Hall, F., Kutler, J., & Nelson, P. (2008). North American forest disturbance mapped from a decadal Landsat record. *Remote sensing of environment, 112,* 2914-2926

Maselli, F., Conese, C., & Petkov, L. (1994). Use of probability entropy for the estimation and graphical representation of the accuracy of maximum likelihood classifications. *ISPRS Journal of Photogrammetry and Remote Sensing, 49,* 13-20

McDowall, D. (1992). *The Kurds: A nation denied*. Harry Ransom Humanities Research Center

Meyer, W.B. (1992). human population growth and global land-use/cover change. *Annual review of ecology and systematics, 23,* 39-61

Naik, P.K., Tambe, J.A., Dehury, B.N., & Tiwari, A.N. (2008). Impact of urbanization on the groundwater regime in a fast growing city in central India. *Environmental Monitoring and Assessment, 146,* 339-373

NASA (2016). NASA's Goddard Space Flight Centre in Greenbelt, Md. In. USA

O'Leary, C.A. (2002). The Kurds of Iraq: Recent history, future prospects. *Middle East Review of International Affairs, 6,* 17-29

Olson, R. (1992). The Kurdish question in the aftermath of the Gulf War: geopolitical and geostrategic changes in the Middle East. *Third Worl Quarterly, 13*

Otukei, J.R., & Blaschke, T. (2010). Land cover change assessment using decision trees, support vector machines and maximum likelihood classification algorithms. *International Journal of Applied Earth Observation and Geoinformation, 12,* S27-S31

Paola, J.D., & Schowengerdt, R.A. (1995). A detailed comparison of backpropagation neural network and maximum-likelihood classifiers for urban land use classification. *IEEE Transactions on Geoscience and Remote Sensing, 33,* 981-996

Paolini, L., Grings, F., Sobrino, J.A., Jiménez Muñoz, J.C., & Karszenbaum, H. (2006). Radiometric correction effects in Landsat multi-date/multi-sensor change detection studies. *International Journal of Remote Sensing, 27*, 685-704

Paul, F. (2000). Evaluation of different methods for glacier mapping using Landsat TM. In, *Proceedings, EARSeL-SIG Workshop*

Paul, F., Kääb, A., Maisch, M., Kellenberger, T., & Haeberli, W. (2002). The new remote-sensing-derived Swiss glacier inventory: I. Methods. *Annals of Glaciology, 34*, 355-361

Peel, M.C., Finlayson, B.L., & McMahon, T.A. (2007). Updated world map of the Köppen-Geiger climate classification. *Hydrol. Earth Syst. Sci, 11*, 1633-1644

Peterson, U., & Aunap, R. (1998). Changes in agricultural land use in Estonia in the 1990s detected with multitemporal Landsat MSS imagery. *Landscape and Urban Planning, 41*, 193-201

Pham, H.M., Yamaguchi, Y., & Bui, T.Q. (2011). A case study on the relation between city planning and urban growth using remote sensing and spatial metrics. *Landscape and Urban Planning, 100*, 223-230

Philip, G. (2002). CORONA satellite photography: an archaeological application from the Middle East. *Antiquity, 76*, 109

Philip, G., Donoghue, D., Beck, A., & Galiatsatos, N. (2002). CORONA satellite photography: an archaeological application from the Middle East. *Antiquity, 76*, 109-118

Philp, R., & Crisp, P. (1982). Surface geochemical methods used for oil and gas prospecting—a review. *Journal of Geochemical Exploration, 17*, 1-34

Porter-Bolland, L., Ellis, E.A., & Gholz, H.L. (2007). Land use dynamics and landscape history in La Montaña, Campeche, Mexico. *Landscape and Urban Planning, 82*, 198-207

Resources, M.o.A.a.W. (2012). Forest. In: General Directorate of Horticulture, Forestry and Rangeland

Richardson, A.J., & Wiegand, C. (1977). Distinguishing vegetation from soil background information.[by gray mapping of Landsat MSS data]

Ridd, M.K., & Liu, J.J. (1998). A comparison of four algorithms for change detection in an urban environment. *Remote sensing of environment, 63*, 95-100

Rigina, O. (2003). Detection of boreal forest decline with high-resolution

panchromatic satellite imagery. *International Journal of Remote Sensing, 24*, 1895-1912

Rocchio, L.E., Hodge, G.M., Arvidson, T., Williams, D.L., & Irons, J.R. (2005). The Landsat Legacy: Tracking down three decades of knowledge. In, *Proceedings of Pecora 16 Symposium, Global priorities in land remote sensing*

Royle, D.D., & Lathrop, R.G. (1997). Monitoring hemlock forest health in New Jersey using Landsat TM data and change detection techniques. *Forest science, 43*, 327-335

Ruelland, D. (2011). Comparison of methods for LUCC monitoring over 50 years from aerial photographs and satellite images in a Sahelian catchment. *International Journal of Remote Sensing, 32*, 1747-1777

Sesnie, S.E., Gessler, P.E., Finegan, B., & Thessler, S. (2008). Integrating Landsat TM and SRTM-DEM derived variables with decision trees for habitat classification and change detection in complex neotropical environments. *Remote sensing of environment, 112*, 2145-2159

Seto, K.C., Woodcock, C., Song, C., Huang, X., Lu, J., & Kaufmann, R. (2002). Monitoring land-use change in the Pearl River Delta using Landsat TM. *International Journal of Remote Sensing, 23*, 1985-2004

Shaban, M., & Dikshit, O. (2001). Improvement of classification in urban areas by the use of textural features: the case study of Lucknow city, Uttar Pradesh. *International Journal of Remote Sensing, 22*, 565-593

Song, C., Woodcock, C.E., Seto, K.C., Lenney, M.P., & Macomber, S.A. (2001). Classification and change detection using Landsat TM data: when and how to correct atmospheric effects? *Remote sensing of environment, 75*, 230-244

Stow, D., Tinney, L., & Estes, J. (1980). Deriving land use/land cover change statistics from Landsat-A study of prime agricultural land

Strahler, A.H. (1980). The use of prior probabilities in maximum likelihood classification of remotely sensed data. *Remote sensing of environment, 10*, 135-163

Sun, Z., Ma, R., & Wang, Y. (2009a). Using Landsat data to determine land use changes in Datong basin, China. *Environmental Geology, 57*, 1825-1837

Sun, Z.Y., Ma, R., & Wang, Y.X. (2009b). Using Landsat data to determine land use changes in Datong basin, China. *Environmental Geology, 57*, 1825-1837

Tang, L., Wu, C., & Chen, Z. (2002). Image dense matching based on region growth with adaptive window. *Pattern Recognition Letters, 23*, 1169-1178

Tappan, G.G. (2000). Use of Argon, Corona, and Landsat imagery to assess 30 years of land resource changes in west-central Senegal. *Photogrammetric engineering and remote sensing, 66*, 727-735

Torres-Vera, M.A., Prol-Ledesma, R.M., & Garcia-Lopez, D. (2009). Three decades of land use variations in Mexico City. *International Journal of Remote Sensing, 30*, 117-138

Townshend, J.R., Masek, J.G., Huang, C., Vermote, E.F., Gao, F., Channan, S., Sexton, J.O., Feng, M., Narasimhan, R., & Kim, D. (2012). Global characterization and monitoring of forest cover using Landsat data: opportunities and challenges. *International Journal of Digital Earth, 5*, 373-397

Tyagi, P., & Bhosle, U. (2011). Atmospheric correction of remotely sensed images in spatial and transform domain. *International Journal of Image Processing, 5*, 564-579

Tyagi, P., & Bhosle, U. (2014). Radiometric correction of Multispectral Images using Radon Transform. *Journal of the Indian Society of Remote Sensing, 42*, 23-34

UNDP (2011). *Drought Impact Assessment, Recovery and Mitigation Framework and Regional Project Design in Kurdistan Region (KR)*. United Nations Development Programmer Iraq

Ur, J. (2003). CORONA satellite photography and ancient road networks: a northern Mesopotamian case study. (Method). *Antiquity, 77*, 102

USGS (2008). Dasymetric mapping techniques. In. United States: United States Geological Survey

USGS (2015). Landsat data. In. United States: USGS

Weber, C., & Puissant, A. (2003). Urbanization pressure and modeling of urban growth: example of the Tunis Metropolitan Area. *Remote sensing of environment, 86*, 341-352

Wilkinson, K. (2006). Satellite imagery as a resource in the prospection for archaeological sites in central Syria. *Geoarchaeology, 21*, 735-750

Wilson, E.H., Hurd, J.D., Civco, D.L., Prisloe, M.P., & Arnold, C. (2003). Development of a geospatial model to quantify, describe and map urban growth. *Remote sensing of environment, 86*, 275-285

Wong, S., & Sarker, M. (2014). Land use/land cover mapping using multi-scale texture processing of high resolution data. In, *IOP Conference Series: Earth and Environmental Science* (p. 012185): IOP Publishing

Xian, G., & Crane, M. (2005). Assessments of urban growth in the Tampa Bay watershed using remote sensing data. *Remote sensing of environment, 97*, 203-215

Xiao, J., Shen, Y., Ge, J., Tateishi, R., Tang, C., Liang, Y., & Huang, Z. (2006). Evaluating urban expansion and land use change in Shijiazhuang, China, by using GIS and remote sensing. *Landscape and Urban Planning, 75*, 69-80

Yadav, P., Kapoor, M., & Sarma, K. (2012). Land use land cover mapping, change detection and conflict analysis of Nagzira-Navegaon corridor, Central India using geospatial technology. *International Journal of Remote Sensing and GIS, 1*, 90-98

Yang, L., Xian, G., Klaver, J.M., & Deal, B. (2003). Urban land-cover change detection through sub-pixel imperviousness mapping using remotely sensed data. *Photogrammetric Engineering & Remote Sensing, 69*, 1003-1010

Yang, X., & Lo, C. (2000). Relative radiometric normalization performance for change detection from multi-date satellite images. *Photogrammetric engineering and remote sensing, 66*, 967-980

Yuan, F., Sawaya, K.E., Loeffelholz, B.C., & Bauer, M.E. (2005). Land cover classification and change analysis of the Twin Cities (Minnesota) Metropolitan Area by multitemporal Landsat remote sensing. *Remote sensing of environment, 98*, 317-328

Zainal, A., Dalby, D., & Robinson, I. (1993). Monitoring marine ecological changes on the east coast of Bahrain with Landsat TM. *Photogrammetric Engineering and Remote Sensing;(United States), 59*

Zoran, M., & Weber, C. (2007). Use of multi-temporal and multispectral satellite data for urban change detection analysis. *Journal of Optoelectronics and Advanced Materials, 9*, 1926-1932

Appendix A: CORONA and Landsat images details

NUMBER	MISSION	MISSION NUMBER	SYSTEM	DATE	SCENE ID	CLOUD COVER
1	CORONA	DS1107-2170DA	KH-4B	2/08/1969	ds1107-2170da091.ntf	0.00%
2	CORONA	DS1107-2170DA	KH-4B	2/08/1969	ds1107-2170da092.ntf	0.00%
3	CORONA	DS1107-2170DA	KH-4B	2/08/1969	ds1107-2170da093.ntf	0.00%
4	CORONA	DS1107-2170DA	KH-4B	2/08/1969	ds1107-2170da094.ntf	0.00%
5	CORONA	DS1107-2170DA	KH-4B	2/08/1969	ds1107-2170da095.ntf	0.00%
6	CORONA	DS1107-2170DA	KH-4B	2/08/1969	ds1107-2170da096.ntf	0.00%
7	CORONA	DS1107-2170DA	KH-4B	2/08/1969	ds1107-2170da097.ntf	0.00%
8	CORONA	DS1107-2170DA	KH-4B	2/08/1969	ds1107-2170da098.ntf	0.00%
9	CORONA	DS1107-2170DA	KH-4B	2/08/1969	ds1107-2170da099.ntf	0.00%
10	CORONA	DS1107-2170DA	KH-4B	2/08/1969	ds1107-2170da100.ntf	0.00%
11	CORONA	DS1107-2170DA	KH-4B	2/08/1969	ds1107-2170da101.ntf	0.00%
12	CORONA	DS1107-2170DA	KH-4B	2/08/1969	ds1107-2170da102.ntf	0.00%
13	CORONA	DS1107-2170DA	KH-4B	2/08/1969	ds1107-2170da103.ntf	0.00%
14	CORONA	DS1107-2170DA	KH-4B	2/08/1969	ds1107-2170da104.ntf	0.00%
15	CORONA	DS1107-2170DA	KH-4B	2/08/1969	ds1107-2170da105.ntf	0.00%
16	CORONA	DS1107-2170DA	KH-4B	2/08/1969	ds1107-2170da106.ntf	0.00%
17	CORONA	DS1107-2170DA	KH-4B	2/08/1969	ds1107-2170da107.ntf	0.00%
18	CORONA	DS1107-2170DA	KH-4B	2/08/1969	ds1107-2170da108.ntf	0.00%
19	CORONA	DS1107-2170DA	KH-4B	2/08/1969	ds1107-2170da109.ntf	0.00%
20	CORONA	DS1107-2170DA	KH-4B	2/08/1969	ds1107-2170da110.ntf	0.00%
21	CORONA	DS1107-2170DA	KH-4B	2/08/1969	ds1107-2170da111.ntf	0.00%
22	CORONA	DS1107-2170DA	KH-4B	2/08/1969	ds1107-2170da112.ntf	0.00%
23	CORONA	DS1107-2170DA	KH-4B	2/08/1969	ds1107-2170da113.ntf	0.00%
24	CORONA	DS1107-2170DA	KH-4B	2/08/1969	ds1107-2170da114.ntf	0.00%
25	CORONA	DS1107-2170DA	KH-4B	2/08/1969	ds1107-2170da115.ntf	0.00%
26	CORONA	DS1107-2170DA	KH-4B	2/08/1969	ds1107-2170da116.ntf	0.00%
27	CORONA	DS1107-2170DA	KH-4B	2/08/1969	ds1107-2170da117.ntf	0.00%
28	CORONA	DS1107-2170DA	KH-4B	2/08/1969	ds1107-2170da118.ntf	0.00%
29	CORONA	DS1107-2170DA	KH-4B	2/08/1969	ds1107-2170da119.ntf	0.00%
30	CORONA	DS1107-2170DA	KH-4B	2/08/1969	ds1107-2170da120.ntf	0.00%
31	CORONA	DS1107-2154DA	KH-4B	3/08/1969	DS1107-2154DA072.tgz	0.00%
32	CORONA	DS1107-2154DA	KH-4B	3/08/1969	DS1107-2154DA073.tgz	0.00%
33	CORONA	DS1107-2154DA	KH-4B	3/08/1969	DS1107-2154DA074.tgz	0.00%
34	CORONA	DS1107-2154DA	KH-4B	3/08/1969	DS1107-2154DA075.tgz	0.00%
35	CORONA	DS1107-2154DA	KH-4B	3/08/1969	DS1107-2154DA076.tgz	0.00%
36	CORONA	DS1107-2154DA	KH-4B	3/08/1969	DS1107-2154DA081.tgz	0.00%
37	CORONA	DS1107-2154DA	KH-4B	3/08/1969	DS1107-2154DA082.tgz	0.00%
38	CORONA	DS1107-2154DA	KH-4B	3/08/1969	DS1107-2154DA083.tgz	0.00%
39	CORONA	DS1107-2154DA	KH-4B	3/08/1969	DS1107-2154DA084.tgz	0.00%

NUMBER	SENSOR	PLATFORM	DATE	LANDSAT SCENE ID	CLOUD COVER	BAND NUMBER	ZONE	PROJECTION	PATH	ROW
1	MSS	LANDSAT 2	23/07/1976	LM21810351976205AAA05.tar	0.00%	4	38	UTM	181	35
2	MSS	LANDSAT 2	23/07/1976	LM21810361976205AAA05.tar	0.00%	4	38	UTM	181	36
3	MSS	LANDSAT 2	24/07/1976	LM21820341976206AAA05.tar	0.00%	4	38	UTM	182	34
4	MSS	LANDSAT 2	24/07/1976	LM21820351976206AAA05.tar	0.00%	4	38	UTM	182	35
5	MSS	LANDSAT 2	7/07/1976	LM21830341976189AAA05.tar	0.00%	4	38	UTM	183	34
6	TM	LANDSAT 4	16/07/1989	LT41680351989197XXX04.tar	10.0%	7	38	UTM	168	35
7	TM	LANDSAT 4	16/07/1989	LT41680361989197XXX03.tar	5.0%	7	38	UTM	168	36
8	TM	LANDSAT 4	7/07/1989	LT41690341989188XXX02.tar	0.00%	7	38	UTM	169	34
9	TM	LANDSAT 4	7/07/1989	LT41690351989188XXX02.tar	0.00%	7	38	UTM	169	35
10	TM	LANDSAT 4	14/07/1989	LT41700341989195XXX02.tar	0.00%	7	38	UTM	170	34
11	TM	LANDSAT 5	1/07/1998	LT51680351998182XXX01.tar	0.00%	7	38	UTM	168	35
12	TM	LANDSAT 5	1/07/1998	LT51680361998182XXX01.tar	0.00%	7	38	UTM	168	36
13	TM	LANDSAT 5	25/08/1998	LT51690341998237AAA01.tar	0.00%	7	38	UTM	169	34
14	TM	LANDSAT 5	25/08/1998	LT51690351998237AAA01.tar	0.00%	7	38	UTM	169	35
15	TM	LANDSAT 5	16/08/1998	LT51700341998228AAA01.tar	0.00%	7	38	UTM	170	34
16	TM	LANDSAT 5	23/07/2006	LT51680352006204MOR00.tar	0.00%	7	38	UTM	168	35
17	TM	LANDSAT 5	23/07/2006	LT51680362006204MOR00.tar	0.00%	7	38	UTM	168	36
18	TM	LANDSAT 5	14/07/2006	LT51690342006195MOR00.tar	0.00%	7	38	UTM	169	34
19	TM	LANDSAT 5	14/07/2006	LT51690352006195MOR00.tar	0.00%	7	38	UTM	169	35
20	TM	LANDSAT 5	21/07/2006	LT51700342006202MOR00.tar	0.00%	7	38	UTM	170	34
21	OLI TIRS	LANDSAT 8	27/06/2014	LC81680352014178LGN00.tar	0.01%	11	38	UTM	168	35
22	OLI TIRS	LANDSAT 8	27/06/2014	LC81680362014178LGN00.tar	0.01%	11	38	UTM	168	36
23	OLI TIRS	LANDSAT 8	4/07/2014	LC81690342014185LGN00.tar	13.30%	11	38	UTM	169	34
24	OLI TIRS	LANDSAT 8	4/07/2014	LC81690352014185LGN00.tar	1.01%	11	38	UTM	169	35
25	OLI TIRS	LANDSAT 8	11/07/2014	LC81700342014192LGN00.tar	0.19%	11	38	UTM	170	34

Appendix B: Accuracy assessment tables

Error matrix calculation for CORONA 1969 point dataset							
	Reference Data						
Classified Data		Built up	Bare land	Forest	Agriculture	row total	User accuracy
	Built up	60	5	1	0	66	91
	Bare land	8	50	4	5	67	75
	Forest	0	0	55	5	60	92
	Agriculture Area	0	5	4	50	59	85
	column total	68	60	64	60	252	
	Producers accuracy	88	83	86	83		
	Overall accuracy	85					
	Kappa coefficient	0.80					

Error matrix calculation for Landsat 1976 point dataset							
	Reference Data						
Classified Data		Built up	Bare land	Forest	Agriculture	row total	User accuracy
	Built up	30	20	0	0	50	60
	Bare land	15	40	0	4	59	68
	Forest	0	0	51	0	51	100
	Agriculture Area	0	0	9	57	66	86
	column total	45	60	60	61	226	
	Producers accuracy	67	67	85	93		
	Overall accuracy	79					
	Kappa coeficient	0.72					

Error matrix calculation for Landsat 1989 point dataset							
	Reference Data						
Classified Data		Built up	Bare land	Forest	Agriculture	row total	User accuracy
	Built up	60	3	0	8	71	85
	Bare land	3	62	0	4	69	90
	Forest	0	11	64	7	82	78
	Agriculture Area	1	2	0	53	56	95
	column total	64	78	64	72	278	
	Producers accuracy	94	79	100	74		
	Overall accuracy	86					
	Kappa coefficient	0.81					

Error matrix calculation for Landsat 1998 point dataset							
	Reference Data						
Classified Data		Built up	Bare land	Forest	Agriculture	row total	User accuracy
	Built up	61	0	0	1	62	98
	Bare land	7	57	1	14	79	72
	Forest	0	0	68	0	68	100
	Agriculture Area	2	2	0	44	49	90
	column total	70	59	69	59	258	
	Producers accuracy	87	97	99	75		
	Overall accuracy	89					
	Kappa coefficient	0.86					

Error matrix calculation for Landsat 2006 point dataset							
	Reference Data						
Classified Data		Built up	Bare land	Forest	Agriculture	row total	User accuracy
	Built up	64	1	0	0	65	98
	Bare land	4	53	0	18	75	71
	Forest	0	0	55	1	56	98
	Agriculture Area	9	18	9	77	113	68
	column total	77	72	64	96	309	
	Producers accuracy	83	74	86	80		
	Overall accuracy	81					
	Kappa coefficient	0.74					

Error matrix calculation for Landsat 2014 point dataset							
	Reference Data						
Classified Data		Built up	Bare land	Forest	Agriculture	row total	User accuracy
	Built up	60	5	0	0	65	92
	Bare land	6	63	1	13	83	76
	Forest	0	0	54	0	54	100
	Agriculture Area	0	0	6	60	66	91
	column total	66	68	61	73	268	
	Producers accuracy	91	93	89	82		
	Overall accuracy	88					
	Kappa coefficient	0.85					

Error matrix calculation Regions 1969 in KM²							
Reference Data							
Classified Data		Built up	Bare land	Forest	Agriculture	row total	User accuracy
	Built up	2.20	0.13	0.07	0.07	2.47	89
	Bare land	1.15	11.43	0.00	0.07	12.65	90
	Forest	0.08	1.75	3.00	0.01	4.83	62
	Agriculture Area	0.12	2.44	0.25	16.31	19.12	85
	column total	3.56	15.74	3.32	16.45	39.07	
	Producers accuracy	62	73	90	99		
	Overall accuracy	84					
	Kappa coefficient	0.76					

Error matrix calculation Regions 1976 in KM²							
Reference Data							
		Built up	Bare land	Forest	Agriculture	row total	User accuracy
Classified Data	Built up	1.16	0.12	0.45	0.00	1.72	67
	Bare land	0.03	10.80	1.15	0.12	12.10	89
	Forest	0.00	0.00	5.85	1.14	6.99	84
	Agriculture Area	0.02	1.10	0.00	2.56	3.68	70
	column total	1.20	12.02	7.45	3.83	24.50	
	Producers accuracy	96	90	79	67		
	Overall accuracy	83					
	Kappa coefficient	0.74					

Error matrix calculation Regions 1989 in KM²							
Reference Data							
Classified Data		Built up	Bare land	Forest	Agriculture	row total	User accuracy
	Built up	3.17	0.06	0.00	0.22	3.45	92
	Bare land	0.12	10.63	0.00	0.17	10.91	97
	Forest	0.00	0.00	4.45	0.00	4.45	100
	Agriculture Area	0.01	0.26	1.52	7.03	8.82	80
	column total	3.30	10.95	5.97	7.41	27.64	
	Producers accuracy	96	97	75	95		
	Overall accuracy	91					
	Kappa coefficient	0.88					

Error matrix calculation Regions 1998 in KM²							
		Reference Data					
		Built up	Bare land	Forest	Agriculture	row total	User accuracy
Classified Data	Built up	13.57	1.18	0.01	0.50	15.26	89
	Bare land	4.09	57.35	1.18	6.15	68.76	83
	Forest	0.00	0.00	6.69	0.07	6.76	99
	Agriculture Area	0.35	4.41	0.08	17.77	22.61	79
	column total	18.01	62.94	7.95	24.49	113.38	
	Producers accuracy	75	91	84	73		
	Overall accuracy	84					
	Kappa coefficient	0.73					

Error matrix calculation Regions 2006 in KM²							
		Reference Data					
		Built up	Bare land	Forest	Agriculture	row total	User accuracy
Classified Data	Built up	5.22	0.12	0.00	0.00	5.34	98
	Bare land	0.16	11.57	0.00	5.74	17.47	66
	Forest	0.00	0.00	7.22	0.00	7.22	100
	Agriculture Area	0.51	7.84	1.97	22.31	32.63	68
	column total	5.89	19.53	9.19	28.04	62.66	
	Producers accuracy	89	59	79	80		
	Overall accuracy	74					
	Kappa coefficient	0.60					

Error matrix calculation Regions 2014 in %							
		Reference Data					
		Built up	Bare land	Forest	Agriculture	row total	User accuracy
Classified Data	Built up	32.45	0.43	0.00	0.23	33.12	98
	Bare land	4.71	97.69	0.01	1.60	104.02	94
	Forest	0.02	0.01	7.91	2.25	10.19	78
	Agriculture Area	0.16	9.08	0.03	17.85	27.12	66
	column total	37.34	107.22	7.95	21.93	174.45	
	Producers accuracy	87	91	100	81		
	Overall accuracy	89					
	Kappa coefficient	0.81					

	Error matrix calculation for CORONA 1969 point dataset							
		Reference Data						
Classified Data		Water	Built up	Bare land	Forest	Agriculture	row total	User accuracy
	Water	65	0	0	0	0	65	100
	Built up	0	60	5	0	0	65	92
	Bare land	0	6	63	1	13	83	76
	Forest	0	0	0	54	0	54	100
	Agriculture Area	0	0	0	6	60	66	91
	column total	65	66	68	61	73	333	
	Producers accuracy	100	91	93	89	82		
	Overall accuracy	91						
	Kappa coefficient	0.88						

Error matrix calculation for Landsat MSS 1976 point dataset								
Reference Data								
Classified Data		Water	Built up	Bare land	Forest	Agriculture	row total	User accuracy
	Water	60	0	0	0	0	60	100
	Built up	0	30	20	0	0	50	60
	Bare land	0	15	40	0	4	59	68
	Forest	0	0	0	51	0	51	100
	Agriculture Area	0	0	0	9	57	66	86
	column total	60	45	60	60	61	286	
	Producers accuracy	100	67	67	85	93		
	Overall accuracy	83						
	Kappa coefficient	0.79						

Error matrix calculation for Landsat TM 1989 point dataset								
Reference Data								
Classified Data		Water	Built up	Bare land	Forest	Agriculture	row total	User accuracy
	Water	66	0	0	0	0	66	100
	Built up	0	60	3	0	8	71	85
	Bare land	0	3	62	0	4	69	90
	Forest	0	0	11	64	7	82	78
	Agriculture Area	0	1	2	0	53	56	95
	column total	66	64	78	64	72	344	
	Producers accuracy	100	94	79	100	74		
	Overall accuracy	89						
	Kappa coefficient	0.86						

Error matrix calculation for the Landsat TM 1998 point dataset								
	Reference Data							
Classified Data		Water	Built up	Bare land	Forest	Agriculture	row total	User accuracy
	Water	76	0	0	0	0	76	100
	Built up	0	61	0	0	1	62	98
	Bare land	0	7	57	1	14	79	72
	Forest	0	0	0	68	0	68	100
	Agriculture Area	0	2	2	0	44	48	92
	column total	76	70	59	69	59	333	
	Producers accuracy	100	87	97	99	75		
	Overall accuracy	92						
	Kappa coefficient	0.90						

Error matrix calculation for the Landsat TM 2006 point dataset								
	Reference Data							
Classified Data		Water	Built up	Bare land	Forest	Agriculture	row total	User accuracy
	Water	65	0	0	0	0	65	100
	Built up	0	64	1	0	0	65	98
	Bare land	0	4	53	0	18	75	71
	Forest	0	0	0	55	1	56	98
	Agriculture Area	0	9	18	9	77	113	68
	column total	65	77	72	64	96	374	
	Producers accuracy	100	83	74	86	80		
	Overall accuracy	84						
	Kappa coefficient	0.80						

Error matrix calculation for the Landsat 8 2014 point dataset								
	Reference Data							
Classified Data		Water	Built up	Bare land	Forest	Agriculture	row total	User accuracy
	Water	65	0	0	0	0	65	100
	Built up	0	60	5	0	0	65	92
	Bare land	0	6	63	1	13	83	76
	Forest	0	0	0	54	0	54	100
	Agriculture Area	0	0	0	6	60	66	91
	column total	65	66	68	61	73	333	
	Producers accuracy	100	91	93	89	82		
	Overall accuracy	91						
	Kappa coefficient	0.88						

Error matrix calculation Regions 1969 in KM²								
	Reference Data							
Classified Data		Water	Built up	Bare land	Forest	Agriculture	row total	User accuracy
	Water	100.98	0.00	0.00	0.00	0.00	100.98	100
	Built up	0.00	2.20	0.13	0.07	0.07	2.47	89
	Bare land	0.00	1.15	11.43	0.00	0.07	12.65	90
	Forest	0.00	0.08	1.75	3.00	0.01	4.83	62
	Agriculture	0.00	0.12	2.44	0.25	16.31	19.12	85
	column total	100.98	3.56	15.74	3.32	16.45	140.05	
	Producers accuracy	100	62	73	90	99		
	Overall accuracy	96						
	Kappa coefficient	0.90						

Error matrix calculation Regions 1976 in KM²								
	Reference Data							
Classified Data		Water	Built up	Bare land	Forest	Agriculture	row total	User accuracy
	Water	4.10	0.00	0.00	0.00	0.00	4.10	100
	Built up	0.00	1.16	0.12	0.45	0.00	1.72	67
	Bare land	0.00	0.03	10.80	1.15	0.12	12.10	89
	Forest	0.00	0.00	0.00	5.85	1.14	6.99	84
	Agriculture	0.00	0.02	1.10	0.00	2.56	3.68	70
	column total	4.10	1.20	12.02	7.45	3.83	28.59	
	Producers accuracy	100	96	90	79	67		
	Overall accuracy	86						
	Kappa coefficient	0.80						

Error matrix calculation Regions 1989 in KM²								
	Reference Data							
Classified Data		Water	Built up	Bare land	Forest	Agriculture	row total	User accuracy
	Water	18.64	0.00	0.00	0.00	0.00	18.64	100
	Built up	0.00	3.17	0.06	0.00	0.22	3.45	92
	Bare land	0.00	0.12	10.63	0.00	0.17	10.91	97
	Forest	0.00	0.00	0.00	4.45	0.00	4.45	100
	Agriculture	0.00	0.01	0.26	1.52	7.03	8.82	80
	column total	18.64	3.30	10.95	5.97	7.41	46.27	
	Producers accuracy	100	96	97	75	95		
	Overall accuracy	95						
	Kappa coefficient	0.93						

Error matrix calculation Regions 1998 in KM²								
	Reference Data							
Classified Data		Water	Built up	Bare land	Forest	Agriculture	row total	User accuracy
	Water	137.71	0.00	0.00	0.00	0.00	137.71	100
	Built up	0.00	13.57	1.18	0.01	0.50	15.26	89
	Bare land	0.00	4.09	57.35	1.18	6.15	68.76	83
	Forest	0.00	0.00	0.00	6.69	0.07	6.76	99
	Agriculture	0.00	0.35	4.41	0.08	17.77	22.61	79
	column total	137.71	18.01	62.94	7.95	24.49	251.09	
	Producers accuracy	100	75	91	84	73		
	Overall accuracy	93						
	Kappa coefficient	0.88						

Error matrix calculation Regions 2006 in KM²								
	Reference Data							
Classified Data		Water	Built up	Bare land	Forest	Agriculture	row total	User accuracy
	Water	94.09	0.00	0.00	0.00	0.00	94.09	100
	Built up	0.00	5.22	0.12	0.00	0.00	5.34	98
	Bare land	0.00	0.16	11.57	0.00	5.74	17.47	66
	Forest	0.00	0.00	0.00	7.22	0.00	7.22	100
	Agriculture	0.00	0.51	7.84	1.97	22.31	32.63	68
	column total	94.09	5.89	19.53	9.19	28.04	156.75	
	Producers accuracy	100	89	59	79	80		
	Overall accuracy	90						
	Kappa coefficient	0.82						

Error matrix calculation Regions 2014 in KM²								
	Reference Data							
Classified Data		Water	Built up	Bare land	Forest	Agriculture	row total	User accuracy
	Water	166.07	0.00	0.00	0.00	0.00	166.07	100
	Built up	0.00	32.45	0.43	0.00	0.23	33.12	98
	Bare land	0.00	4.71	97.69	0.01	1.60	104.02	94
	Forest	0.00	0.02	0.01	7.91	2.25	10.19	78
	Agriculture	0.00	0.16	9.08	0.03	17.85	27.12	66
	column total	166.07	37.34	107.22	7.95	21.93	340.52	
	Producers accuracy	100	87	91	100	81		
	Overall accuracy	95						
	Kappa coefficient	0.92						

Appendix C: From-To change detection detailed results

Change detection "From To", Areas KM²						
LULC Classes	**1969-1976**	**1976-1989**	**1989-1998**	**1998-2006**	**2006-2014**	**1969-2014**
Agriculture no change	1904.1	1029.3	1766.9	2702.5	1175.8	653.9
Bare land no change	21368.0	25950.1	28953.3	15994.4	15060.1	20063.2
Built up no change	20.2	35.2	110.1	128.3	209.8	45.0
Forest no change	2780.0	1215.2	1189.5	4598.5	6970.6	3738.0
Water no change	355.5	270.1	331.5	413.2	367.4	261.5
Total of unchanged classes	**26427.9**	**28500.0**	**32351.3**	**23836.8**	**23783.7**	**24761.6**
Agriculture to bare land	9836.0	4769.6	6397.5	603.4	15276.3	10374.0
Agriculture to built up	10.8	24.6	30.0	22.2	624.1	624.6
Agriculture to forest	385.4	12.1	2249.8	133.2	1538.3	477.0
Agriculture to water	51.7	34.4	88.2	13.8	31.1	58.5
Total agriculture Conversion	**10283.8**	**4840.7**	**8765.5**	**772.6**	**17469.9**	**11534.1**
Bare land to agriculture	3257.7	7191.2	1671.4	15238.1	798.2	1303.6
Bare land to built up	19.6	100.7	31.3	67.9	404.6	538.6
Bare land to forest	2019.6	39.3	1886.2	4157.4	481.1	4765.5
Bare land to water	82.5	51.0	88.5	14.9	13.3	76.5
Total Bare land Conversion	**5379.4**	**7382.2**	**3677.4**	**19478.3**	**1697.3**	**6684.2**
Built up to agriculture	10.6	6.7	18.3	32.5	1.7	4.8
Built up to bare land	45.2	9.6	37.5	10.6	6.9	27.4
Built up to forest	2.9	0.0	0.4	0.3	0.2	1.6
Built to water	0.8	0.0	0.9	1.0	0.4	0.9
Total built up Conversion	**59.5**	**16.4**	**57.0**	**44.4**	**9.2**	**34.7**
Forest to agriculture	685.6	2184.7	5.1	623.4	160.9	160.7
Forest to bare land	2019.5	1787.8	72.9	104.7	1741.9	1541.6
Forest to built up	0.9	4.8	0.0	0.1	14.9	43.4
Forest to water	16.9	3.7	0.1	0.6	3.3	19.2
Total forest Conversion	**2722.9**	**3981.0**	**78.1**	**728.9**	**1920.9**	**1764.9**
Water to agriculture	12.2	120.4	13.5	49.2	13.9	27.0
Water to bare land	64.5	113.6	11.6	44.3	59.9	140.1
Water to built	0.1	1.8	1.3	0.5	0.9	2.8
Water to forest	6.7	1.0	1.4	2.1	1.4	7.6
Total water Conversion	**83.6**	**236.8**	**27.7**	**96.0**	**76.2**	**177.6**
Total of changed classes	**18529.2**	**16457.0**	**12605.7**	**21120.2**	**21173.4**	**20195.4**
Grand Total	**44957.1**	**44957.1**	**44957.1**	**44957.1**	**44957.1**	**44957.1**

Change detection "From To", areas in % in respect to unchanged areas only						
LULC Classes	**1969-1976**	**1976-1989**	**1989-1998**	**1998-2006**	**2006-2014**	**1969-2014**
Agriculture unchanged	7.2	3.6	5.5	11.3	4.9	2.6
Bare land unchanged	80.9	91.1	89.5	67.1	63.3	81.0
Built up unchanged	0.1	0.1	0.3	0.5	0.9	0.2
Forest unchanged	10.5	4.3	3.7	19.3	29.3	15.1
Water unchanged	1.3	0.9	1.0	1.7	1.5	1.1
Total of unchanged	**100.0**	**100.0**	**100.0**	**100.0**	**100.0**	**100.0**

Change detection "From To", Areas in % in respect to changed areas only						
LULC Classes	**1969-1976**	**1976-1989**	**1989-1998**	**1998-2006**	**2006-2014**	**1969-2014**
Agriculture to bare land	53.1	29.0	50.8	2.9	72.1	51.4
Agriculture to built up	0.1	0.1	0.2	0.1	2.9	3.1
Agriculture to forest	2.1	0.1	17.8	0.6	7.3	2.4
Agriculture to water	0.3	0.2	0.7	0.1	0.1	0.3
Bare land to agriculture	17.6	43.7	13.3	72.1	3.8	6.5
Bare land to built up	0.1	0.6	0.2	0.3	1.9	2.7
Bare land to forest	10.9	0.2	15.0	19.7	2.3	23.6
Bare land to water	0.4	0.3	0.7	0.1	0.1	0.4
Built up to agriculture	0.1	0.0	0.1	0.2	0.0	0.0
Built up to bare land	0.2	0.1	0.3	0.1	0.0	0.1
Built up to forest	0.0	0.0	0.0	0.0	0.0	0.0
Built to water	0.0	0.0	0.0	0.0	0.0	0.0
Forest to agriculture	3.7	13.3	0.0	3.0	0.8	0.8
Forest to bare land	10.9	10.9	0.6	0.5	8.2	7.6
Forest to built up	0.0	0.0	0.0	0.0	0.1	0.2
Forest to water	0.1	0.0	0.0	0.0	0.0	0.1
Water to agriculture	0.1	0.7	0.1	0.2	0.1	0.1
Water to bare land	0.3	0.7	0.1	0.2	0.3	0.7
Water to built up	0.0	0.0	0.0	0.0	0.0	0.0
Water to forest	0.0	0.0	0.0	0.0	0.0	0.0
Total changed	**100.0**	**100.0**	**100.0**	**100.0**	**100.0**	**100.0**

Appendix D: From-To approach detailed results for three cities

Built area changes within 20 km radius, areas in km²							
Epochs		1969-1976	1976-1989	1989-1998	1998-2006	2006-2014	1969-2014
Duhok	Agriculture lost and built up gain	1.56	7.07	2.93	1.30	56.63	45.82
	Bare land lost and built up gain	1.70	6.22	2.02	2.99	20.75	35.53
	Forest lost and built up gain	0.37	0.68		0.01	0.50	10.51
	Built up lost and agriculture gain	1.19	0.59	1.54	3.71	0.05	0.26
	Built up lost and bare land gain	0.71	0.74	4.63	0.58	0.16	0.96
	Built up lost and forest gain	0.19		0.11		0.01	0.08
	Built up lost and water gain						0.03
	Built up unchanged	0.60	2.89	10.59	11.26	15.34	1.36

Epochs		1969-1976	1976-1989	1989-1998	1998-2006	2006-2014	1969-2014
Erbil	Agriculture lost and built up gain	2.6	3.7	6.3	1.8	132.5	206.7
	Bare land lost and built up gain	3.3	31.3	6.6	23.4	84.3	69.6
	Forest lost and built up gain		0.1				0.3
	Built up lost and agriculture gain	1.0	1.2	0.6	2.9	0.2	0.3
	Built up lost and bare land gain	4.0	1.5	6.9	1.4	0.5	0.5
	Built up unchanged	8.1	11.3	39.0	47.6	72.2	12.3

Epochs		1969-1976	1976-1989	1989-1998	1998-2006	2006-2014	1969-2014
Sulamani	Agriculture lost and built up gain	2.9	0.2	1.7	2.9	84.0	86.5
	Bare land lost and built up gain	5.8	11.6	4.1	9.9	67.4	91.1
	Forest lost and built up gain	0.0	0.3			1.1	3.6
	Water lost and built up gain						0.0
	Built up lost and agriculture gain	0.1	1.2	0.9	1.5	0.1	0.1
	Built up lost and bare land gain	2.2	2.0	2.7	0.4	0.4	0.6
	Built up lost and forest gain	0.1				0.0	0.1
	Built up unchanged	7.9	13.4	21.9	25.8	38.1	9.5

Built area gain, lose, and net within 20 km radius, areas in km² and %							
	Epochs	1969-1976	1976-1989	1989-1998	1998-2006	2006-2014	1969-2014
Duhok	Built up lost	2.1	1.3	6.3	4.3	0.2	1.3
	Built up gain	4.8	14.6	6.5	8.0	77.9	92.1
	Net gain	**2.7**	**13.2**	**0.2**	**3.7**	**77.7**	**90.8**
	Built up unchanged	0.6	2.9	10.6	11.3	15.3	1.4
Erbil	Built up lost	5.0	2.8	7.5	4.3	0.7	1.2
	Built up gain	5.9	35.1	12.9	25.2	216.7	276.7
	Net gain	**0.9**	**32.3**	**5.4**	**21.0**	**216.1**	**275.5**
	Built up unchanged	8.1	11.3	39.0	47.6	72.2	12.3
Sulamani	Built up lost	2.4	3.2	3.6	1.9	0.5	0.8
	Built up gain	8.7	12.1	5.8	12.9	152.5	181.2
	net gain	**6.3**	**8.9**	**2.1**	**11.0**	**152.0**	**180.4**
	Built up unchanged	7.9	13.4	21.9	25.8	38.1	9.5

	Epochs	1969-1976	1976-1989	1989-1998	1998-2006	2006-2014	1969-2014
Duhok	Agriculture lost and built up gain	1.6	7.1	2.9	1.3	56.6	45.8
	Bare land lost and built up gain	1.7	6.2	2.0	3.0	20.7	35.5
	Net from bare land and agriculture	**3.3**	**13.3**	**5.0**	**4.3**	**77.4**	**81.4**
Erbil	Agriculture lost and built up gain	2.6	3.7	6.3	1.8	132.5	206.7
	Bare land lost and built up gain	3.3	31.3	6.6	23.4	84.3	69.6
	Net from bare land and agriculture	**5.9**	**35.1**	**12.9**	**25.2**	**216.7**	**276.3**
Sulamani	Agriculture lost and built up gain	2.9	0.2	1.7	2.9	84.0	86.5
	Bare land lost and built up gain	5.8	11.6	4.1	9.9	67.4	91.1
	Net from bare land and agriculture	**8.7**	**11.8**	**5.8**	**12.9**	**151.4**	**177.6**

	Epochs	1969-1976	1976-1989	1989-1998	1998-2006	2006-2014	1969-2014
Duhok	Agriculture lost and built up gain	48	53	59	30	73	56
	Bare land lost and built up gain	52	47	41	70	27	44
	Net from bare land and agriculture	**100**	**100**	**100**	**100**	**100**	**100**
Erbil	Agriculture lost and built up gain	44	11	49	7	61	75
	Bare land lost and built up gain	56	89	51	93	39	25
	Net from bare land and agriculture	**100**	**100**	**100**	**100**	**100**	**100**
Sulamani	Agriculture lost and built up gain	34	2	29	23	55	49
	Bare land lost and built up gain	66	98	71	77	45	51
	Net from bare land and agriculture	**100**	**100**	**100**	**100**	**100**	**100**

Appendix E: Direction of expansion for three cities

Duhok/area (km²)	Buffer distances	1969	1976	1989	1998	2006	2014
East	1 KM	0.40	0.38	0.42	0.42	0.42	0.53
	5 KM	0.01	0.10	0.04	0.37	3.39	3.42
	10 KM	0.02			0.07	0.04	0.08
	15 KM	0.12		0.21	0.87	1.81	2.14
	20 KM						
North	1 KM	0.38	0.44	0.48	0.45	0.45	0.45
	5 KM	0.03	0.54	0.62	0.54	2.59	2.70
	10 KM	0.01	0.05	0.05	0.06	0.06	0.11
	15 KM	0.07	0.14	0.01	0.04	0.44	0.66
	20 KM	0.07	0.11		0.08		0.14
North East	1 KM	0.32	0.31	0.32	0.31	0.31	0.53
	5 KM	0.61	0.88	1.19	1.32	1.54	1.58
	10 KM	0.04	0.06	0.23	0.56	0.48	0.70
	15 KM	0.10		0.46	0.30	0.33	1.20
	20 KM	0.09		0.24	0.05	0.17	0.30
North West	1 KM	0.53	0.55	0.54	0.49	0.50	0.50
	5 KM	0.06	0.29	1.39	1.38	2.91	3.61
	10 KM	0.04		0.20	0.05	1.59	1.67
	15 KM	0.10	0.12	0.01	0.24		0.45
	20 KM	0.12	0.04		0.03		0.19
South	1 KM	0.32	0.25	0.40	0.43	0.43	0.49
	5 KM	0.06	0.32	5.16	5.19	1.61	1.73
	10 KM			0.24	0.37	0.47	0.52
	15 KM	0.11					0.11
	20 KM	0.19					0.19
South East	1 KM	0.35	0.33	0.43	0.41	0.42	0.49
	5 KM	0.28	0.15	0.23	0.73	2.83	2.99
	10 KM				0.00		0.00
	15 KM	0.03		0.00	0.61	0.94	1.43
	20 KM	0.05	0.16	0.27	0.19	0.19	0.69
South West	1 KM	0.32	0.36	0.39	0.43	0.45	0.49
	5 KM	0.15	0.84	1.01	1.26	3.15	3.57
	10 KM	0.03		0.00	0.06	0.09	0.10
	15 KM	0.61	0.86	1.04	0.37	0.02	1.97
	20 KM	0.13					0.13
West	1 KM	0.40	0.67	0.65	0.65	0.64	0.67
	5 KM	1.74	2.19	5.50	5.26	5.99	6.54
	10 KM	0.10		1.36	1.16	0.88	2.21
	15 KM	0.14	0.03	0.48	0.48	1.24	2.35
	20 KM	0.11	0.02	0.46	0.48	0.46	0.66

Erbil/area (km²)	Buffer distances	1969	1976	1989	1998	2006	2014
East	1 KM	0.39	0.42	0.61	0.62	0.61	0.62
	5 KM	0.35	0.35	2.27	3.50	3.66	11.09
	10 KM	0.06		0.03	0.05	0.13	21.88
	15 KM	0.02		0.78	0.78	0.78	0.78
	20 KM						
North	1 KM	0.46	0.48	0.53	0.51	0.53	0.50
	5 KM	0.70	1.50	1.21	1.41	2.41	11.17
	10 KM	0.09	0.49	0.30	0.07	0.44	15.32
	15 KM	0.09	0.15	0.28	0.34	0.37	0.48
	20 KM	0.00	0.00				0.00
North East	1 KM	0.40	0.48	0.49	0.49	0.49	0.49
	5 KM	0.61	0.77	4.14	5.48	5.84	8.30
	10 KM	0.06	0.19	1.01	1.69	1.46	11.61
	15 KM	0.00			0.00	0.00	0.00
	20 KM	0.00		0.71	0.17	0.09	0.74
North West	1 KM	0.45	0.47	0.43	0.44	0.45	0.46
	5 KM	1.45	2.44	5.02	4.11	6.30	13.34
	10 KM	0.19	0.00	0.69	0.91	1.56	37.43
	15 KM	0.14	0.12	0.06	0.12		0.22
	20 KM	0.08	0.06		0.03		0.10
South	1 KM	0.45	0.41	0.41	0.42	0.44	0.48
	5 KM	1.25	1.33	2.12	2.81	3.87	11.78
	10 KM	0.06		0.76	1.22	1.03	26.44
	15 KM						
	20 KM						
South East	1 KM	0.46	0.42	0.61	0.63	0.61	0.62
	5 KM	0.89	0.90	5.01	5.81	6.57	16.44
	10 KM	0.06		1.05	2.57	3.74	28.61
	15 KM			0.06	0.11	0.12	0.11
	20 KM	0.05	0.39	0.08	0.02	0.02	0.34
South West	1 KM	0.48	0.49	0.58	0.57	0.58	0.58
	5 KM	0.27	0.57	5.54	5.53	6.06	11.86
	10 KM	0.13		0.74	0.39	0.66	19.35
	15 KM	0.03		0.76	0.76	0.14	0.77
	20 KM						
West	1 KM	0.38	0.39	0.36	0.35	0.37	0.42
	5 KM	0.34	1.34	3.40	2.68	3.92	12.41
	10 KM	0.43		1.15	1.25	3.29	49.10
	15 KM	0.05	0.04	1.05	1.51	1.58	1.72
	20 KM	0.11	0.14	0.84	0.89	0.72	1.89

Sulamani/area (km^2)	Buffer distances	1969	1976	1989	1998	2006	2014
East	1 KM	0.00	0.02	0.02	0.03	0.02	0.02
	5 KM	0.48	1.39	2.75	2.80	2.81	4.68
	15 KM	0.02		0.05	0.06	0.03	19.95
	20 KM	0.11			0.01		1.63
	20 KM						
North	1 KM		0.04	0.04	0.03	0.03	0.03
	5 KM	0.45	0.41	2.62	2.89	3.02	3.21
	10 KM	0.01	0.07	0.07	0.07	0.07	0.07
	15 KM	0.05	0.12	0.17	0.12	0.14	8.42
	20 KM	0.07	0.06				2.78
North East	1 KM	0.01	0.01	0.00	0.01	0.01	0.01
	5 KM	0.13	2.04	2.15	2.19	3.02	3.25
	10 KM	0.06	0.15	0.16	0.16	0.16	0.16
	15 KM	0.04			0.06	0.02	9.06
	20 KM	0.21		0.32	0.24	0.28	8.83
North West	1 KM	0.04	0.06	0.03	0.01	0.04	0.05
	5 KM	0.49	1.88	2.13	1.52	2.07	2.51
	10 KM	0.12	0.01	1.08	1.08	1.09	1.09
	15 KM	0.09	0.13	0.02	0.02		16.70
	20 KM	0.19	0.05		0.07		2.53
South	1 KM	0.06	0.01	0.06	0.07	0.07	0.07
	5 KM	0.75	0.65	1.33	1.34	6.09	6.09
	10 KM	0.12		0.18	0.09	1.29	1.68
	15 KM	0.17					5.19
	20 KM	0.03					5.88
South East	1 KM	0.00	0.01	0.01	0.01	0.01	0.01
	5 KM	0.34	0.06	1.35	1.34	1.44	4.72
	10 KM			0.11	0.03	0.08	0.10
	15 KM	0.11			0.02	0.01	4.61
	20 KM	0.19	0.20	0.11	0.11	0.13	2.13
South West	1 KM	0.01	0.08	0.07	0.07	0.06	0.07
	5 KM	0.93	0.68	1.60	2.54	2.82	4.57
	10 KM	0.07		0.33	0.24	2.15	2.64
	15 KM	0.01		0.24	0.05		12.05
	20 KM	0.14					2.79
West	1 KM	0.04	0.01	0.05	0.05	0.07	0.09
	5 KM	0.59	1.45	1.52	0.51	0.70	5.27
	10 KM	0.28		2.16	2.27	2.57	3.11
	15 KM	0.31	0.70	0.95	0.96	0.94	41.40
	20 KM	0.19		0.08	0.09	0.09	19.67

Appendix F: CORONA and Landsat raw images

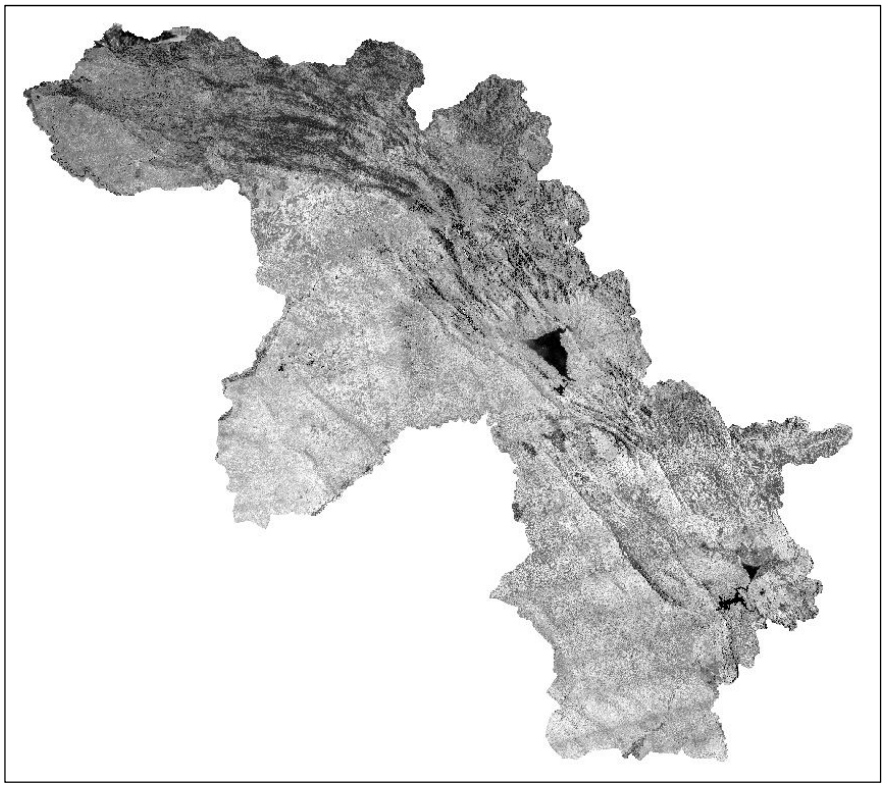

1969 CORONA image

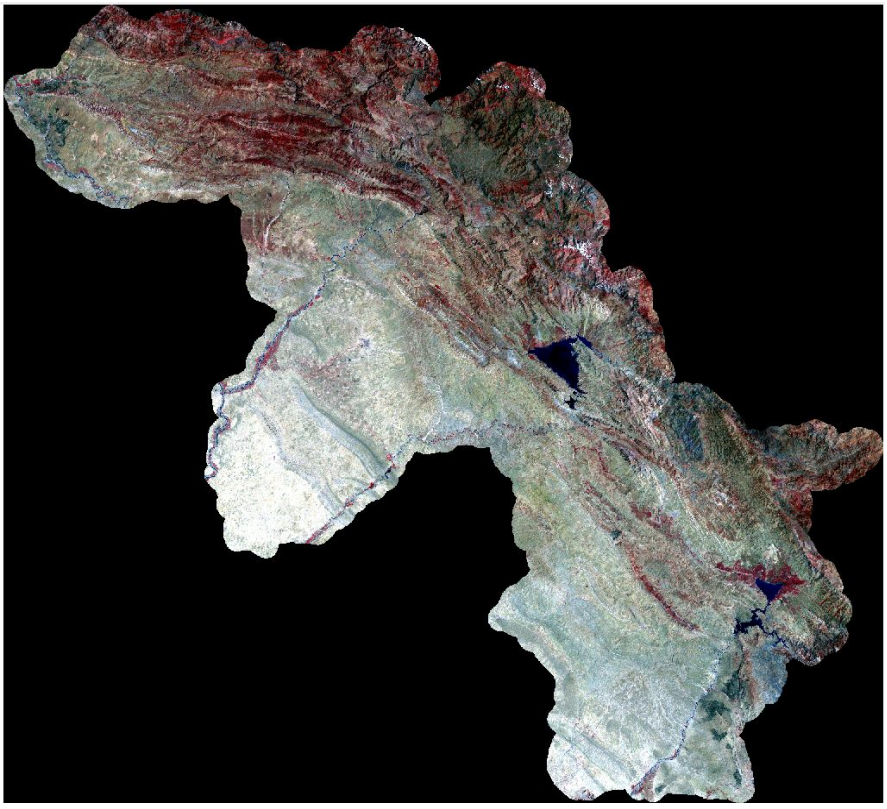

1976 Landsat 2 image

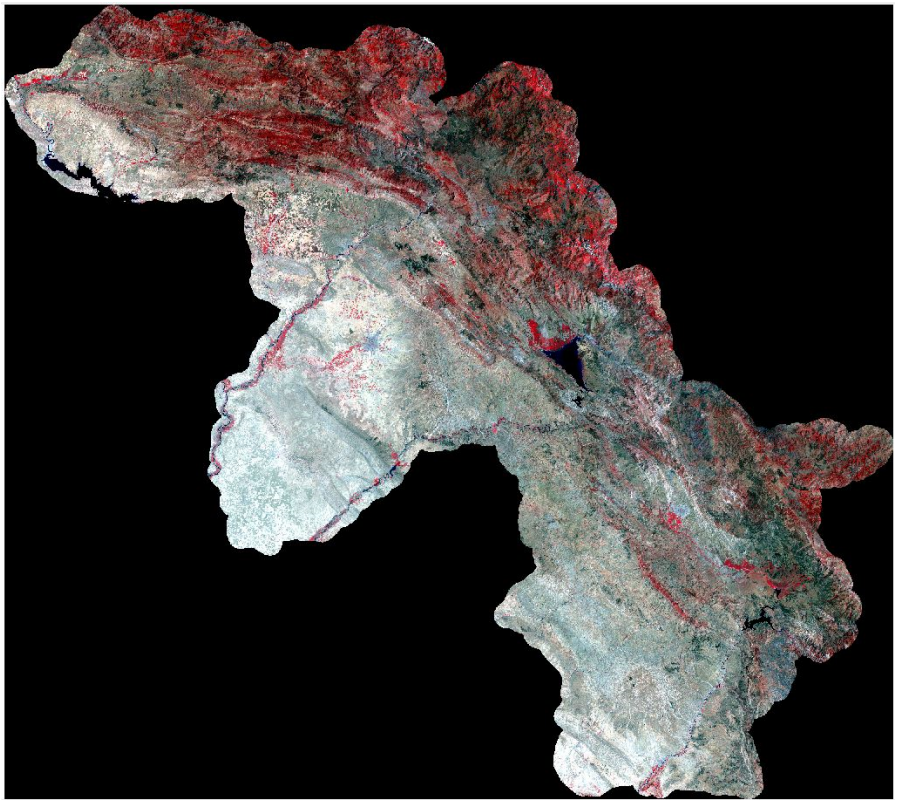

1989 Landsat 4 image

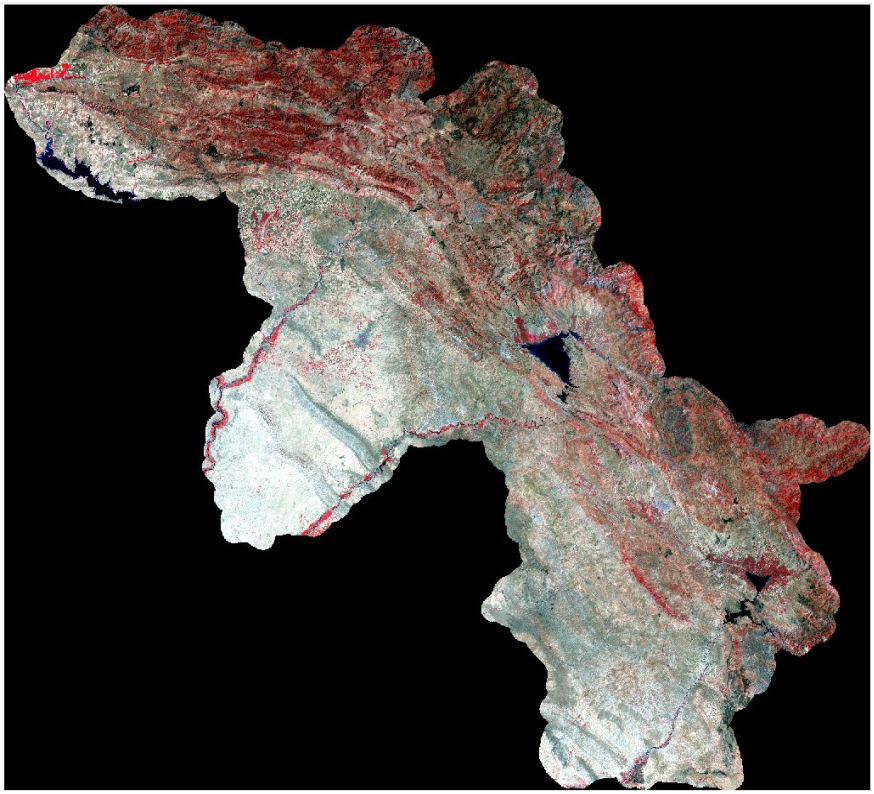

1998 Landsat 5 image

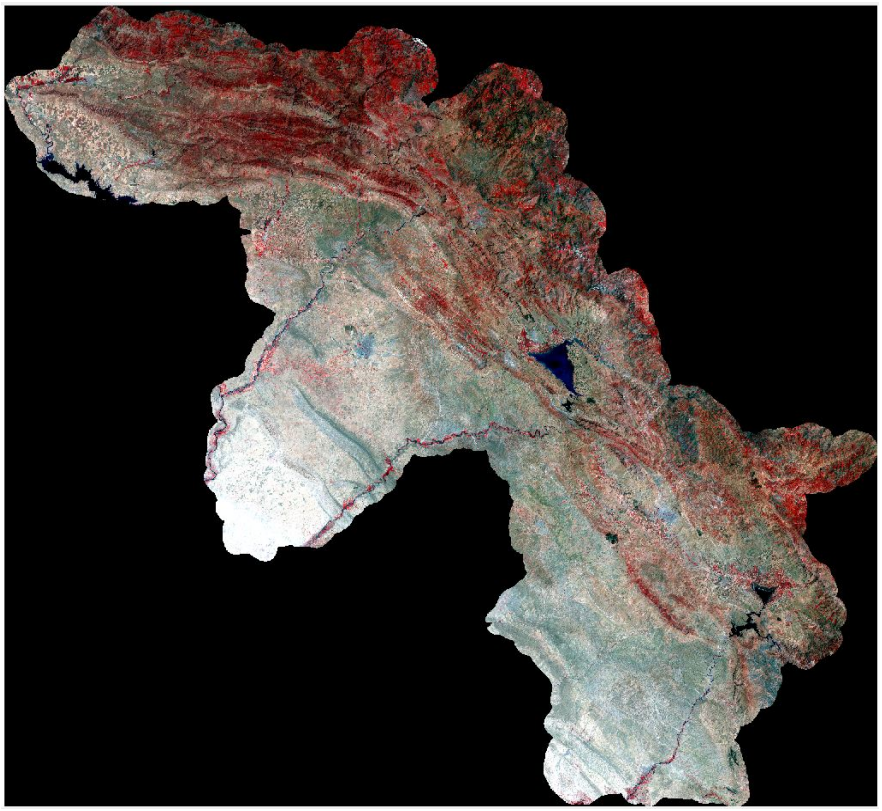

2006 Landsat 5 image

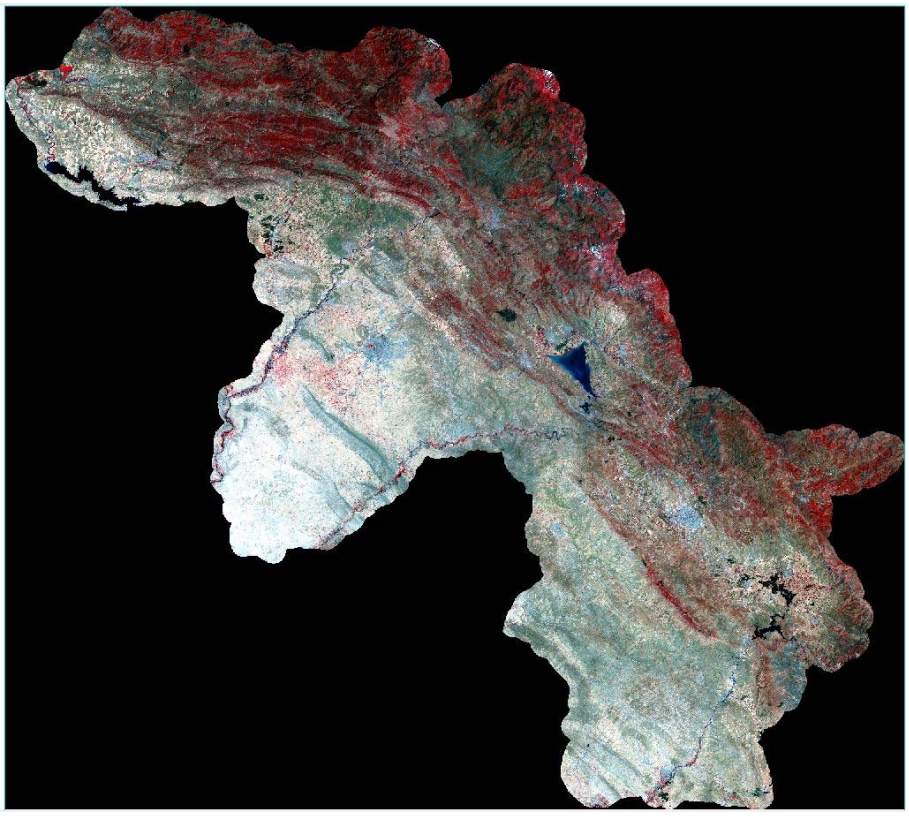

2014 Landsat 8 image